

**UNIVERSIDADE FEDERAL DE MINAS GERAIS**

**PROGRAMA DE PÓS-GRADUAÇÃO EM SANEAMENTO,  
MEIO AMBIENTE E RECURSOS HÍDRICOS**

**EVALUATION OF MEMBRANE  
DISTILLATION FOR THE TREATMENT OF  
SURFACE WATER DURING EMERGENCY  
SITUATIONS**

**Luiza de Barros Grossi**

**Belo Horizonte**

**2018**

**EVALUATION OF MEMBRANE  
DISTILLATION FOR THE TREATMENT OF  
SURFACE WATER DURING EMERGENCY  
SITUATIONS**

**Luiza de Barros Grossi**

**Luiza de Barros Grossi**

**EVALUATION OF MEMBRANE DISTILLATION FOR  
THE TREATMENT OF SURFACE WATER DURING  
EMERGENCY SITUATIONS**

Dissertação apresentada ao Programa de Pós-Graduação em Saneamento, Meio Ambiente e Recursos Hídricos da Universidade Federal de Minas Gerais como requisito parcial à obtenção do título de Mestre em Saneamento, Meio Ambiente e Recursos Hídricos.

Área de Concentração: Meio Ambiente

Linha de Pesquisa: Caracterização, prevenção e controle da poluição

Orientadora: Profa. Míriam Cristina Santos Amaral Moravia

Belo Horizonte  
Escola de Engenharia da UFMG  
2018

**Luiza de Barros Grossi**

**EVALUATION OF MEMBRANE DISTILLATION FOR  
THE TREATMENT OF SURFACE WATER DURING  
EMERGENCY SITUATIONS**

Master thesis presented to the Post-Graduate Program in Sanitation, Environment and Water Resources of the Federal University of Minas Gerais as a partial requirement to obtain the title of Master in Sanitation, Environment and Water Resources.

Focus area: Environment

Research line: Characterization, prevention and control of pollution

Advisor: Prof. Míriam Cristina Santos Amaral Moravia

Belo Horizonte  
School of Engineering, Federal University of Minas Gerais  
2018

G878e

Grossi, Luíza de Barros.

Evaluation of membrane distillation for the treatment of surface water during emergency situations [manuscrito] / Luíza de Barros Grossi.- 2018. 108 f, enc.: il.

Orientadora: Míriam Cristina Santos Amaral Moravia.

Mestrado (dissertação) - Universidade Federal de Minas Gerais, Escola de Engenharia.

Bibliografia: f. 100-108.

1. Engenharia sanitária - Teses. 2. Meio ambiente - Teses. 3. Águas superficiais - Teses. 4. Água - Purificação - Teses. I. Moravia, Míriam Cristina Santos Amaral. II. Universidade Federal de Minas Gerais. Escola de Engenharia. III. Título.

CDU: 628(043)



UNIVERSIDADE FEDERAL DE MINAS GERAIS

Escola de Engenharia

Programa de Pós-Graduação em Saneamento, Meio Ambiente e Recursos Hídricos

Avenida Antônio Carlos, 6627 - 4º andar - 31270-901 - Belo Horizonte - BRASIL

Telefax: 55 (31) 3409-1882 - posgrad@desa.ufmg.br

<http://www.smarh.eng.ufmg.br>

## FOLHA DE APROVAÇÃO

Evaluation Of Membrane Distillation For The Treatment Of Surface Water During  
Emergency Situations

**LUIZA DE BARROS GROSSI**

Dissertação defendida e aprovada pela banca examinadora constituída pelos Senhores:

*Miriam C.S. Amaral Moravia*

Profª MÍRIAM CRISTINA SANTOS AMARAL MORAVIA

*Lisete Celina Lange*

Profª LISÉTE CELINA LANGE

*C. P. B.*  
Prof. CRISTIANO PIACSEK BORGES

Aprovada pelo Colegiado do PG SMARH

*N. de Oliveira Nascimento*

Prof. Nilo de Oliveira Nascimento  
Coordenador

Versão Final aprovada por

*Miriam C.S. Amaral Moravia*

Profª. Miriam Cristina Santos Amaral Moravia  
Orientadora

Belo Horizonte, 20 de março de 2018.

## AGRADECIMENTOS

Acredito que os agradecimentos de uma dissertação venham antes do texto justamente pois, se não fossem pelas pessoas que nos auxiliaram durante esta caminhada, não haveria texto algum. No entanto, apesar de confiar à memória (sempre falha) a impossível tarefa de lembrar de todos aqueles que fizeram parte desta etapa, tento aqui deixar um registro escrito dos que foram indispensáveis durante este tempo.

Ao universo por abrir tantas portas durante a minha caminhada e aos meus pais por terem me ensinado a reconhecer estas oportunidades e aproveitá-las com leveza e responsabilidade.

À minha orientadora Míriam por ter contribuído tanto para a minha formação, me oferecendo inúmeras oportunidades e por confiar no meu trabalho.

À minha família do coração que, independente do parentesco ou não, são as pessoas que fazem meus dias mais felizes. Se você chegou até aqui e está lendo isso, pode acreditar, este agradecimento é para você e é de todo o meu coração. Tenha certeza que sem você eu não estaria aqui e se você considera isso uma vitória, vem comemorar comigo porque ela é sua também!

Aos amigos e colegas do DESA e do GEAPS que, apesar de se encaixarem no parágrafo acima, merecem um destaque especial por serem pessoas que foram indispensáveis para a minha formação e realização deste trabalho: Laura, Bárbara e Priscila; vocês me ajudaram tanto (e desde o início da minha vida no mundo das membranas) que eu não tenho palavras pra expressar o que eu sinto, eu só consigo sorrir. Agradeço profundamente também aos demais integrantes do projeto e companheiros de perrengue: Ramatisa, Cecília, Cíntia, Clara e Mateus; podem acreditar que, sem vocês, não haveria mestrado.

Aos professores da banca, Profa. Liséte Lange e Prof. Cristiano Piacsek, que gentilmente aceitaram avaliar e contribuir com o melhoramento deste trabalho.

Aos parceiros externos ao DESA e que colaboraram para a realização das diversas etapas deste trabalho: INCT – ACQUA Instituto Nacional de Ciência e Tecnologia em Recursos

Minerais, Água e Biodiversidade pelas análises de ICP-OES; Orlando do Departamento de Engenharia Metalúrgica da UFMG pelas análises de ângulo de contato; Centro de Microscopia da UFMG e Departamento de Engenharia Química da PUC Minas pelas imagens de microscopia eletrônica e EDX; CEFET pelas análises de infravermelho.

Aos recursos fornecidos pela FAPEMIG ao projeto intitulado *Tratamento Avançado De Água Para Abastecimento Com Vistas Ao Atendimento Em Situações Emergenciais*, sob o Edital 04/2016 e à CAPES pela bolsa concedida.

Muito obrigada!



## RESUMO

A presença sistêmica de poluentes em corpos d'água e o risco de eventos de grande potencial poluidor – como o rompimento de barragens de mineração – são problemas enfrentados pela sociedade moderna. Além das consequências ambientais, a contaminação severa de águas superficiais dificulta fortemente ou até inviabiliza o tratamento da mesma com vistas ao abastecimento público. Assim, uma solução a curto prazo é o desenvolvimento de rotas de tratamento avançado que possam ser utilizadas durante estes momentos. No entanto, para que sejam eficazes, estas rotas devem ser robustas e pautadas em preceitos sustentáveis. Neste contexto, a destilação assistida por membranas (DM) é reportada na literatura como um processo de separação robusto e com baixo requerimento energético, quando associada à uma fonte de energia alternativa. Tendo em vista o contexto brasileiro de disponibilidade de energia solar e a potencialidade apresentada pela destilação por membranas quando conjugada à fontes renováveis, este trabalho visou avaliar tecnicamente a viabilidade do uso da DM no tratamento de águas superficiais seriamente contaminadas com rejeitos de barragem de minério de ferro. Aspectos como pré-tratamento, temperatura e vazão foram avaliados em escala de bancada, assim como a ação de diferentes agentes de limpeza e a estabilidade da membrana quando exposta a longo prazo à água contaminada. Nestes casos, observou-se que o pré-tratamento é recomendado para alimentações cuja turbidez excede 300NTU, e a ultrafiltração demonstrou os melhores resultados do ponto de vista técnico. Ainda, a 70°C e velocidade linear de 0.18 m/s o sistema demonstrou melhor eficiência energética. Observou-também que água destilada a 60°C foi o agente de limpeza com melhor desempenho entre os testados, mantendo tanto a integridade da membrana quanto restaurando o fluxo de permeado inicial. Por fim, os fenômenos de transferência de massa e calor do sistema foram matematicamente modelados, a fim de servir como base para a concepção e construção de um módulo em escala semi-piloto. Neste caso, foi possível modelar a extensão da membrana com uma precisão de no mínimo 80%, e os resultados obtidos para um módulo com área ativa de 0.3 m<sup>2</sup> indicaram que os modelos permaneceram válidos para membranas maiores.

**Palavras-chave:** Destilação por membranas, águas superficiais, barragem de minério de ferro, condições operacionais, vida útil, design de módulo.

## ABSTRACT

The continued pollution of water bodies and the possibility of acute pollution events – such as the collapse of tailing dams – are problems faced by the modern society. Aside the environmental effects of it, this severe contamination can difficult or even impair the surface water treatment to public supply, which leads to a state of emergency during certain situations. As a short-term solution to at least diminish the chaos provoked by the water shortage, the establishment of advanced water treatment routes based on sustainable principles is a feasible alternative. Membrane distillation (MD) is a technology reported by the literature as a robust and low energy demand (when associated to alternatives sources of heating) separation process. Having in sight the Brazilian context of wide solar availability and the potentiality of solar-driven membrane distillation systems, this work aimed to evaluate technical aspects of MD treating surface water contaminated with tailings from an iron mining dam. Aspects such as feed pretreatment, temperature and flow rate were assessed in bench-scale, as well as the impacts of different cleaning agents and membrane ageing. In these cases, it was observed that for feeds whose turbidity was above 300 NTU, a pretreatment should be carried out, and ultrafiltration is the most suitable technology from the technical point of view. In addition, at 70°C and 0.18 m/s, the system presented its best energy efficiency without compromising the permeate quality. Regarding the cleaning agents, deionized water at 60°C demonstrated the best cleaning efficiency among the agents tested, being able to restore the membrane initial permeate flux without compromising its integrity. Furthermore, the mass and heat phenomena that took place in the system were mathematically modelled, in order to assist the design of a semi-pilot membrane distillation module. The models presented an accuracy of at least 80%, and similar results were found the the semi-pilot simulation, which indicates that the model remained valid for a module with a total active area of 0.3m<sup>2</sup>.

**Keywords:** Membrane distillation, surface water, iron tailing dam, operational conditions, membrane ageing, module design.

# TABLE OF CONTENTS

LIST OF FIGURES .....	viii
LIST OF TABLES .....	x
LIST OF ABBREVIATIONS, ACRONYMS AND SYMBOLS .....	xiii
<b>CHAPTER 1: INTRODUCTION .....</b>	<b>1</b>
1.1 BACKGROUND AND JUSTIFICATION .....	2
1.2 OBJECTIVE.....	6
1.2.1 <i>General objective</i> .....	6
1.2.2 <i>Specific objectives</i> .....	6
1.3 DOCUMENT STRUCTURE .....	6
<b>CHAPTER 2: PRODUCTION OF DRINKING WATER IN EMERGENCY SITUATIONS USING MEMBRANE DISTILLATION: AN EVALUATION OF THE MAIN OPERATIONAL PARAMETERS .....</b>	<b>7</b>
2.1 INTRODUCTION.....	8
2.2 MATERIALS AND METHODS .....	11
2.2.1 <i>Sample collection, characterization, and preparation</i> .....	11
2.2.2 <i>Experimental setup</i> .....	13
2.2.3 <i>Membrane characteristics</i> .....	14
2.2.4 <i>Experimental procedure</i> .....	15
2.2.5 <i>Analytical methods</i> .....	16
2.2.6 <i>Calculations</i> .....	16
2.3 RESULTS AND DISCUSSION .....	20
2.3.1 <i>MD performance</i> .....	20
2.3.2 <i>Pretreatment</i> .....	24

2.3.3	<i>Feed temperature</i> .....	30
2.3.4	<i>Cross-flow velocity</i> .....	36
2.4	CONCLUSION .....	40
<b>CHAPTER 3: MEMBRANE DISTILLATION APPLIED TO THE TREATMENT OF SURFACE WATER CONTAMINATED AFTER THE BREAK OF FUNDÃO'S MINING TAILING DAM: A STUDY OF MEMBRANE FOULING, CLEANING, AND AGEING .....</b>		
<b>42</b>		
3.1	INTRODUCTION .....	43
3.2	MATERIALS AND METHODS .....	45
3.2.1	<i>Effluent characterization</i> .....	45
3.2.2	<i>Experimental set up</i> .....	47
3.2.3	<i>MD Membrane</i> .....	47
3.2.4	<i>Fouling evaluation</i> .....	47
3.2.5	<i>Chemical cleaning</i> .....	48
3.2.6	<i>Membrane ageing</i> .....	49
3.2.7	<i>Analytical Methods</i> .....	51
3.3	RESULTS AND DISCUSSION .....	51
3.3.1	<i>Fouling evaluation</i> .....	51
3.3.2	<i>Chemical cleaning</i> .....	55
3.3.3	<i>Membrane ageing</i> .....	59
3.4	CONCLUSION .....	62
<b>CHAPTER 4: THERMAL BOUNDARY LAYER AND MASS FLUX PREDICTION MODELS FOR THE DESIGN OF A SEMI-PILOT MEMBRANE DISTILLATION STACK CELL .....</b>		
<b>63</b>		
4.1	INTRODUCTION .....	64
4.2	THEORY .....	65

4.2.1	<i>Thermal Boundary Layer Estimation</i> .....	66
4.2.2	<i>Mass flux prediction</i> .....	72
4.3	<b>MATERIALS AND METHODS</b> .....	76
4.3.1	<i>Membrane characteristics</i> .....	76
4.3.2	<i>Experimental setup</i> .....	76
4.3.3	<i>Experimental procedure</i> .....	77
4.3.4	<i>Mass flux prediction</i> .....	78
4.3.5	<i>Convective heat transfer analysis</i> .....	78
4.3.6	<i>Thermal boundary layer estimation</i> .....	79
4.4	<b>RESULTS AND DISCUSSION</b> .....	81
4.4.1	<i>Experiments</i> .....	81
4.4.2	<i>Mass flux prediction</i> .....	81
4.4.3	<i>Convective heat transfer analysis</i> .....	82
4.4.4	<i>Thermal boundary layer estimation</i> .....	83
4.4.5	<i>Stack module design</i> .....	89
4.5	<b>CONCLUSION</b> .....	93
	<b>CHAPTER 5: FINAL CONSIDERATIONS</b> .....	<b>94</b>
	<b>CHAPTER 6: SUGGESTIONS FOR FUTURE WORK</b> .....	<b>97</b>
	<b>CHAPTER 7: REFERENCES</b> .....	<b>99</b>

## LIST OF FIGURES

<b>Figure 2.1</b> – Schematic of the WTP and sampling point.....	11
<b>Figure 2.2</b> – Schematic of the DCMD bench-scale unit.....	14
<b>Figure 2.3</b> – Curve of dosage as a function of the residual turbidity for the pH's 8.14.....	25
<b>Figure 2.4</b> – Experimental and predicted mean flux, and final permeate conductivity for the evaluated temperatures, Water recovery fraction of 65% .....	31
<b>Figure 2.5</b> – Experimental and predicted Qspec for the evaluated temperatures.....	32
<b>Figure 2.6</b> – Permeate flux, pump requirement and final conductivity for each of the assessed cross-flow velocities .....	36
<b>Figure 3.1</b> – Schematic of the DCMD bench-scale unit.....	47
<b>Figure 3.2</b> – Flux decay and conductivity over time for the solution.....	52
<b>Figure 3.3</b> – SEM and EDX for the (a) virgin and (b) fouled membrane.....	54
<b>Figure 3.4</b> – EDX mapping of the fouled membrane (Al: Green, Fe: Red, O: Yellow, Si: Pink and F: Blue) .....	55
<b>Figure 3.5</b> – Cleaning efficiency, average water contact angle and SEM images (70x) for the virgin, fouled and after each of the chemical agents used.....	56
<b>Figure 3.6</b> – Flux decay over time for the effluent in which WC = water cleaning and CC = chemical cleaning with HCl 2% w/v .....	58
<b>Figure 3.7</b> – EDX mapping for the fouled membrane after cleaning with DI water and HCl (Al: Green, Fe: Red, O: Yellow, Si: Pink and F: Blue).....	58
<b>Figure 3.8</b> – SEM images for the membranes at days 0, 120 and 210 (5000x), membrane main characteristics, and EDX mapping for the membrane at day 210 .....	60

<b>Figure 3.9</b> – EDX mapping for the membrane at day 210.....	61
<b>Figure 3.10</b> – SEM images and EDX mapping for the membrane subjected to solution + DI water at 60°C .....	62
<b>Figure 4.1</b> – Representation of the system in the rectangular coordinate system used .....	66
<b>Figure 4.2</b> – Schematic of the DCMD bench-scale unit.....	77
<b>Figure 4.3</b> – Thermal boundary layer height predicted by the temperature profile resultant from the modelling in feed and permeate channels for condition (a) A; (b) B and (c) C .....	85
<b>Figure 4.4</b> – Illustration of $\Delta T$ behavior delivered specifically by the temperature profiles solutions of each of the three feed inlet temperature condition.....	87
<b>Figure 4.5</b> – Illustration of $\Delta P$ behavior delivered specifically by the temperature profiles solutions of each of the three feed inlet temperature condition.....	88
<b>Figure 4.6</b> – Thermal boundary layer height predicted by the temperature profile resultant from the modelling in feed and permeate channels for the stack module designed .....	91
<b>Figure 4.7</b> – Illustration of $\Delta T$ behavior delivered specifically by the temperature profiles solutions for the small pilot .....	92
<b>Figure 4.8</b> – Stack module schematics and image .....	93

## LIST OF TABLES

<b>Table 2.1</b> – Mean and standard deviation for the main physical-chemical parameters and their respective legal limits according to the Administrative Ordinance 2914.....	12
<b>Table 2.2</b> – Semi-quantitative analysis of the sludge used in the synthetic solutions .....	12
<b>Table 2.3</b> – Physicochemical characterization of the synthetic solutions.....	13
<b>Table 2.4</b> – Membrane main characteristics .....	14
<b>Table 2.5</b> – Assessment of feed temperature and cross-flow velocity in MD performance ....	16
<b>Table 2.6</b> – Blocking filtration laws .....	19
<b>Table 2.7</b> – $J/J_0$ and blocking filtration type for the synthetic solutions with different turbidities.....	22
<b>Table 2.8</b> – Resistances, wetting rate and wetting time for the synthetic solutions with different turbidities .....	23
<b>Table 2.9</b> – Permeates characterization for a recovery fractions of 82% (56NTU), 56%(300NTU), 45% (10,000NTU) and 46% (20,000NTU).....	24
<b>Table 2.10</b> – Physicochemical characterization of the solution before and after their respective pretreatment.....	25
<b>Table 2.11</b> – Normalized flux ( $J/J_0$ ) and blocking filtration type for the solutions with and without the pretreatment stage.....	28
<b>Table 2.12</b> – Resistances, wetting rate and wetting time for the synthetic solutions for the solutions with and without the pretreatment stage. ....	29
<b>Table 2.13</b> – MD Permeate quality for each of the cases .....	30



<b>Table 2.14</b> – Resistances in the membrane distillation system for each of the temperatures assessed.....	32
<b>Table 2.15</b> – Physical-Chemical characterization of the generated permeates for each of the assessed temperatures .....	34
<b>Table 2.16</b> – Metals and ions characterization of the generated permeates.....	35
<b>Table 2.17</b> – Boundary layer resistances in the membrane distillation system for each of the cross-flow velocities assessed .....	36
<b>Table 2.18</b> – Physical-Chemical characterization of the generated permeates.....	38
<b>Table 2.19</b> – Metals and ions characterization of the generated permeates.....	39
<b>Table 3.1</b> – Physical-chemical characterization of the effluent and semi-quantitative analysis of the sludge used during the tests.....	46
<b>Table 3.2</b> – Pre-selected cleaning agents, their respective concentrations, and temperature ..	49
<b>Table 3.3</b> – Flux decay, blocking filtration type, resistances and wetting characteristics after 6h of filtration (Temperature: 40°C, Flow rate; 33L/h) .....	53
<b>Table 4.1</b> – Membrane main characteristics and air thermal conductivity for the set of temperatures used during the experiments .....	76
<b>Table 4.2</b> – Process conditions established to provide data to assist on the modelling.....	78
<b>Table 4.3</b> – Experimental data for each process condition .....	81
<b>Table 4.4</b> – Corresponding linear regression equation and $R^2$ for each of the heat coefficient correlations .....	82
<b>Table 4.5</b> – Comparison between experimental data and constant wall temperature model energy variation predictions .....	83

<b>Table 4.6</b> – Respective temperature profile solutions obtained for feed and permeate channels for each feed inlet temperature condition modelled .....	86
<b>Table 4.7</b> – Operational conditions, membrane dimensions, expected flux, and permeate production.....	90
<b>Table 4.8</b> – Respective temperature profile solutions obtained for feed and permeate channels for the stack module designed .....	91

## LIST OF ABBREVIATIONS, ACRONYMS AND SYMBOLS

$a$  – Constant of equation 4.12

$A$  – Cross section area of the channel

$A_m$  – Membrane area

AGMD – Air gap membrane distillation

ALUM – Aluminum sulfate

$b$  – Constant of equation 4.12

$c$  – Constant of equation 4.12

$C$  – Membrane distillation coefficient

$C_p$  – Liquid specific heat capacity

CA – Contact Angle

CE – Cleaning Efficiency

$D$  – Hydraulic diameter

DCMD – Direct contact membrane distillation

DI – Deionized

$E$  – Power requirement

ED – Electrodialysis

EDX – Energy Dispersive X-ray

FEAM – State Environmental Regulatory Foundation

$h$  – Convective heat transfer coefficient

$H$  – Half of the channel's thickness value

$\Delta H_g$  – Specific vapor enthalpy gradient

$\Delta H_{vap}$  – Liquid-vapour enthalpy gradient

ICP-OES – Inductively Coupled Plasma optical emission spectrometry

$J_0$  – Initial permeate flux

$J$  – Permeate flux

$J_{exp}$  – Expected permeate flux

$k$  – thermal conductivity coefficient

$k_f$  – Air thermal conductivity

$k_m$  – Membrane thermal conductivity

$K_m$  – membrane heat transfer coefficient

$k_s$  – PTFE thermal conductivity

$K_{complete}$  – Hermia's parameter to complete blocking law

$K_{standard}$  – Hermia's parameter to standard blocking law

$K_{intermediate}$  – Hermia's parameter to intermediate blocking law

$K_{cake}$  – Hermia's parameter to cake blocking law

LEP – Liquid entry pressure

$m_d$  – Distillate mass

MD – Membrane distillation

$N$  – Constant of equation 4.12

NF – Nanofiltration

$Nu$  – Nusselt number

$P$  – Pressure (Pa)

PP – Polypropylene

$\Delta p$  – Vapor pressure difference

$P_1$  – Vapor pressure at feed membrane surface

$P_2$  – Vapor pressure at permeate membrane surface

$P_f$  – Vapor pressure at feed bulk

$P_p$  – Vapor pressure at permeate bulk

$P$  – Perimeter of the channel

$Pr$  – Prandtl number

PTFE – Polytetrafluoroethylene

$q''_m$  – Conductive heat transferred to the membrane

$q''_v$  – phase transition heat

$Q$  – Flow rate

$Q_{\text{spec}}$  – Amount of heat required to generate 1kg of permeate

RE – Renewable energy

Re – Reynolds number

RO – Reverse Osmosis

$R_{\text{fb}}$  – Feed boundary layer resistance

$R_{\text{pb}}$  – Permeate boundary layer resistance

$R_{\text{m}}$  – Membrane resistance

$R_{\text{total}}$  – Total resistance

$R_{\text{fouling}}$  – Fouling resistance

SEM – Scanning Electron Microscopy

SGMD – Sweep gas membrane distillation

SNIS – National System for Information about Sanitation

TN – Total Nitrogen

TOC – Total Organic Carbon

TP – Temperature polarization

TPC – Temperature polarization coefficient

$T_{\infty,p}$  – Feed bulk temperature

$T_{\infty,f}$  – Permeate bulk temperature

$T_{w,f}$  – Feed interfacial temperature

$T_{w,p}$  – Permeate interfacial temperature

TS – Total Solids

TSS – Total Suspended Solids

$u_m$  – Mean fluid velocity

$u$  – Velocity in  $x$  direction

VMD – Vacuum membrane distillation

$v$  – Velocity in  $y$  direction

$w$  – Velocity in  $z$  direction

WTP – Water Treatment Plant

### **Greek letters**

$\rho$  – Density

$\emptyset$  – Membrane porosity

$\eta$  – Pump efficiency

$\xi$  – Overall convective heat

$\delta_T(x)$  – Thermal boundary layer height

$\varepsilon$  – Membrane thickness

# **CHAPTER 1**

---

## **INTRODUCTION**



## **1.1 BACKGROUND AND JUSTIFICATION**

The variety of pollutants disposed in rivers and lakes has increased worldwide due to anthropic activities developed without a proper control, specially regarding pollution. Among these pollutants, organic load, trace metals, contaminants from industrial wastewater, pesticides and pharmaceuticals can be highlighted as the ones of major concern to society, including in Brazil (YABE and OLIVEIRA, 1998; IGAM, 2014; ANDRADE et al., 2011; EPA, 2016).

In the Minas Gerais state context, in addition to the chronical pollution already lived for decades, the water bodies are also subjected to the possibility of acute pollution resulted from the collapse of mining tailing dams. In the state, mining is considered the major economical activity, representing 24.4% of the industrial share (IBRAM, 2016). As a consequence, according to the State Environmental Regulatory Foundation – FEAM (2016), Minas Gerais currently counts with 737 mining tailing dams, and some of them are in a very precarious situation, such as the one that collapsed in the cities of Mariana (2015), Itabirito (2014), Miraf (2007) and São Sebastião das Águas Claras (2001) – (WISE URANIUM PROJECT, 2016).

Despite the undeniable importance that river restoration and an effective control of pollution at the source have in order to build a more sustainable scenario, such actions still have a way to go in Brazil, and their results may take some time to be felt. Nevertheless, the effects of pollutions have already been faced by the population. In the water management context, this asks for the development of routes for advanced water treatment that are more robust than the conventional treatment widely adopted, and can be also used during emergencies.

As a case study to evaluate the feasibility and applicability of such routes, the water from river Doce in the region of Governador Valadares city was chosen. The valley of river Doce is a mesoregion that houses 8.9% of Minas Gerais state's population, distributed in 84 cities. Governador Valadares, the biggest city among them, has a population estimated in 400,000 inhabitants (FUNDAÇÃO JOÃO PINHEIRO, 2000), and its occupation was established in the beginning of the 20<sup>th</sup> century, after the construction of a railroad connecting the states of Minas Gerais and Espírito Santo (FAVERO, 2001).

Even with an well-established occupation for over 100 years, the sewage collection and treatment is still poor in the region. According to the National System for Information about Sanitation – SNIS, there is no sewage treatment in Governador Valadares, which places the city in the last place in the Ranking for Basic Sanitation for the 100 biggest cities in Brazil.

Besides the organic load that arises from the incorrect sewage disposal, the River Basin Committee of river Doce – CBH-Doce indicated as factors of pressure for the rapid deterioration of the water quality in the region aspects such as erosion and incorrect industrial wastewater, and classifies the region as Class 2, according to the CONAMA Resolution 357 (BRASIL, 2005). In addition, a diagnose from the committee done in 2005 also pointed out the vulnerability of the potable water distribution during accidental pollutions (CBH-Doce, 2005).

In November 2015, the water degradation was aggravated by the collapse of Fundão’s dam, located 363 km away from Governador Valadares. The wave of 40m cubic meters destroyed villages and flowed on down river Doce, being considered Brazil’s worst environmental disaster. After this event, the conventional treatment widely employed in the region – that consisted of railing, coagulation with polyaluminium chloride, filtration and disinfection - was not enough to properly treat the water for public supply. As an emergency action, the local agency replaced the normal coagulant agent to tannin, considered as more effective than the regular one. Despite being able to produce water with quality as required by law, the amount of sludge generated was widely increased, which increased both costs and environmental impacts of the treatment. It is noteworthy that before the reestablishment of the service, a 10-day interruption in the water supply was suffered in Governador Valadares, being responsible for a severe water crisis in the city. The effects of these lack of planning during emergencies can still be felt in the region, where even after 2 years of the event and a normal water distribution several people still do not trust in the water quality.

Besides the amount of suspended solids disposed on the river due to the wave passage, a secondary phenomenon was also observed: several industries along the riverside seized the opportunity to release its own industrial wastewater without a proper treatment. As a consequence, the water became not only contaminated by tailings from an iron dam, but also by trace metals and other pollutants, which impaired even more the water quality.

By seeing this scenario, the establishment of advanced water treatment solutions is an important alternative to be considered in order mitigate or at least diminish the vulnerability of the potable water distribution during adverse situations. Among the suitable technologies to this application, the membrane technology can be highlighted. According to Baker (2004), the membrane separation processes use membranes as selective barriers able to control the permeation of chemical species through its structure. This occurs under the presence of a driving force, that may be thermal, electrical or arise from a concentration or pressure difference (HABERT, BORGES and NOBREGA, 2006). The significant development experienced by the membrane technologies and its unique characteristics – such as absence or low demand for chemicals, modular design and high selectivity (ACERO et al., 2010) have led to an expressive increase in the use of membranes in the last years (BBC, 2011).

Currently, reverse osmosis (RO) is the leading technology in desalination (BBC, 2014), being also successfully used to remove multiple contaminants from groundwater (RICHARDS et al., 2011). However, the associated costs to its implementation in Brazil is still a challenge, and as an alternative to it, membrane distillation (MD) is a promising solution, specially when combined with thermal renewable energy (RE) sources (BAKER, 2004).

Membrane distillation is a thermally driven process in which a hydrophobic, microporous membrane is used to separate two phases with different temperatures. The existing vapor pressure gradient between both phases is responsible for driving the passage of vapor from the hot to the cold side (DÍEZ and GONZÁLEZ, 2000; KHAYET, 2011). The hydrophobic nature of the membrane allows that only vapor goes through it, thus addressing a theoretical rejection of 100% for non-volatile solutes (AL-OBAIDANI et al., 2008). MD can be performed under four different configurations, characterized mainly by the difference in which the cold phase is presented. They are as following: (a) Air Gap Membrane Distillation (AGMD), where an air gap is placed between the membrane and the cold solution; (b) Sweep Gas Membrane distillation, in which an inert gas is used to sweep the permeate; (c) Vacuum Membrane Distillation, that besides the presence of the temperature difference, also subjects the permeate under vacuum conditions; and (d) Direct Contact Membrane Distillation (DCMD), where the cold solution is in direct contact with the membrane, resulting in a mixture between cold solution and permeate (ALKHUDHIRI, DARWISH and HILAL, 2012).

In MD, the major energetic requirement is demanded for heating the feed, and a minor part is used by the pumps, since it consists of a non pressure-oriented process (MERICQ, LABORIE and CABASSUD, 2009). By developing a RE-MD unit, one is expected to deliver an advanced treatment option able to provide water with high quality even in remote areas with no grid connection. In this context, as sources of heat supply, Drioli, Ali and Macedonio (2015) quote the industrial residual heat, geothermal and solar energy.

In the Brazilian context, the use of solar energy as a source for both heat and electric energy is very attractive. According to Pereira et al. (2006), the average sunlight irradiation is high and presents little fluctuations over the year throughout the entire country. Besides, the price for installation and operation of photovoltaic cells has experienced a continued decrease in the last few years (BNDES, 2014) and, consequently, a growth of 350% in its utilization was observed in 2015 alone.

Even with the applicability that membrane distillation may have in Brazil, the technology is still very little explored nationally, and as far as the author is concerned, experiences of its conjugation with solar energy in the country have not yet been published; in fact, only two works regarding MD could be attributed to Brazilian scientists (PANTOJA, NARIYOSHI and SECKLER, 2014; NARIYOSHI and PANTOJA, 2014). On the international context, however, several studies were performed, including the successful construction and operation of pilot plants, as reported by Schwantes et al. (2013), Guillén- Burrieza et al. (2012), Banat and Jwaied (2010), and Khan and Martin (2014), for example.

The potentiality of membrane distillation for ensuring water with good quality for people even in off-grid localities is huge, but yet, little explored in Brazil. Thus, this work aims to be a first step towards a study to evaluate under which conditions will MD be a feasible alternative in Brazil. It is noteworthy to mention that this study is part of a bigger research project that covers others aspects of MD such as the mechanisms of pharmaceuticals retention, design, efficiency and economic aspects of a solar-driven MD unit. Besides developing national technology focused on improving the access of water to people, the work also intends to contribute to properly characterize and understand the changes that may occur in the water quality of a river after suffering from an acute pollution event.

## **1.2 OBJECTIVE**

### **1.2.1 General objective**

The aim of this master thesis is to investigate both operational and design aspects of membrane distillation by treating surface damaged water, using the water from river Doce collected in Governador Valadares as a case study.

### **1.2.2 Specific objectives**

- Observe the effect of feed turbidity in the MD performance;
- Evaluate the effects of pretreatment on MD performance treating the water collected in Governador Valadares;
- Define the most suitable operational conditions for temperature and cross-flow velocity, in bench scale;
- Assess membrane fouling, ageing, and define a cleaning procedure to it;
- Model the heat and mass transfer that takes place in the MD system;
- Model and estimate the thermal boundary layer profile of the system;
- Propose a module stack design for the flat sheet direct contact membrane distillation process, based on the models previously developed for heat, mass transfer, and thermal boundary layer.

## **1.3 DOCUMENT STRUCTURE**

This master thesis is divided into 7 chapters: Chapter 1 is an introduction and contains a theme presentation, objectives and the document structure; Chapter 2 addresses objectives 1 to 3; Chapter 3 presents the results for membrane fouling, ageing and cleaning procedure (objective 4); Chapter 4 comprehends the development of models to heat and mass transfer, as well as for the thermal boundary layer estimation, and the module design proposition (objectives 5 to 7). Finally, Chapters 5, 6 and 7 contain the final considerations, suggestions to future work and the references, respectively.

## **CHAPTER 2**

---

# **PRODUCTION OF DRINKING WATER IN EMERGENCY SITUATIONS USING MEMBRANE DISTILLATION: AN EVALUATION OF THE MAIN OPERATIONAL PARAMETERS**

## **2.1 INTRODUCTION**

Iron mining activity brings several environmental impacts, including tailing dams. Despite the control strategies used to avoid accidents, these dams are subjected to collapse, and when this happens, both environment and society undergo for a period of severe stress. In 2015, for example, a considerable part of southeast Brazil was impacted by the collapse of a dam whose contamination plume reached the basin of an important river - Doce. Besides the environmental losses, the extremely high concentration of Total Suspended Solids (TSS) and other contaminants in the raw water (originated also from the incorrect disposal of other industrial wastewater along the riverside) impaired the water distribution, since there was no route of treatment available and able to properly treat the water in that situation. This event caused a severe water stress in major cities and elucidated the urgent need for developing alternative routes of treatment able to ensure water of good quality even during emergency situations.

As a robust and highly selective technology that may be suitable, membrane distillation (MD) can be highlighted. MD is a process in which the driving force is the temperature difference between two phases separated by a microporous and hydrophobic membrane. The existing vapor pressure gradient leads the passage of water vapor from the hot – feed - to the cold side – permeate (QU et al., 2009), and in most cases a temperature difference of 30°C is enough to promote vapor permeation. Since the membrane possesses hydrophobic characteristics, only vapor is capable of passing across it, thus addressing a theoretical rejection of 100% for non-volatile solutes (AL-OBAIDANI et al., 2008). In addition, MD is capable of concentrating solutions until its saturation point without any significant loss on permeate flux, since it consists of a non-pressure oriented process, unlike nanofiltration (NF) and reverse osmosis (RO) (FRANCIS et al., 2014).

When compared to NF, RO, and electrodialysis (ED), membrane distillation has some advantages, such as: (a) low operating temperature, which allows its association to energy sources such as geothermal, solar and industrial residual heat; (b) operation at room pressure, which increases the system's security and decreases costs of equipment; (c) membrane fouling is less severe (MANNA and PAL, 2016).

Membrane distillation can be performed under four configurations that differ one from another by the nature of permeate cooling: Air Gap Membrane Distillation (AGMD), Vacuum Membrane Distillation (VMD), Sweep Gas Membrane Distillation (SGMD) and Direct Contact Membrane Distillation (DCMD). Among them, DCMD is widely employed to desalination and concentration of aqueous solutions, due to its operational simplicity when compared to the others (ALKHUDHIRI et al., 2012). For DCMD, mass transfer is a three-step process, involving; (a) diffusive transport from bulk feed to the membrane surface; (b) diffusive and convective transport of the water vapor across the membrane pores; and (c) vapor condensation at the membrane interface, in which the cold permeate stream can be found (CATH, ADAMS and CHILDRESS, 2004).

As major parameters that affect DCMD performance, feed temperature and flow rate can be cited (CRISCUOLI, CARNEVALI and DRIOLI, 2008). By increasing the temperature gradient between the two phases, the vapor pressure difference is also increased, which enhances the permeate flux. Since temperature and vapor pressure are exponentially related, a change at higher temperatures (feed side) will affect more significantly the permeate flux than those observed for lower temperatures (permeate side). Indirectly though, temperature difference affects the temperature polarization (TP) phenomena, which plays an important role in the process efficiency (BAKER, 2004). An increase in temperature difference will increase mass transfer, which that heat will be transferred at a higher rate. As a result, the real temperature difference between both sides of the membrane will represent a lower fraction of the temperature difference between the bulk of the two phases. Then, due to the higher intensity of temperature polarization, an increase in the temperature difference induced in the system becomes less significant as it is made bigger (MANAWI et al., 2014a).

Regarding flow rate, it can be seen that it has an inverse relationship with the temperature polarization phenomenon. By increasing flow rate, the Reynolds (Re) number is also increased, i.e., the bigger is the turbulence of the system, which diminishes the thermal boundary layer width. Consequently, the temperature polarization effect is diminished, thus increasing the process overall efficiency (CAMACHO et al., 2013). However, the hydrodynamic pressure has a quadratic relationship with the flow rate, and an increase of pressure may reduce the effect of the turbulence increase, in cases which the membrane is compressible (ZHANG, GREY and LI, 2012). In addition, the superficial liquid – membrane



tension (responsible for allowing only the passage of vapor) is ensured mainly during operations performed under the Liquid Entry Pressure (LEP) (LAWSON and LLOYD, 1997). LEP is defined as the minimum transmembrane pressure demanded to overcome the hydrophobic forces and from which the liquid starts to penetrate the membrane pore. When LEP is exceeded, the wetting phenomenon is observed, thus compromising the membrane selectivity (GUILLÉN-BURRIEZA et al., 2016).

Like all other membrane processes, fouling is the major obstacle for membrane distillation, since it adds resistance to water permeation (thus diminishing water flux) and causes progressive membrane wetting (GRYTA 2008; GRYTA et al., 2009). A fouling control strategy commonly used in most membrane-based processes is feed pretreatment, but it is mainly neglected in membrane distillation studies. However, despite the lower tendency of fouling when compared to pressure-oriented processes, MD is also benefited from feed pretreatment, since it prevents the wetting phenomenon by diminishing fouling in the membrane surface (GRYTA et al., 2009). In this context, ultrafiltration, regular filtration and coagulation are effective techniques commonly used for this purpose (PROFIO et al., 2011; WANG et al., 2008). By removing suspended solids from feed, these pretreatment help to decrease fouling and, consequently, operational costs.

Lately, MD has experienced an expressive increase in its use due to the development of new membranes and systems that are more energetically efficient (CAMACHO et al., 2014; JANSEN et al., 2013). Membrane distillation can be employed for several applications, including desalination, wastewater treatment, concentration of non-volatile compounds, separation of volatiles, and water purification (WANG and CHUNG, 2015). For this latter application, the wide ability of MD to successfully remove non-volatile compounds adds considerable importance to the technology in the context of purifying waters whose quality has been seriously damaged by different types of compounds.

Thus, by seeing the potentiality of membrane distillation to purify water even at serious degrees of contamination, this work aimed to assess the influence of operational parameters such as pretreatment, feed temperature and flow rate (cross-flow velocity) on the performance of a flat sheet direct contact membrane distillation bench scale system treating surface water contaminated after the break of an iron ore tailing dam.

## 2.2 MATERIALS AND METHODS

### 2.2.1 Sample collection, characterization, and preparation

The raw water collections were performed quarterly, during one hydrological year, at the intake of the Water Treatment Plant (WTP) in Governador Valadares (geographical coordinate 18°51'50.45 "S and 41°56'46.86" W), after the phase of railing (Figure 2.1). Governador Valadares is located 363km away from the area where the dam broke, and despite being relatively distant, it was also severely impacted after the passage of the contamination plume. In fact, the water turbidity in this region experienced values between 100,000 (during the passage of the plume) and 300 NTU (few months after the event) (IGAM, 2106).

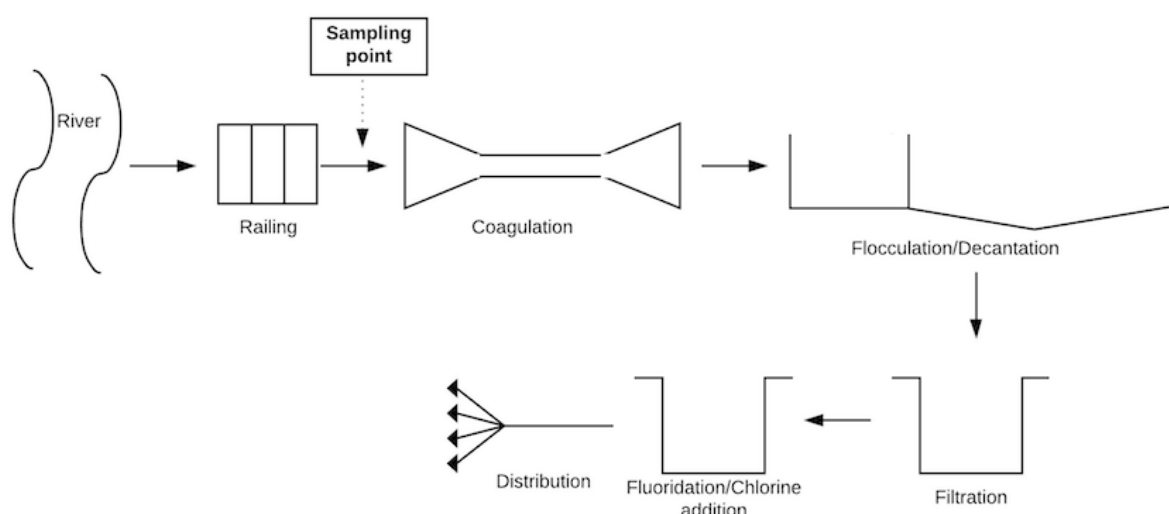


**Figure 2.1** – Schematic of the WTP and sampling point

After collected, the samples were stored at 4 °C and brought to room temperature before their use. Table 2.1 presents the mean and standard deviations values for the main physical-chemical parameters, metals concentration, and its respective maximum concentration permitted by the Administrative Ordinance 2914 from the Brazilian Health Ministry (BRASIL, 2011).

**Table 2.1** – Mean and standard deviation for the main physical-chemical parameters and their respective legal limits according to the Administrative Ordinance 2914

Parameter	Average	Brazilian legal limit	Parameter	Average	Brazilian legal limit
<b>pH</b>	7.09 ± 0.03	~6	<b>Toxicity</b>	not toxic	not toxic
<b>Conductivity (µS/cm)</b>	128.0 ± 28.0	-	<b>NH<sub>4</sub><sup>+</sup> (mg/L)</b>	<1.25	-
<b>Turbidity (NTU)</b>	22.6 ± 19.2	1	<b>Ca (mg/L)</b>	4.3 ± 0.9	500*
<b>Perceived color (mg Pt-Co/L)</b>	131 ± 53	15	<b>Mg (mg/L)</b>	1.6 ± 0.4	
<b>Real color (mg Pt-Co/L)</b>	41.2 ± 39.1	-	<b>Na (mg/L)</b>	2.9 ± 1.0	200
<b>TS (mg/L)</b>	202 ± 45	-	<b>K (mg/kg)</b>	2.5 ± 0.4	-
<b>TSS (mg/L)</b>	10 ± 7	-	<b>Fe (mg/kg)</b>	0.6 ± 0.5	0.3
<b>TOC (mg/L)</b>	1.74 ± 0.82	-	<b>Al (mg/kg)</b>	0.4 ± 0.3	0.2
<b>TN (mg/L)</b>	0.98 ± 0.49	-	<b>As (ppb)</b>	8.0 ± 0	10
<b>Alkalinity (mg CaCO<sub>3</sub>/L)</b>	17.4 ± 10.1		<b>Pb (ppb)</b>	5.0 ± 0	10
<b>Total Coliforms (NMP.100mL<sup>-1b</sup>)</b>	<1	absence in 100 mL	<b>Si (mg/kg)</b>	6.6 ± 1.8	-
<b>E. Coli (NMP.100mL<sup>-1b</sup>)</b>	<1	absence in 100 mL			

\*The Administrative Ordinance 2914 defines the maximum permitted value of 500 mg/L for Hardness (the sum of Mg and Ca concentrations).

In addition, to simulate the conditions after the break of the iron mining tailing dam, synthetic water with different turbidities were prepared. In order to do so, a sludge collected alongside the river Doce (in the same location of the water collection) was used. Table 2.2 brings a semi-quantitative analysis of the sludge used to prepare the solutions.

**Table 2.2** – Semi-quantitative analysis of the sludge used in the synthetic solutions

Composition	SiO <sub>2</sub>	Al <sub>2</sub> O <sub>3</sub>	Fe <sub>2</sub> O <sub>3</sub>	K <sub>2</sub> O	Others
Sludge	57.64%	19.02%	17.43%	1.59%	4.32%

Taking into consideration the turbidities registered by IGAM for the raw water after the passage of the contamination plume, turbidities of 20,000 NTU, 10,000 NTU, and 300 NTU were chosen as representatives for different conditions found on the river water on the days that followed the event. Table 2.3 present the physical-chemical characterization of the synthetic solutions used.

**Table 2.3** – Physicochemical characterization of the synthetic solutions

<b>Solutions</b>	<b>pH</b>	<b>Conductivity (mS/cm)</b>	<b>Turbidity (NTU)</b>	<b>Real color (mg Pt-Co/L)</b>	<b>TS (g/L)</b>	<b>TSS (g/L)</b>	<b>Alkalinity (mgCaCO<sub>3</sub>/L)</b>
1	7.01	0.002	56	110	0.193	0.020	29
2	8.14	0.020	300	187	0.205	0.145	29
3	6.81	119.7	10,000	254	9.8	8.5	52
4	6.61	149.6	20,000	291	21.5	19.3	64

### 2.2.2 Experimental setup

Tests were carried out in a custom built lab-scale direct contact membrane distillation (DCMD) setup (Figure 2.2). The system was equipped with two diaphragm pumps (one for feed and another for distillate flows, Provitec GA5200 MB), two supply tanks, a semi-analytical balance (for distillate weighting, Shimadzu UX6200H), a hot plate with magnetic stirrer (for feed heating, Solab SL-91), a cooling system for permeate and a Teflon module (Sterlitech CFO42D) with a total membrane active area of 0.004209m<sup>2</sup> (STERLITECH CORPORATION, 2017).

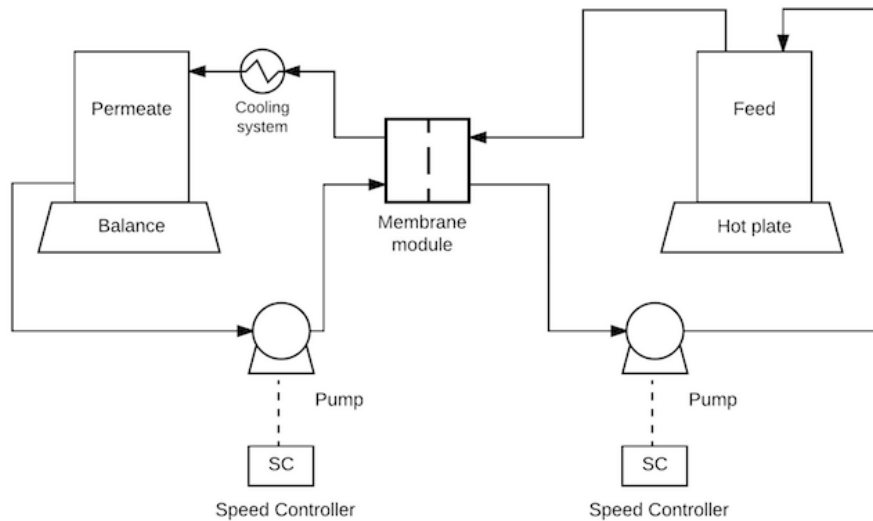


**Figure 2.2** – Schematic of the DCMD bench-scale unit

### 2.2.3 Membrane characteristics

A flat sheet polytetrafluoroethylene (PTFE) in a non-woven polypropylene support membrane supplied by Sterlitech was used in all experiments. Membrane main characteristics are presented in Table 2.4.

**Table 2.4** – Membrane main characteristics

Parameter	Value	Unit	Reference
Membrane material	PTFE	-	Sterlitech Corporation
Average pore size	0.2	$\mu\text{m}$	
Liquid entry pressure	<14.5	Psi	
Membrane porosity	0.7	$\mu\text{m}$	Xu et al. (2016)
Membrane overall thickness	170	$\mu\text{m}$	Manawi et al. (2014b)
PTFE thermal conductivity	0.25	W/m.K	Price and Jarrat (2002)
Air thermal conductivity	0.020 – 0.022	W/m.K	Phattaranawik et al. (2003)
Membrane thermal conductivity	0.0918	W/m.K	Equation 2.11

#### 2.2.4 Experimental procedure

The effects of feed pretreatment, temperature and cross-flow velocity were independently investigated for MD in bench scale. In this regard, 2L of surface water as feed and 1L of distillate water as cooling solution circulated in batch mode until a water recovery fraction between 65% - 85% was attained. Permeate flow was continuously measured by means of a semi-analytical balance and the membrane flux was calculated from this value. Temperature and conductivity were measured at the permeate and feed bulks.

After that, three different feed pretreatments were assessed and compared. In order to do so, samples of the Solution 2 from Table 2.3 (turbidity of 300 NTU) were subjected to filtration (JP 42 filter, average pore size: 2 $\mu$ M), ultrafiltration (average pore size 0.04 $\mu$ m, pressure 0.8bar, water recovery fraction 80%) and coagulation/flocculation (200mg/L aluminum sulfate). The coagulating agent dosage was defined after the construction of a curve of dosage as a function of the final turbidity. After that, the fixed-dose of coagulating agent was added during the fast mixing step (120 rpm during 2 minutes) and then the slow mixture stage (20 rpm) took place for 20 minutes. The supernatant was collected after 2 hours of settling.

Tests with the results from ultrafiltration, filtration and coagulation were conducted under temperature and cross-flow velocity of 60°C and 0.10 m/s, respectively. The pH, conductivity, and permeate flux were monitored over time. In addition, a blank test was carried out with the solution without pretreatment. Fouling was evaluated by means of blocking filtration model, resistance to filtration, wetting time and wetting rate.

To observe the effects of feed temperature and cross-flow velocity on the membrane distillation performance, experiments were performed according to Table 2.5.

**Table 2.5** – Assessment of feed temperature and cross-flow velocity in MD performance

Assessed parameter	Fixed parameter	Conditions evaluated	Unit	Equivalent flow rate (L/h)	Re	Cooling side temperature (°C)
Temperature	Cross-flow Velocity (0.1 m/s)	40	°C	0.55	581	25
		50				
		60				
		70				
Cross-flow Velocity	Temperature (60°C)	0.050	m/s	0.275	290	
		0.100		0.550	581	
		0.183		1.0	810	
		0.273		1.5	1056	

By the end of each of the tests from Table 2.5, the membrane was cleaned with distilled water in an ultrasound batch during 20 minutes.

### 2.2.5 Analytical methods

The river Doce's raw water and permeate were characterized according to the following physical-chemical parameters: pH (Qualxtron QX 1500 pH meter, method 4500B), Conductivity (Hanna HI 9835 Conductivity Meter, method 2510B), Turbidity (Hach 2100AN Turbidimeter, method 2130B), Color (Hach Spectrophotometer DR 2800, method 2120B), Total Solids (TS) (method 2540A), Total Suspended Solids (TSS) (method 2540B), Alkalinity (method 2320), Total Coliforms (method 9221), and E. Coli (method 1603), in compliance with the Standard Methods for the Examination of Water and Wastewater (APHA, 2012). In addition, it was also quantified Total Organic Carbon (TOC) (Shimadzu TOC-V CNP), Ca, Mg, Na, K, Fe, Al, As, Pb (Inductively Coupled Plasma optical emission spectrometry (ICP-OES), and NH<sub>4</sub><sup>+</sup> (Ionic Chromatographer). The sludge was semi-quantitative analyzed by energy dispersive X-ray (EDX).

### 2.2.6 Calculations

In order to calculate permeate mass flux, Equation 2.1 was used.

$$J = \frac{m_2 - m_1}{(t_2 - t_1) \times A_m} \quad \text{Equation 2.1}$$

Where  $J$  is the permeate flux;  $t_1$  and  $t_2$  are the time;  $m_2 - m_1$  is the increase in the permeate mass between times  $t_1$  and  $t_2$ ; and  $A_m$  is the membrane area.

To estimate the expected flux, Equation 2.2 was used (KHAYET, 2011)

$$J_{exp} = C\Delta p \quad \text{Equation 2.2}$$

In the previous equation,  $C$  is named membrane coefficient;  $J_{exp}$  is the mass flux across the membrane; and  $\Delta p$  is the vapour pressure difference between both interfaces. For the different liquid-gas phase equilibria states of water, its vapour pressure relates to temperature as shown in Equation 2.3 (KHAYET, 2011).

$$P = EXP\left(23.238 - \frac{3841}{T-45}\right) \quad \text{Equation 2.3}$$

For the calculation of the resistances, Equations 2.4 to 2.6 were used (SRISURICHAN et al., 2006).

$$R_{fb} = \frac{P_f - P_1}{J} \quad \text{Equation 2.4}$$

$$R_m = \frac{P_1 - P_2}{J} \quad \text{Equation 2.5}$$

$$R_{pb} = \frac{P_2 - P_p}{J} \quad \text{Equation 2.6}$$

In which  $R_{fb}$ ,  $R_m$ , and  $R_{pb}$  stand for feed boundary layer, membrane, and permeate boundary layer resistances. In addition,  $P_1$  and  $P_2$  represent the vapor pressure at feed and permeate membrane surface,  $P_f$ ,  $P_p$  the vapor pressure at the bulk feed and permeate, and  $J$ , the permeate flux. Pressures were calculated according to Equation 2.3 and temperatures at the membrane surface were estimated according to Equations 2.7 and 2.8 (SRISURICHAN et al., 2006).



$$T_{w,f} = \frac{h_m \left( T_p + \left( \frac{h_f}{h_p} \right) T_f \right) + h_f T_f - J \Delta H_v}{h_m + h_f \left( 1 + \frac{h_m}{h_p} \right)} \quad \text{Equation 2.7}$$

$$T_{w,p} = \frac{h_m \left( T_f + \left( \frac{h_p}{h_f} \right) T_p \right) + h_p T_p - J \Delta H_v}{h_m + h_p \left( 1 + \frac{h_m}{h_f} \right)} \quad \text{Equation 2.8}$$

Where  $T_{w,f}$ ,  $T_{w,p}$ ,  $T_f$  and  $T_p$  represent the temperatures at interface and bulk for feed and permeate, respectively;  $h_m$ ,  $h_p$ , and  $h_f$  stand for the convective heat transfer coefficient of the membrane, permeate and feed; and  $\Delta H_v$  is the vaporization heat.

The temperature polarization coefficient (TPC) was estimated by Equation 2.9 (SRISURICHAN et al., 2006).

$$TPC = \frac{T_{w,f} - T_{w,p}}{T_f - T_p} \quad \text{Equation 2.9}$$

To evaluate the temperatures assessed, the amount of heat necessary to generate 1kg of permeate ( $Q_{spec}$ ) was calculated according to Equation 2.10 (CAMACHO et al., 2013).

$$Q_{spec} = \frac{\frac{k_m}{\epsilon} \times (T_{\infty,f} - T_{\infty,p}) + J \times \Delta H_g}{m_d} \quad \text{Equation 2.10}$$

Where  $Q_{spec}$  is the amount of heat required to generate 1kg of permeate;  $k_m$  is the membrane thermal conductivity;  $\epsilon$  is the membrane thickness;  $\Delta H_g$  specific vapor enthalpy deviation at  $T_f$  and  $T_p$ ; and  $m_d$  is the mass of produced permeate.

In addition, membrane thermal conductivity was calculated according to Equation 2.11 (BEJAN, 2004; PHATTARANAWIK, JIRARATANANON & FANE, 2003).

$$k_m = (1 - \phi)k_s + \phi k_f \quad \text{Equation 2.11}$$

Where  $\phi$ ,  $k_s$ , and  $k_f$  stand for the membrane porosity, and the thermal conductivity of each of the individual solid and vapor phases, respectively.

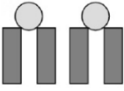
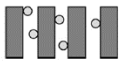
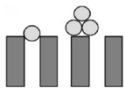
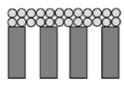
To the cross-flow velocity assessment, the pump power requirement  $E$  for each of the pumps was calculated according to Equation 2.12 (SETHI & WIESNER, 2000).

$$E = \frac{P \times Q}{\eta} \quad \text{Equation 2.12}$$

In which  $E$  is the power requirement;  $P$  is the pressure;  $Q$  is the flow rate; and  $\eta$  is the pumps efficiency, estimated in 70%.

In order to understand how feed turbidity would affect MD performance, the five solutions (Table 2.3) were filtered. As a mean to elucidate the fouling phenomenon, the Hermia model was used (YUAN, KOCIC and ZYDNEY, 2002; HERMIA, 1982; JACOB et al., 1998; BLANPAIN and LALANDE, 1997). By adding the cake erosion model, Hermia's law can be adapted to cross-flow filtration mode, according to Table 2.6 (SRISURICHAN, JIRARATANANON and FANE, 2006). In addition, the resistance to filtration, wetting time (the time it took for the conductivity to start rising) and wetting rate (the observed rise in conductivity over time) were also calculated.

**Table 2.6 – Blocking filtration laws**

Law	Schematics	Linearized equation	N
Complete blocking model		$-\ln\left(\frac{J_o}{J}\right) - 1 = Kt$	3
Standard blocking model		$\frac{J_o}{J} - 1 = Kt$	3/2
Intermediate blocking model		$\sqrt{\frac{J_o}{J}} - 1 = Kt$	1
Cake blocking model		$\left(\frac{J_o}{J}\right)^2 - 1 = Kt$	0

## 2.3 RESULTS AND DISCUSSION

### 2.3.1 MD performance

Considering the scenario of the application of MD for producing drinking water during emergency situations, it is important to evaluate the robustness of the process, since it will be used to treat water with adverse qualities. Regardless of the quality of the water to be treated, it is desirable that the process exhibits high rejection efficiencies and low fouling potential. In the specific case study, the water turbidity of the river Doce ranged from 100,000 to 1,000 NTU during the first month after the break of Fundão mining tailings dam, and remained between 50 – 500 NTU in the months that followed the event (IGAM, 2016).

To see the effect of feed turbidity in the MD performance, the technology was evaluated for the treatment of water with turbidity values between 56 and 20,000 NTU. Table 2.7 presents the results for flux decay and blocking filtration model adjustment (Hermia's model adapted to cross-flow filtration) and Table 2.8 depicts the resistances, wetting rate and wetting time for the solutions tested.

By analyzing Table 2.7, it was noticed a subtle flux decline for the turbidity of 56 NTU (6%), whereas from 300 NTU on, the flux decline did not vary much, and remained around 22%. This decline can be attributed in all cases to the formation of a fouling layer that added extra resistance to filtration ( $R_{\text{fouling}}$  in Table 2.8). The differences found for the  $R_{\text{fouling}}$  values can be explained both by the feed turbidity and the models adjustments for the fouling characterization. At 56NTU,  $R_{\text{fouling}}$  value was the lowest (58 Pa/kg.m<sup>2</sup>.h) and caused mainly by complete and standard blocking pore. For the other turbidities, however, the best adjustments and K values were related to cake formation, which increased along with turbidity from 300 to 10,000 NTU, but remained constant after this value. This constancy may be attributed to the fact that even doubling the turbidity of the solution, most of the suspended solids deposited very rapidly in the feed tank despite its constant agitation, and thus did not reach the MD system. As a consequence, the actual amount of suspended solids did not vary much, thus addressing little changes in the  $R_{\text{fouling}}$  values from 10,000 to 20,000 NTU.

Nevertheless, when comparing  $R_{\text{fouling}}$  and  $R_{\text{fb}}$ , it can be seen that  $R_{\text{fb}}$  is still the major resistance to filtration in all cases. This can be attributed to the fouling layer's composition, since silica – which is expected to be the main solute considering the sludge composition presented in Table 2.2 – is used to have little influence on flux decline for DCMD (QIN et al., 2018), thus attributing only 22% of flux decay during the filtration. Yet, despite its lack of influence on flux decline, the formation of the fouling layer contributed to the wetting phenomenon, as it can be seen by the values for wetting rate and wetting time, that became notable in the experiments with feed at higher turbidities.

**Table 2.7** –  $J/J_0$  and blocking filtration type for the synthetic solutions with different turbidities  
(Water recovery fraction, 40%; Feed temperature: 60°C)

Feed Turbidity (NTU)	Flux decay			Blocking filtration type ( $\text{min}^{-1}$ )			
	$J_0$ ( $\text{kg/m}^2\cdot\text{h}$ )	$J$ ( $\text{kg/m}^2\cdot\text{h}$ )	$J/J_0$	$K_{\text{complete}}$ Value ( $R^2$ )	$K_{\text{intermediate}}$ Value ( $R^2$ )	$K_{\text{standard}}$ Value ( $R^2$ )	$K_{\text{cake}}$ Value ( $R^2$ )
56	17.1	16.1	94.2%	<b>0.03 (0.87)</b>	0.04 (0.86)	<b>0.02 (0.87)</b>	0.08 (0.84)
300	17.2	13.5	78.5%	0.02 (0.85)	0.02 (0.86)	0.008 (0.85)	<b>0.04 (0.87)</b>
10,000	13.4	10.3	77.3%	0.03 (0.88)	0.04 (0.89)	0.02 (0.89)	<b>0.09 (0.90)</b>
20,000	13.4	10.9	81.5%	0.01 (0.94)	0.01 (0.85)	<b>0.01 (0.95)</b>	<b>0.02 (0.95)</b>

**Table 2.8** – Resistances, wetting rate and wetting time for the synthetic solutions with different turbidities  
(Water recovery fraction, 40%, Feed temperature: 60°C)

Feed Turbidity (NTU)	Resistance* (Pa/Kg.m <sup>2</sup> .h)					Wetting rate (μS.cm <sup>-1</sup> /min)	Wetting time (min)
	R <sub>fb</sub>	R <sub>pb</sub>	R <sub>m</sub>	R <sub>fouling</sub>	R <sub>tot</sub>		
56	562	292	130	58	1042	-	-
300	587	295	126	215	1223	0.08	104
10,000	600	245	386	327	1558	0.09	123
20,000	545	250	390	328	1513	0.06	125

\*  $R_{fb}$  = Feed boundary resistance,  $R_{pb}$  = Permeate boundary resistance,  $R_m$  = Membrane resistance,  $R_{fouling}$  = Fouling resistance, and  $R_{tot}$  = Total resistance

In addition to fouling characterization and flux decline, Table 2.9 presents the permeate characterization for the tests performed. A high removal for all the assessed parameters was attained, despite the differences in the wetting time and rate. This can be attributed to the dilution effect, since the permeate is aggregated to the initial distilled water in the DCMD configuration. In all cases, the legal parameters from the Administrative Ordinance 2914 from the Brazilian Health Minister (BRASIL, 2011) were attended .

**Table 2.9** – Permeates characterization for a recovery fractions of 82% (56NTU), 56%(300NTU), 45% (10,000NTU) and 46% (20,000NTU)

<b>Feed Turbidity (NTU)</b>	<b>pH</b>	<b>Conductivity (<math>\mu\text{S/cm}</math>)</b>	<b>Turbidity (NTU)</b>	<b>Perceived color (mg Pt-Co/L)</b>
56	6.09	5.63	0.156	0
	-	96.5%	99,0%	100%
300	5.9	13.6	0.107	0
	-	99.9%	99.9%	100%
10,000	5.4	26.9	0.605	6
	-	99.9%	99.9%	97.6%
20,000	6.5	24.6	0.604	3
	-	99.9%	99.9%	99.0%

As it can be noticed, the presence of solids into the feed did not affect severely the MD performance. However, at higher turbidities, a pretreatment should be carried out in order to avoid a premature membrane damage and to improve the permeate flux and quality.

### 2.3.2 Pretreatment

In order to define a suitable pretreatment, filtration, ultrafiltration and coagulation were compared. However, prior to this, a proper amount of aluminum sulfate for the coagulation experiment was defined. In order to do so, a curve of dosage as a function of the residual turbidity was built for the pH's of 8.14 (GUEDES et al. 2004), presented in Figure 2.4.

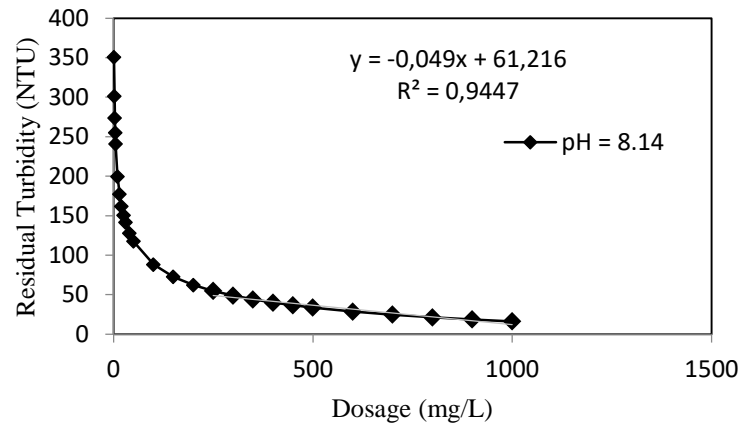


**Figure 2.3** – Curve of dosage as a function of the residual turbidity for the pH's 8.14

It can be seen from Figure 2.3. that as of 200mg/L, any significant decay of the final turbidity was observed, which can be observed from the linear adjustment made for the final portion of the curve. From this experimental fact, the coagulant dosage was set as 200mg/L of aluminum sulfate.

In addition to coagulation, both filtration and ultrafiltration were tested as pretreatment options. Table 2.10 presents the main physical-chemical characterization of the solutions before and after the pretreatment.

**Table 2.10** – Physicochemical characterization of the solution before and after their respective pretreatment

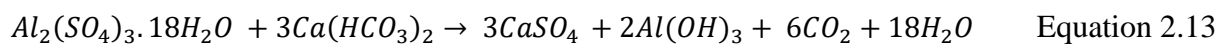
<b>Pretreatment</b>	<b>pH</b>	<b>Conductivity (<math>\mu</math>S/cm)</b>	<b>Turbidity (NTU)</b>	<b>TSS (g/L)</b>	<b>TS (g/L)</b>
No	8.6	205	300	0.145	0.205
Coagulation	4.3	542	75.6	0.002	0.076
Removal	-	99.1%	74.8%	98.6%	62.9%
Filtration	8.5	200	15.4	0*	0*
Removal	-	2.4%	5.1%	100%	100%
Ultrafiltration	8.5	192	0.11	0*	0*
Removal	-	6.3%	99.9%	100%	100%

*\*Not detectable by APHA Methods 2540A and 2540B*

In Table 2.10, a drastic reduction of all the monitored parameters was observed after all pretreatments, except for conductivity. Moreover, the prominent decrease in the pH of the



product from the coagulation can be explained by the chemistry of the aluminum sulfate (since an alkalizing agent was not added in order to diminish costs and avoid future membrane scaling). By adding ALUM to the solution, it reacts with the alkalinity present in the water (normally in the  $\text{HCO}_3^-$  form). This reaction produces carbon dioxide, that reacts with water, producing carbonic acid, that normally dissociate, hereby producing bicarbonate, carbonate and  $\text{H}^+$ . Once  $\text{H}^+$  is generated, the pH is expected to drop, but not very intensively, since carbonic is a weak acid. The general mechanisms of ALUM in the water are described in Equations 2.13 to 2.15 (WANG et al., 2008).



After their respective pretreatment, all solutions were separately fed into the MD system. Results for flux decay and blocking filtration model adjustment (Hermia's model adapted to cross-flow filtration) are presented in Table 2.11, and Table 2.12 depicts the resistances, wetting rate and wetting time for each of the assays.

By comparing the  $J/J_0$  ratio, it can be noticed that all pretreatments were effective in reducing the flux decay, being ultrafiltration the most effective one, with a flux decrease of 6% after 5h of filtration. This reduction can be attributed to the effectiveness in reducing the amount of suspended solids from the raw solution, which contributed to avoid the formation of the fouling layer, as presented by the  $R_{\text{fouling}}$  in Table 2.12. Moreover, Table 2.12 also shows that the wetting tendency observed for the raw solution was prevented both by filtration and ultrafiltration. In this case, the action of the coagulation was not able to avoid wetting, and this can be explained by the mechanisms involved in the process; despite reducing the initial turbidity, the ALUM forms positive charged species in the water. Since the PTFE membrane has a negative zeta potential (LIU, CHEN and ZHU, 2018; AN et al., 2016), once in contact with these solutions, the interaction between membrane and positive particles is favored, which can contribute to membrane wetting. In addition, the increase in the conductivity

observed for the supernatant indicates a bigger ions concentration in the feed for this case, which can also contribute for fouling.

**Table 2.11** – Normalized flux ( $J/J_0$ ) and blocking filtration type for the solutions with and without the pretreatment stage. Coagulation (ALUM 200 mg/L); Filtration (JP 42 filter, average pore size:  $2\mu\text{M}$ ); Ultrafiltration (average pore size  $0.04\mu\text{m}$ , pressure 0.8bar, water recovery fraction 80%)  
(Temperature:  $60^\circ\text{C}$ , Flow rate: 33 L/h)

Pretreatment	Flux decay			Blocking filtration type ( $10^3 \cdot \text{min}^{-1}$ )			
	Jo ( $\text{kg}/\text{m}^2 \cdot \text{h}$ )	J ( $\text{kg}/\text{m}^2 \cdot \text{h}$ )	J/Jo	$K_{\text{complete}}$ Value ( $R^2$ )	$K_{\text{intermediate}}$ Value ( $R^2$ )	$K_{\text{standard}}$ Value ( $R^2$ )	$K_{\text{cake}}$ Value ( $R^2$ )
No	17.2	13.5	78.2%	1.50 (0.85)	1.82 (0.86)	0.83 (0.85)	<b>4.45 (0.87)</b>
Coagulation	13.2	8.5	64.4%	<b>1.19 (0.91)</b>	2.11 (0.88)	<b>0.78 (0.91)</b>	8.5 (0.78)
Filtration	16.8	13.3	79.4%	1.02 (0.95)	<b>1.23 (0.95)</b>	0.57 (0.95)	<b>3.19 (0.94)</b>
Ultrafiltration	18.6	17.6	94.8%	<b>0.73 (0.88)</b>	<b>0.77 (0.87)</b>	0.37 (0.87)	1.62 (0.85)

**Table 2.12** – Resistances, wetting rate and wetting time for the synthetic solutions for the solutions with and without the pretreatment stage. Coagulation (ALUM 200 mg/L); Filtration (JP 42 filter, average pore size: 2 $\mu$ M); Ultrafiltration (average pore size 0.04 $\mu$ m, pressure 0.8bar, water recovery fraction 80%). - Temperature: 60°C, Cross-flow velocity: 0.1 m/s

Pretreatment	Resistance (Pa/Kg.m <sup>2</sup> .h)					Wetting rate ( $\mu$ S.cm <sup>-1</sup> /min)	Wetting time (min)
	R <sub>fb</sub>	R <sub>pb</sub>	R <sub>m</sub>	R <sub>fouling</sub>	R <sub>tot</sub>		
No	587	295	126	219	1227	0.083	104
Filtration	567	237	173	254	1232	-	-
Coagulation	597	250	384	527	1758	0.010	100
Ultrafiltration	504	301	137	0	855	-	-

Aside from flux decay, Table 2.13 presents the quality of the permeate obtained for each of the cases. It can be inferred that a high removal was attained in all cases. The lowest removal of conductivity for the supernatant from the coagulation can be attributed to the wetting observed after 100 minutes of filtration.

**Table 2.13** – MD Permeate quality for each of the cases

<b>Pretreatment</b>	<b>pH</b>	<b>Conductivity</b>	<b>Turbidity</b>
	<b>-</b>	<b>(<math>\mu\text{S/cm}</math>)</b>	<b>(NTU)</b>
No	5.9	13.6	0.107
Removal	-	93.7%	99.9%
Coagulation	5.9	23.6	0.143
Removal	-	88.5%	99.9%
Filtration	6.4	14	0.005
Removal	-	93.2%	99.9%
Ultrafiltration	5.9	12.72	0.001
Removal	-	93.8%	100%

In sight of the results obtained both for flux decay and permeate quality, it can be concluded that despite being much less sensitive to feed quality than pressure-oriented processes, membrane distillation is still benefited from feed pretreatment, specially as a mean to prevent membrane wetting. Moreover, among the pretreatments tested, ultrafiltration presented the most interesting results both for flux decline and wetting time, being thus the most technically recommended in this case.

### 2.3.3 Feed temperature

Figure 2.4 presents the experimental and expected flux decay and the conductivity for the tests with temperatures of 40°C, 50°C, 60°C and 70°C. As expected, an increase in temperature increased the mean permeate flux non-linearly (YUNA et al., 2006) (Figure 2.4). However, a deviation from the predicted flux was observed. This can be attributed to the temperature polarization phenomenon, that yielded coefficients (TPC) of 0.51, 0.36, 0.34, and 0.24 for the temperatures of 40°C, 50°C, 60°C, and 70°C, respectively. This shows that the TP increased by increasing the temperature (LAWAL and KHALIFA 2014).

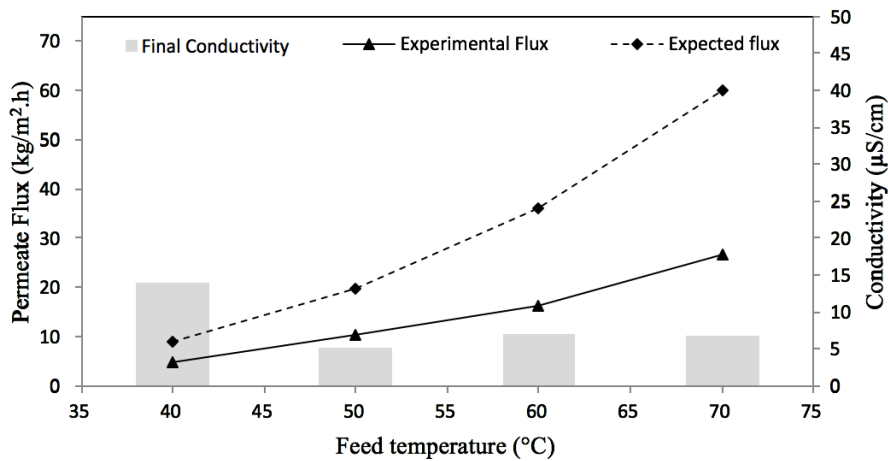


**Figure 2.4** – Experimental and predicted mean flux, and final permeate conductivity for the evaluated temperatures, Water recovery fraction of 65%

In addition, the conductivity value was maintained below 7.1  $\mu\text{S}/\text{cm}$  for temperatures above 50°C. This indicates that in none of these cases the wetting phenomenon was observed. On the other hand, at 40°C, a wetting time of 50h and wetting rate of 0.004  $\mu\text{S}/\text{cm}\cdot\text{min}$  ( $R^2 = 0.90$ ) were found, which justifies the bigger permeate final conductivity reported in this case. This can be explained by the time difference between tests. Since the water flux is lower at lower temperatures, the time it took to attain a similar water recovery fraction was greater at 40°C. As a consequence, the system experienced more intermittencies over night, which is reported by few authors as a factor responsible for enhancing membrane wetting (GUILLENBURRIEZA et al., 2013; SAFFARINI et al., 2012). Once the system is switched off, the decrease in the temperature can lead to the condensation of the water vapor inside the membrane pores. These ‘water bridges’ that are formed during this period allow the passage of solutes to the permeate side, thus increasing the permeate conductivity (GUILLENBURRIEZA et al., 2016). Indeed, if taken into consideration the time it took by other tests to attain 65% of recovery (between 660-1740 min), the permeate conductivity in the test of 40°C was around  $6.5 \pm 1.9 \mu\text{S}$  in this case, which is consistent to a non-wetted situation.

Figure 2.5 presents the the specific heat ( $Q_{spec}$ ) required in the MD operation at the evaluated temperatures.

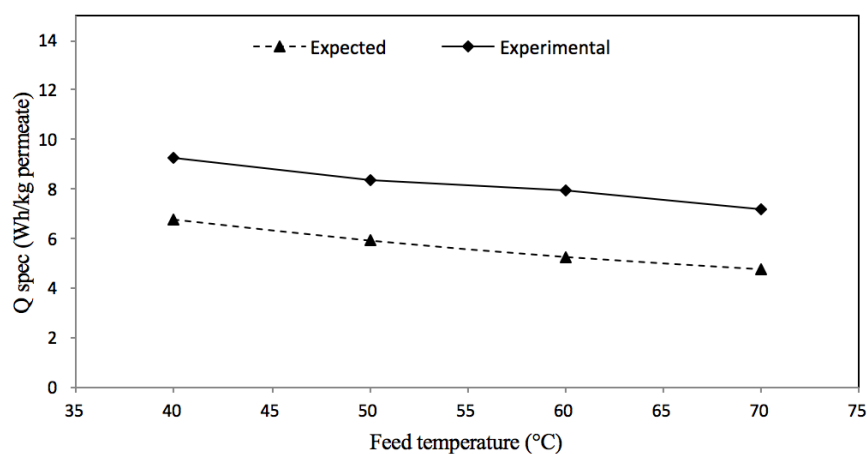


**Figure 2.5** – Experimental and predicted  $Q_{\text{spec}}$  for the evaluated temperatures

Since the amount of specific heat is inversely proportional to the permeate flux, the experimental heat was found bigger than the theoretical for all temperatures assessed, which can also be justified by the temperature polarization effect. That means that the extra amount of heat provided to keep feed at their bulk temperature (that is entire considered during the theoretical calculation) is not fully transferred to the membrane surface and increase the temperature gradient as it was supposed to do; in this case, what actually happen is an increase in the thermal boundary layer thickness, as it can be seen from Table 2.14. However, it is important to highlight that even presenting a lower TP ratio (i.e., a bigger temperature polarization),  $Q_{\text{spec}}$  presented its lowest value at 70°C.

**Table 2.14** – Resistances in the membrane distillation system for each of the temperatures assessed

Resistance (Pa/kg.m <sup>2</sup> .h)	40°C	50°C	60°C	70°C
$R_{fb}$	296	405	475	838
$R_{pb}$	215	246	278	321
$R_m$	391	260	141	38

Table 2.14 depicts a prominent increase in the resistance of the boundary layer from the feed side due to an increase in TP. In addition, a tendency of decrease of  $R_m$  by the increase of temperature was also observed. This may be attributed to the inverse relationship between  $R_m$  and the membrane mass transfer coefficient ( $K_m$ );  $K_m$  is proportional to the diffusivity ( $PD_{wa}$ )

and consequently to temperature, since  $PD_{wa} = 4.46 \times 10^{-6} T^{2.334}$  (SRISURICHAN et al., 2006).

When assessing the temperature effect on MD performance, permeate quality should also be taken into consideration. Tables 2.15 and 2.16 present the physicochemical characterization of the permeates.



**Table 2.15** – Physical-Chemical characterization of the generated permeates for each of the assessed temperatures under the following conditions:

Flow rate: 33 L/h, Water recovery fractions: 65% (40°C), 72% (50°C), 75% (60°C), and 76% (70°C)

<b>Permeate</b>	<b>pH</b>	<b>Conductivity (<math>\mu\text{S/cm}</math>)</b>	<b>Turbidity(NTU)</b>	<b>Apparent color (mg Pt-Co/L)</b>	<b>Real color (mg Pt-Co/L)</b>	<b>TOC (mg/L)</b>	<b>Alkalinity (mg <math>\text{CaCO}_3/\text{L}</math>)</b>
Raw water	7.05	161	56.5	196	110	2.53	29.0
40°C	6.08	17.0	0.108	9	0	1.48	0
% Removal	-	89.5%	99.8%	95.4%	100%	41.9%	100%
50°C	6.05	7.48	0.115	9	< 3	1.10	< 1
% Removal	-	95.4%	99.8%	95.4%	100%	56.5%	100%
60°C	6.09	7.60	0.156	9	< 3	1.01	< 1
% Removal	-	95.3%	99.0%	95.4%	100%	60.1%	100%
70°C	6.68	8.64	0.25	9	< 3	0.80	< 1
% Removal	-	94.6%	99.6%	95.4%	100%	68.4%	100%

**Table 2.16** – Metals and ions characterization of the generated permeates

<b>Permeate</b>	<b>NH<sub>4</sub><sup>+</sup> (mg/L)</b>	<b>Ca (mg/L)</b>	<b>Mg (mg/L)</b>	<b>Na (mg/L)</b>	<b>Fe* (mg/kg)</b>	<b>Al* (mg/kg)</b>	<b>As* (ppb)</b>	<b>Pb* (ppb)</b>
Raw water	< 1.25	3.7	1.17	2.43	1.40	0.60	8	5
40°C	< 1.25	0.11	< 0.001	0.37	< 0.001	< 0.001	< 2	< 1
% Removal	-	97.1%	99.9%	84.7%	99.9%	99.8%	75.0%	80.0%
50°C	< 1.25	0,03	< 0.001	0.35	< 0.001	< 0.001	< 2	< 1
% Removal	-	99.3%	99.9%	85.4%	99.9%	99.8%	75.0%	80.0%
60°C	< 1.25	<0.01	< 0.001	0.34	< 0.001	< 0.001	< 2	< 1
% Removal	-	99.7%	99.9%	85.8%	99.9%	99.8%	75.0%	80.0%
70°C	< 1.25	0.26	< 0.001	0.66	< 0.001	< 0.001	< 2	< 1
% Removal	-	92.9%	99.9%	72.8%	99.9%	99.8%	75.0%	80.0%

*\*Minimal removal presented, since MD reduced the metals concentration below the detection limits for the permeates.*

The removal of almost every assessed solute was above 85% . The exception lies on TOC, in which the deviation can be attributed to passage of volatile solutes across the membrane. In addition, the final conductivity of the permeate generated at 40°C is the higher among them, which is attributed to the wetting phenomenon that occurred after 50h of filtration.

### 2.3.4 Cross-flow velocity

Figures 2.6 and Table 2.17 present the average permeate flux, pump requirement, and permeate conductivity and the resistances for each of the assessed velocities, respectively.

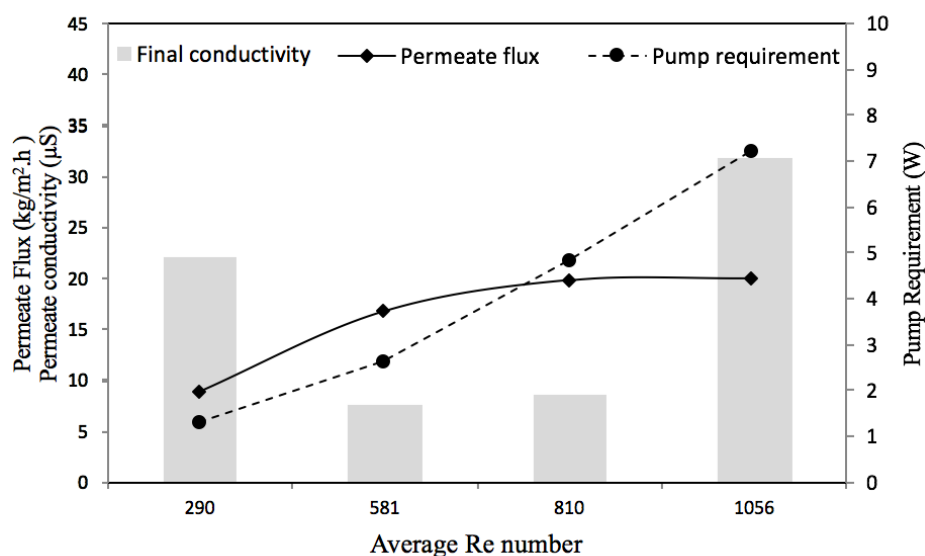


**Figure 2.6** – Permeate flux, pump requirement and final conductivity for each of the assessed cross-flow velocities. Temperature: 60°C, Water recovery fractions: 27% (0.05 m/s), 52% (0.10m/s), 61% (0.18m/s), and 60% (0.27m/s), time of filtration: 15h

**Table 2.17** – Boundary layer resistances in the membrane distillation system for each of the cross-flow velocities assessed

Resistance (Pa/kg.m <sup>2</sup> .h)	290	581	810	1056
R <sub>fb</sub>	688	575	527	462
R <sub>pb</sub>	212	278	317	347

It can be observed from Figure 2.6 that the permeate flux increased by the increase of the cross-flow velocity. This can be explained by the fact that by increasing  $Re$ , the promoted turbulence diminishes the thickness of the thermal boundary layer, as presented in Table 2.17. This approximates the bulk and membrane surface temperature, thus diminishing energy waste and, consequently, increasing permeate flux and process efficiency. In addition, as predicted by Khayet and Matsuura (2011), an asymptotic behavior for permeate flux at higher velocities was observed. In the current case, it initiated at the cross-flow velocity of 0.183 m/s ( $Re = 810$ ). This means that after this threshold value, any increase in the cross-flow velocity did not affect the system in a significant way; it just increased its energetic requirement, since the pump requirement is directly proportional to the cross-flow velocity of the process.

Besides the permeate flux behavior, the permeate quality was assessed in each of the cases, since the cross-flow velocity may contribute to elevate the hydrodynamic pressure of the system that, once exceeds the Liquid Entry Pressure of the membrane, may wet it and harm the permeate quality. Table 2.18 and 2.19 present the result for the characterization of the permeates from all tests.

**Table 2.18** – Physical-Chemical characterization of the generated permeates under the following conditions: Temperature: 60°C, Water recovery fractions: 60% (0.05 m/s), 52% (0.10m/s), 61% (0.18m/s), and 60% (0.27m/s)

<b>Permeate</b>	<b>pH</b>	<b>Conductivity (<math>\mu\text{S/cm}</math>)</b>	<b>Turbidity (NTU)</b>	<b>Perceived color (mg Pt-Co/L)</b>	<b>Real color (mg Pt-Co/L)</b>	<b>TOC (mg/L)</b>	<b>Alkalinity (mg <math>\text{CaCO}_3/\text{L}</math>)</b>
Raw water	7.05	161	56.5	196	110	2.53	29
0.05 m/s	6.4	22.2	0.372	21	0	1.01	0
% Removal	-	89.7%	99.3%	89.3%	100%	60.1%	100%
0.10 m/s	6.05	7.6	0.248	3	< 3	1.47	<1
% Removal	-	93.1%	99.6%	98.5%	100%	41.9%	100%
0.18 m/s	6.21	8.6	0.194	3	< 3	1.25	<1
% Removal	-	89.3%	99.7%	98.5%	100%	50.6%	100%
0.27 m/s	6.31	31.8	0.176	3	< 3	0.92	<1
% Removal	-	89.6%	99.7%	98.5%	100%	63.6%	100%

**Table 2.19** – Metals and ions characterization of the generated permeates

<b>Permeate</b>	<b>NH<sub>4</sub><sup>+</sup> (mg/L)</b>	<b>Ca (mg/L)</b>	<b>Mg (mg/L)</b>	<b>Na (mg/L)</b>	<b>Fe* (mg/kg)</b>	<b>Al* (mg/kg)</b>	<b>As* (ppb)</b>	<b>Pb* (ppb)</b>
Raw water	< 1.25	3.7	1.17	2.43	1.40	0.60	8	5
0.05 m/s	< 1.25	< 0.01	0.17	0.54	< 0.001	< 0.003	< 4	< 1
% Removal	-	99.7%	85.5%	77.8%	99.9%	99.5%	50.0%	80.0%
0.10 m/s	< 1.25	< 0.01	< 0.001	0.34	< 0.001	< 0.003	< 4	< 1
% Removal	-	99.7%	99.9%	86.0%	99.9%	99.5%	50.0%	80.0%
0.18 m/s	< 1.25	< 0.01	0.15	0.48	< 0.001	< 0.003	< 4	< 1
% Removal	-	99.7%	87.2%	80.2%	99.9%	99.5%	50.0%	80.0%
0.27 m/s	< 1.25	< 0.01	< 0.002	0.41	< 0.001	< 0.003	< 4	< 1
% Removal	-	99.7%	99.8%	83.1%	99.9%	99.5%	50.0%	80.0%

\* Minimal removal presented, since MD reduced the metals concentration below the detection limits for the permeates.

As it can be seen from Tables 2.18 and 2.19, a high removal of the main solutes was attained at all velocities assessed. Conversely, during the cross-flow velocities of 0.05 and 0.27m/s, membrane wetting was observed, and can be explained for different reasons. At the cross-flow velocity of 0.05m/s, for example, the wetting time of 25.3h and wetting rate of 0.01 ( $R^2 = 0.94$ ) are attributed to the effects of dry-out that happens due to intermittent operation (GUILLEN-BURRIEZA et al., 2013). On the other hand, at 0.27m/s, the wetting time was 2.3 h and the wetting rate, 0.05  $\mu\text{S}/\text{cm}\cdot\text{min}$  ( $R^2 = 0.95$ ). This short wetting time indicates that wetting took place from the beginning of operation, which indicates that the hydrodynamic pressure applied to the membrane was the preponderant factor to cause membrane wetting. In this case, the liquid pressure overcame the membrane LEP, thus compromising its hydrophobicity. Yet, the dilution effect present in DCMD still contributed to yield high removal efficiencies. TOC deviations happened for the same reason explained in section 2.3.2.

## **2.4 CONCLUSION**

An experimental study was conducted to investigate the influence of parameters such as pretreatment, feed temperature and cross-flow velocity on the performance of the MD process for the purification of surface water during emergency situations (such as after the collapse of dams). When treating solutions with different turbidities, it was noticed that a feed turbidity until 300 NTU did not affect the membrane performance very severely, since no wetting time or wetting rate were observed. However, at higher turbidities, a pretreatment should be carried out in order to avoid a premature membrane damage. In this context, the ultrafiltration presented the best technical, results both for preventing flux decay and wetting time.

Regarding the effect of feed temperature, it was observed a deviation between the expected and the experimental flux, which can be attributed to the temperature polarization phenomenon. In addition, this effect was made greater for higher temperatures, due to the increase in the thermal boundary layer resistances. Conversely, the minimum amount of heat demanded for generating 1kg of permeate was found for the temperature of 70°C, being thus the recommended temperature in these case, since all permeates had similar characteristics.

Finally, for the cross-flow velocity assessment, it was noticed that an increase in the Re number increased the permeate flux, fact that could be attributed to a depletion in the thermal boundary resistance observed at higher cross-flow velocities. However, this decrease is less prominent after the threshold value of 0.18 m/s, from which the energy added to increase cross-flow velocity did not contribute to a better efficiency of the process and may also compromise the permeate quality, since membrane wetting was observed very early at 0.27m/s.



## **CHAPTER 3**

---

# **MEMBRANE DISTILLATION APPLIED TO THE TREATMENT OF SURFACE WATER CONTAMINATED AFTER THE BREAK OF FUNDÃO'S MINING TAILINGS DAM: A STUDY OF MEMBRANE FOULING, CHEMICAL CLEANING, AND AGEING**

### **3.1 INTRODUCTION**

Tailing dams are a commonly used strategy in the mining sector to dispose waste. Despite its relatively low cost, if not properly maintained, they are subjected to collapse, as it happened in Brazil in 2015. The break of Fundão's dam disposed 40m cubic meter of tailings composed mainly of silica, alumina and hematite in an important river of the country. The wave not only killed most of the live from that habitat but also impaired the water supply alongside the river for several days, since the turbidity experienced after this event was too high to be treated via coagulation (the standard treatment in the region). This caused a severe water stress that elucidated the need for the development of alternative routes.

As an option to address this issue, membrane distillation (MD) can be employed due to its robustness and ability to work with alternative sources of energy at low pressure, thus diminishing its operational costs (PHATTARANAWIK et al., 2008). Membrane distillation is a thermally driven separation process in which a hydrophobic membrane allows the passage of water vapor from the hot (feed) to the cold (permeate) side (CURCIO and DRIOLI, 2005). As observed in Chapter 2, MD presents a lower propensity for fouling, specially if compared to pressure-oriented processes such as reverse osmosis (RO) and nanofiltration (NF). Nevertheless, this is still the major drawback from MD, since it has a negative influence to the selectivity of the membrane (GRYTA, 2008).

Fouling is generally defined as the accumulation of unwanted materials at the surface or inside the pores of the membrane, therefore impairing its permeation flux and selectivity (GRYTA, 2007). According to Tijing et al. (2015), four main factors are preponderant to fouling formation: (a) foulant characteristics; (b) membrane properties; (c) operational conditions; and (d) feed water characteristics. The formation of inorganic salt scaling, particulate fouling, biological fouling, or chemical membrane degradation (CURCIO et al., 2010; GRYTA, 2007; GRYTA, 2012) inside the membrane pores or on its surface (KNYAZKOVA and MAYNAROVICH, 1999) is intrinsically related to the interaction between those four factors, and will consequently dictate what mitigation action should be taken in order to avoid it (GRYTA and TOMASZEWSKA, 2001).

In membrane distillation, fouling deposition decreases the membrane hydrophobicity, causing the membrane wetting. In this case, liquid starts to penetrate the membrane pores, reducing its selectivity and impairing its goals of separation (WARSINGER et al., 2015). This phenomenon has been reported for several types of foulant agents (GUILLEN-BURRIEZA et al., 2014; GE et al., 2014; WANG and LIN, 2017), including silica and iron oxide (DARTON et al., 2004; GRYTA, 2007). Besides, the existence of a fouling layer adds both thermal and hydraulic resistance to the system, thus increasing the temperature polarization effect (CURCIO et al., 2010; SRISURICHAN, JIRARATANANON and FANE, 2005; HSU, CHENG and CHIOU, 2002).

As strategies employed to control fouling or restore wetted membranes, feed pretreatment, cleaning procedures with distilled water or cleaning agents followed by air drying, blowing with inert gas, and changing the liquid entrapped inside the pores with another lower surface tension liquid (such as alcohols) followed by air drying can be highlighted (SCHÄFER, FANE and WAITE, 2005; SANMARTINO, KHAYET and GARCÍA-PAYO, 2017). Nevertheless, despite the benefits from feed pretreatment, periodical cleaning is often the only way to restore the membrane initial permeate flux (KLÜPFEL and FRIMMEL, 2010). Cleaning is a process that can involve both chemical and physical interactions. The chemical reaction between the agent and the fouling layer lessens the structural integrity of the latter, thus facilitating its mechanical removal (AGUIAR et al., 2018). In contrast, the mass transport of solutes between bulk and membrane surface is mainly governed by physical interactions (SOHRABI et al., 2011). According to Andrade et al. (2017), the ideal cleaning agent should be able to remove the fouling layer without compromising the membrane structure. Thus, the choice of the chemical agent is directed mainly by the type of fouling and the membrane materials, in which they normally have either acid, basic or chelating characteristics.

According to Peng et al. (2015), an effective control of fouling and improvement of cleaning are the main responsible factors for slowing down membrane ageing in MD. Membrane ageing can be defined as the changes that happen to the membrane's properties over time and it is also directly dependent on the effluent characteristics, operation conditions, fouling rate and cleaning cycles. Despite being a comparative

analysis, it is indispensable to a better function of membrane systems, since it can result in a decreased process productivity, alteration of the membrane properties and retention efficiency, and increase in the cleaning frequency (REGULA et al., 2014).

Seeing the importance of fouling and cleaning assessment to the good and long-term performance of MD systems, this work aimed to investigate MD fouling during the treatment of a water contaminated mostly with silica, alumina and hematite originated from an iron mining tailing dam, and also the suitability of different chemical substances as cleaning agents in this case. Moreover, it was also intended to evaluate the effects of a long-term exposure of a PTFE membrane to this solution and periodic cleaning.

## **3.2 MATERIALS AND METHODS**

### **3.2.1 Effluent characterization**

Tests were conducted with a synthetic water prepared from the sludge of the river Doce collected in Governador Valadares six months after the break of Fundão's dam. Despite being collected 363 km away from the point of rupture of the iron tailing dam, the sludge's composition is in accordance to the what literature reports to the area of the accident. According to Andrade (2014), the geology found in the region of Mariana (MG) is rich in filitos made from aluminosilicate (ANDRADE, 2014). After the iron beneficiation, the aluminum oxide normally increase its fraction at the thinnest tailings fractions, probably associated with the silt + clay fraction (GOMES 2009). As a consequence, more than 50% of the tailings can be composed of  $Al_2O_3$  and  $Si_2O_3$ . The main physical-chemical characteristics of the solution and a semi-quantitative analysis of the sludge and the solution are presented in Table 3.1.

**Table 3.1** – Physical-chemical characterization of the effluent and semi-quantitative analysis of the sludge used during the tests

<b>Sample</b>	<b>pH</b>	<b>Conductivity (mS/cm)</b>	<b>Turbidity (NTU)</b>	<b>TS (g/L)</b>	<b>TSS (g/L)</b>	<b>SiO<sub>2</sub> (g/L) or %</b>	<b>Al<sub>2</sub>O<sub>3</sub> (g/L) or %</b>	<b>Fe<sub>2</sub>O<sub>3</sub> (g/L) or %</b>	<b>K<sub>2</sub>O (g/L) or %</b>	<b>Others (g/L) or %</b>
Solution	6.81	60.9	5,000	8.5	9.8	19.2*	6.3*	5.8*	0.5*	1.4*
Sludge	-	-	-	-	-	57.64%**	19.02%**	17.43%**	1.59%**	4.32%**

\*Estimated concentration for the solution (33.3g of sludge/L of solution); \*\*Sludge semi-quantitative analysis by EDX

### 3.2.2 Experimental set up

Tests were carried out in a direct contact membrane distillation (DCMD) bench scale unit (Figure 3.1). The system was equipped with two diaphragm pumps (one for feed and another for distillate flows, Provitec GA5200 MB), two supply tanks, a semi-analytical balance (for distillate weighting, Shimadzu UX6200H), a hot plate with magnetic stirrer (for feed heating, Solab SL-91), a cooling system for permeate and a Teflon module (Sterlitech CFO42D). The total membrane active area was 0.004209m<sup>2</sup> (STERLITECH CORPORATION, 2017).

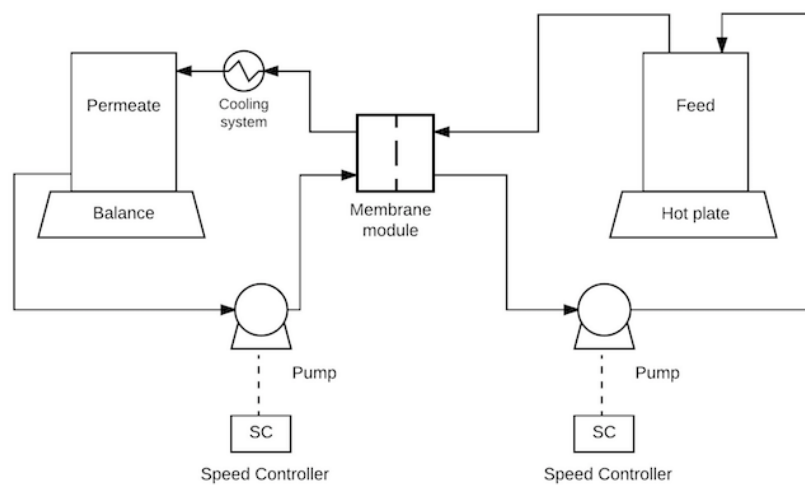


**Figure 3.1** – Schematic of the DCMD bench-scale unit

### 3.2.3 MD Membrane

A flat sheet polytetrafluoroethylene (PFTE) in a non-woven polypropylene support membrane supplied by Sterlitech was used. Prior to all experiments, the membrane was cleaned with deionized water in an ultrasound bath during 20 minutes, in order to remove any residual component. Membrane main characteristics are presented in Table 2.4.

### 3.2.4 Fouling evaluation

The main foulants were evaluated after 6h of filtration. In order to do so, 2L of the synthetic water were transferred to the feed tank, along with 1L of distillate water in the

permeate side. Both streams were recirculated in counter-current during 6h at 33L/h and temperatures of 40°C and 25°C, respectively. The total pressure difference across the membrane module during testing was always less than 10 kPa.

Permeate flow was continuously measured by means of a balance and the membrane flux was calculated from this value according to Equation 3.2.

$$J = \frac{m_2 - m_1}{(t_2 - t_1) \times A_m} \quad \text{Equation 3.1}$$

Where  $J$  is the permeate flux;  $t_1$  and  $t_2$  are the time;  $m_2 - m_1$  is the increase in the permeate mass between times  $t_1$  and  $t_2$ ; and  $A_m$  is the membrane area.

At the end of the operation, the membrane was dried at room temperature (25°C). In order to assess fouling, SEM/EDX and water contact angle (CA) analysis were performed. In addition, the resistances to filtration were calculated according to Equations 2.3 to 2.7 (SRISURICHAN, JIRARATANANON and FANE, 2006). The membrane blocking pore models was adjusted to the Hermia's law adapted to cross-flow filtration mode, (SRISURICHAN et al., 2006) and the wetting rate and wetting time were estimated as the rise observed in the conductivity ( $\mu\text{S}/\text{cm}\cdot\text{min}$ ) and the time the conductivity started to rise, respectively.

### 3.2.5 Chemical cleaning

Four pre-selected cleaning agents, besides water at the temperatures of 60°C and 25°C were tested against its cleaning effectiveness towards the PTFE membrane, as it can be seen in Table 3.2.

**Table 3.2** – Pre-selected cleaning agents, their respective concentrations, and temperature

Cleaning agent	Concentration (m/v)	Temperature
DI water 1	-	25°C
DI water 2	-	60°C
HCl	2%	
EDTA	3%	25°C
NaOH	1%	
Citric Acid	2%	

Cleaning tests consisted of (a) measurement of the initial water flux to determine  $J_{virgin}$ ; (b) subject the membrane to fouling; (c) recirculation of distilled water and flux measurement to determine  $J_{fouled}$ ; (d) accomplish the cleaning procedure; (e) measurement of the water flux after the cleaning procedure to calculate  $J_{cleaned}$ . The fouling procedure was the same as described in section 3.4.4 to fouling evaluation.

The cleaning procedure was accomplished by replacing the content of the feed tank with 1L of the cleaning solution and recirculating it during 30 minutes at 33L/h. Temperatures varied from solution to solution and are described in Table 3.2. The cleaning efficiency of each agent was calculated according to Equation 3.3.

$$Cleaning\ Efficiency = \frac{J_{cleaned} - J_{fouled}}{J_{virgin} - J_{fouled}} \quad \text{Equation 3.3}$$

In which  $J$  stands for the membrane flux in each of the cases written in subscribe.

In order to evaluate any possible change in the membrane surface when exposed to the cleaning agents, SEM images and water contact angle were held for each of the assessed cases.

### 3.2.6 Membrane ageing

Membrane ageing was evaluated by exposing three fragments of membrane continuously to the solution described in section 3.2.1, under the temperature of  $60^\circ \pm 5^\circ\text{C}$ . The first fragment was evaluated without any cleaning procedure, and the other



two were soaked, monthly, during 30 minutes to: (a) DI water at 60°C and (b) HCl 2% w/v.

In order to assess the flux decline and the saline retention, the fragment was subjected to the following procedure: before its immersion and at every 30 days after the beginning of the experiment, during 210 days, the fragment was placed in the MD unit and had its water flux at the temperatures of 50°C, 60°C and 70°C measured, and its salt rejection tested for a NaCl 4.5% w/v solution. The salt rejection experiments were conducted at 60°C and 33 L/h. They consisted of placing 0.5L of a 4.5% w/v NaCl solution into the feed stream and 0.5L of distilled water in the permeate side. Mass and permeate conductivity were monitored over time, until a water recovery fraction of 30% was attained. In addition, the other fragment subjected to regular cleaning was assessed regarding its flux decline and salt retention at 210, following the same procedure described by the fragment without cleaning. In all cases, the salt rejection factor was calculated according to Equation 3.4 (ALKHUDHIRI & HILAL, 2017).

$$\text{Salt rejection factor} = \left(1 - \frac{C_p}{C_{f,avr}}\right) \times 100 \quad \text{Equation 3.4}$$

In Equation 3.4.,  $C$  is the salt concentration in  $p$  (permeate) and  $f$  (feed) streams. Since the DCMD configuration was used, the permeate was added to the initial distillate. Thus, in order to calculate the salt rejection more accurately, the concentrations of both permeate and feed were estimated through a NaCl standard curve, that related the solution concentration and its respective conductivity. For the permeate, the conductivity obtained in the final distillate (a mixture between permeate and DI water), was transformed in salt concentration and then divided by the real permeate mass, thus obtaining its real concentration. In addition to permeability and saline retention, the fragments of the membrane correspondent to the days 0, 120, 180, and 210 were morphologically analyzed by SEM/EDX and water contact angle. The wetting rate and wetting time were also calculated.

### **3.2.7 Analytical Methods**

The solution was characterized according to the following physical-chemical parameters: pH (Qualxtron QX 1500 pH meter, method 4500B), Conductivity (Hanna HI 9835 Conductivity Meter, method 2510B), Turbidity (Hach 2100AN Turbidimeter, method 2130B), Total Solids (TS) (method 2540A) and Total Suspended Solids (TSS) (method 2540B).

After the experimental procedure (sections 3.2.4, 3.2.5, and 3.2.6), the membrane was dried at room temperature (approximately 25°C) and subjected to the following analysis for morphological and chemical characterization: scanning electron microscopy (SEM) with energy dispersive X-ray (EDX), and water contact angle.

Images of membrane surface were obtained by SEM and the content of the surface elements was analysed by EDX spectroscopy. Before the scanning, samples were coated with a 5nm-Au/Pd alloy. SEM and EDX were conducted with a FEI Quanta 200 scanning microscopy and a FIB Quanta FEG 3D, respectively, except for the aged samples subjected to a cleaning procedure with DI water. In this case, SEM and EDX were carried out in a Jeol JSM-IT300. At least 5 images were obtained for each membrane in all cases. Water contact angle was carried out in an DIGIDROP-DI Goniometer equipped with a CCD camera and an automated dispenser, using the standard sessile drop method. For each sample, three droplets of 6µL were analysed, in order to define an average contact angle.

## **3.3 RESULTS AND DISCUSSION**

### **3.3.1 Fouling evaluation**

Figure 3.2 and Table 3.3 show the flux decay, the blocking filtration model, the resistances, wetting time and rate for the solution, respectively. It can be seen that after 6 hour of filtration, the flux decreased 52.9%. This can be associated mainly to the fouling layer formed during the process, which increased the resistance to filtration ( $R_{\text{fouling}}$  in Table 3.3), thus decreasing the permeate flux (CURCIO et al., 2010). This

fouling layer is caused mainly due to cake formation, since  $K_{\text{cake}}$  (Table 3.3) revealed to be the biggest value and presented the best adjustment.

In addition to flux decline, Figure 3.2 also presents an increase in the permeate conductivity over time. This can be explained by the deposition of inorganic matter over the membrane surface, which may have caused progressive membrane wetting. As indicatives of membrane wetting, the water contact angle decrease from  $119.2 \pm 1.0^\circ$  (virgin membrane) to  $65.5 \pm 0.5^\circ$  (fouled membrane after 6hr of filtration), the wetting rate was estimated in  $0.068 \mu\text{S}/\text{cm}\cdot\text{min}$  ( $R^2 = 0.96$ ) and the wetting time, 120 minutes.

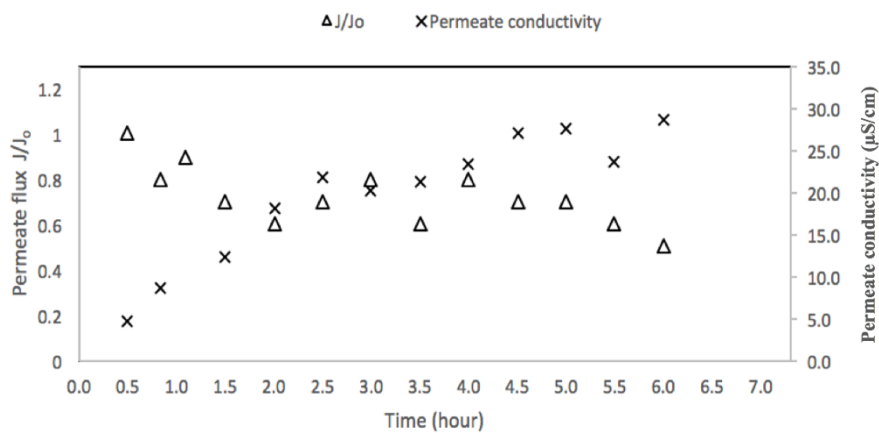


**Figure 3.2** – Flux decay and conductivity over time for the solution

**Table 3.3** – Flux decay, blocking filtration type, resistances and wetting characteristics after 6h of filtration (Temperature: 40°C, Flow rate; 33L/h)

<b>Flux decay and Blocking filtration type (<math>10^3 \text{ min}^{-1}</math>)</b>		<b>Resistances (<math>\text{Pa/Kg.m}^2.\text{h}</math>)</b>	
$J_{\text{water}}$ ( $\text{kg/m}^2.\text{h}$ )	9.10	$R_{\text{fb}}$	458
$J_{\text{eff}}$ ( $\text{kg/m}^2.\text{h}$ )	8.57	$R_{\text{pb}}$	170
$J_{\text{final}}$ ( $\text{kg/m}^2.\text{h}$ )	4.29	$R_{\text{m}}$	208
$J/J_0$	0.47	$R_{\text{fouling}}$	203
$K_{\text{complete}}$ Value ( $R^2$ )	0.98 (0.89)	$R_{\text{tot}}$	1039
$K_{\text{intermediate}}$ Value ( $R^2$ )	1.25 (0.91)	<b>Wetting characteristics</b>	
$K_{\text{standard}}$ Value ( $R^2$ )	0.55 (0.90)	Wetting rate ( $\mu\text{S.cm}^{-1}/\text{min}$ )	0.068
$K_{\text{cake}}$ Value ( $R^2$ )	3.22 (0.92)	Wetting time (min)	120

\*  $R_{\text{fb}}$  = Feed boundary resistance,  $R_{\text{pb}}$  = Permeate boundary resistance,  $R_{\text{m}}$  = Membrane resistance,  $R_{\text{fouling}}$  = Fouling resistance, and  $R_{\text{tot}}$  = Total resistance

When assessing the fouling layer, a SEM/EDX analysis indicated the presence of several inorganic compounds deposited as amorphous structures in the membrane surface, where Fe, Si and Al can be highlighted because of its abundance (Figure 3.3 and 3.4). This can be explained by the composition of the synthetic solution, that possesses an elevated concentration of  $\text{Al}_2\text{O}_3$  and  $\text{SiO}_2$  (Table 3.1).

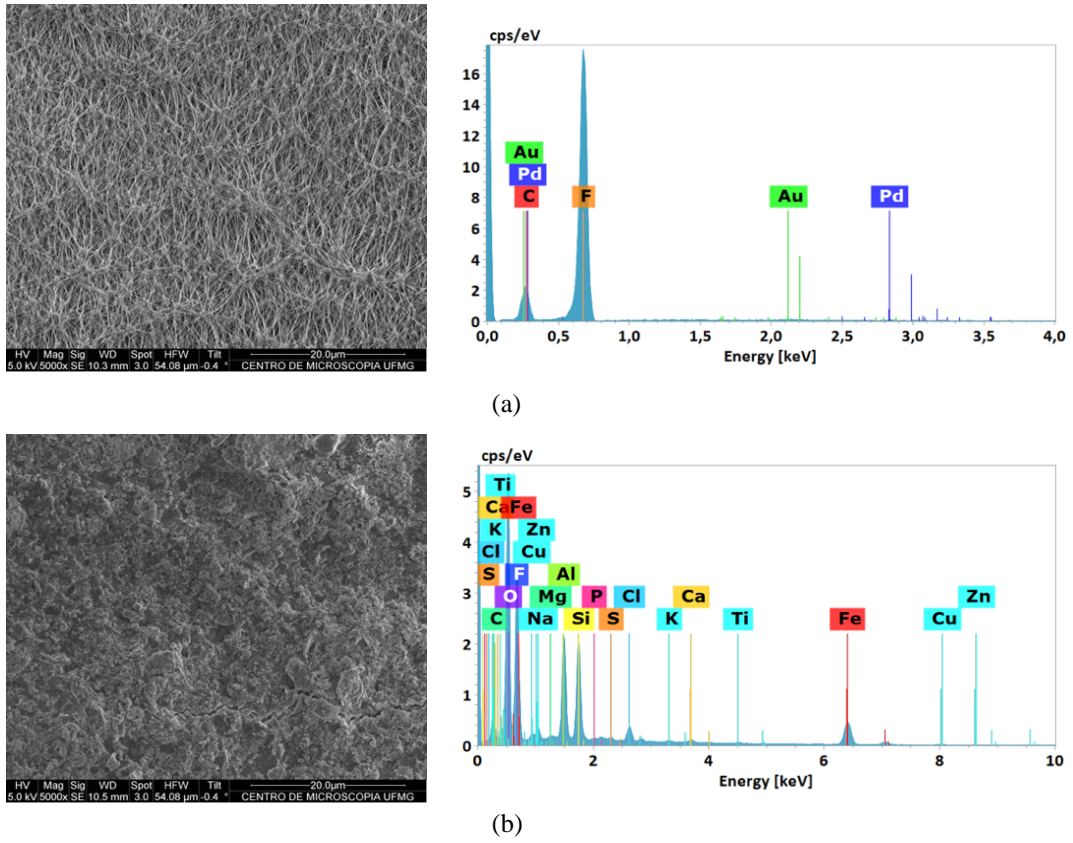


**Figure 3.3** – SEM and EDX for the (a) virgin and (b) fouled membrane

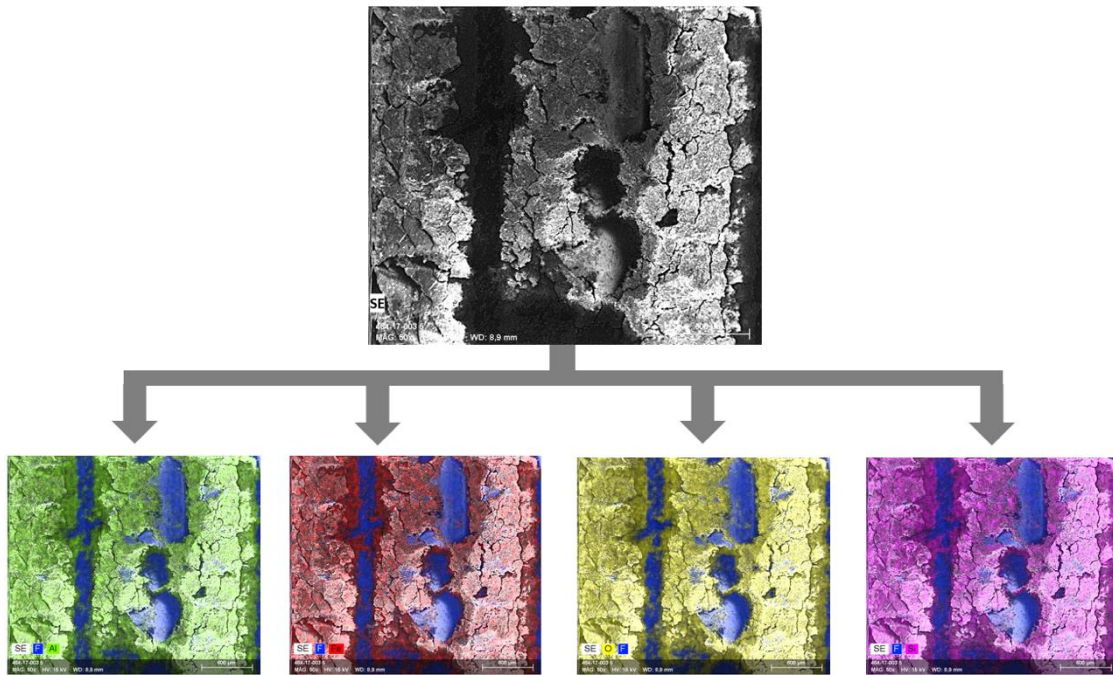


**Figure 3.4** – EDX mapping of the fouled membrane (Al: Green, Fe: Red, O: Yellow, Si: Pink and F: Blue)

It is noteworthy that the fouling layer found in the membrane surface caused a considerable flux decline, despite its main constituents – iron oxide and silica – being reported as porous at a certain degree (GRYTA, 2007; QIN et al., 2018), which are not expected to severely influence the permeate flux. However, the main difference between those references and the assessed case is concentration of these foulants in feed, that is considerably bigger in the present case (here, the concentration of Si is 4 times higher than reported by QIN et al (2018), for example). This amount of solids was so high that the formed fouling layer presented expressive  $R_{fouling}$  and  $Kc_{ake}$ , thus reducing flux throughout the filtration.

### 3.3.2 Chemical cleaning

Figure 3.5 presents the cleaning efficiency, the average contact angle (CA) and the SEM image for each of the evaluated membrane cleaning agents for a single step. The decrease in the membrane water flux after the effluent treatment varied from 50% to 60%.

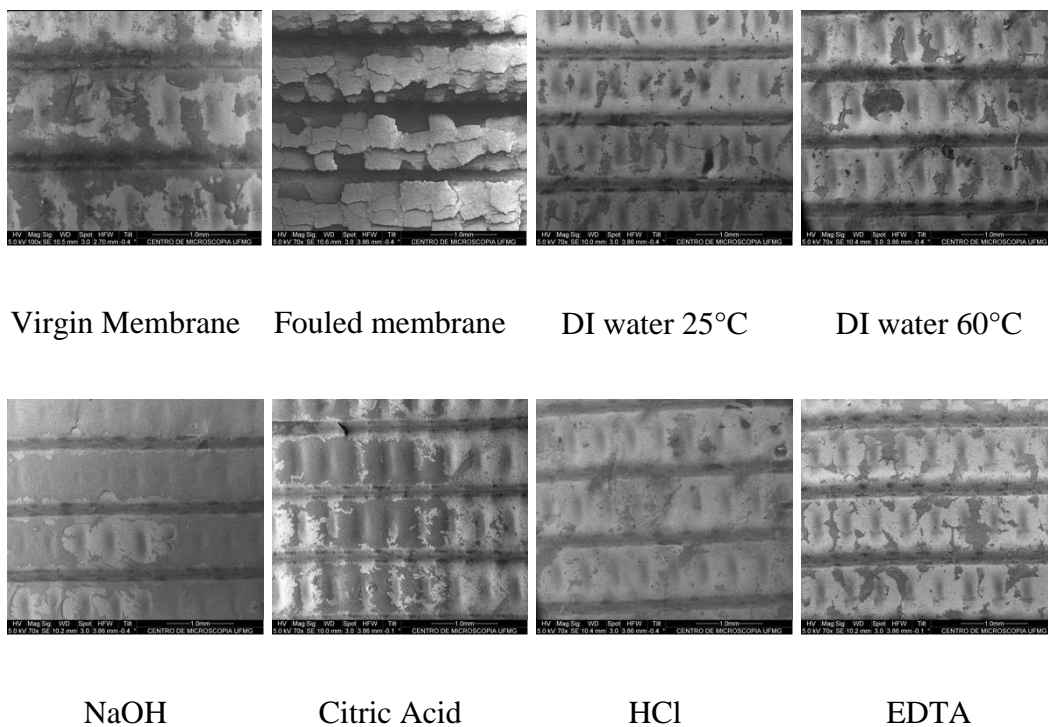
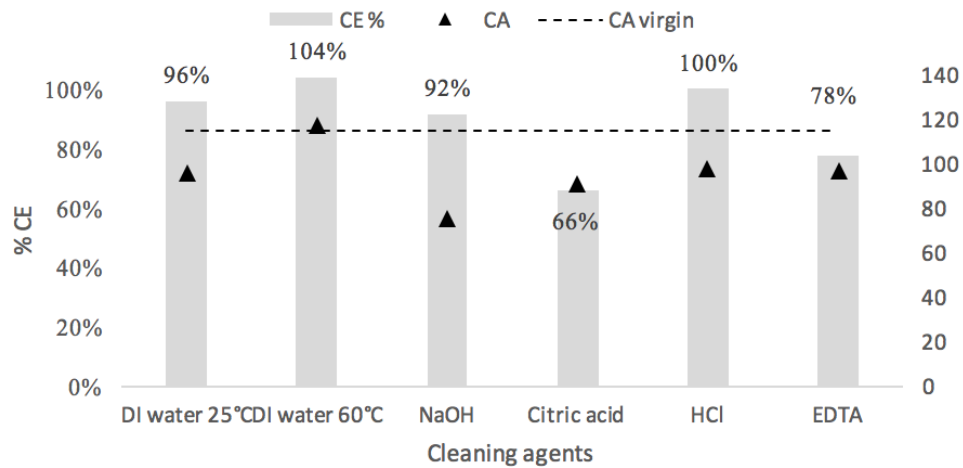


**Figure 3.5** – Cleaning efficiency, average water contact angle and SEM images (70x) for the virgin, fouled and after each of the chemical agents used

As it can be seen from Figure 3.5, DI water at 60°C and HCl presented the best overall results, which can be explained by the fact that by increasing temperature or decreasing

the pH, the solubility of major metals is also increased, which can facilitate their removal. Moreover, a high efficiency was also found for NaOH, that is related to ability of basis to reduce the interaction between the membrane and silica (GWON et al., 2003). However, the use of sodium hydroxide may have a negative effect in the membrane, since the water contact angle measured after the cleaning procedure was  $75.3 \pm 5.1^\circ$ , which may indicate that the selective layer was jeopardized during the process. The low performance of the citric acid can be attributed to the fouling layer characteristics; as it is mainly composed by metals oxide, the effects of pH and temperature are the most preeminent. It is known that citric acid acts mainly on  $\text{CaCO}_3$ , which is not the main foulant in the assessed case (GRYTA, 2008). Besides, citric acid is a weak acid, and as consequence, the pH of the resulting solution was not low enough to facilitate the oxides dissolution, thus impairing its cleaning efficiency.

In order to compare the gain that using HCl would bring (or not) to the process, Figure 3.7 shows the flux profile for an entire cycle of filtration, including cleaning procedures with both water at  $60^\circ\text{C}$  and HCl. By substituting DI water to the effluent, the flux decreased in 30%, which is associated to vapor pressure reduction experienced by solutions with salt content, when compared to the vapor pressure of pure water. As it can be observed, this effect is reversible just by changing the solution again by DI water ('WC' in Figure 3.6). During the water cleaning, the ratio  $J/J_{\text{water}}$  was 93% and increase for 100% after 30 minutes, and, as a consequence, the HCl stage had no effect in the cycle.



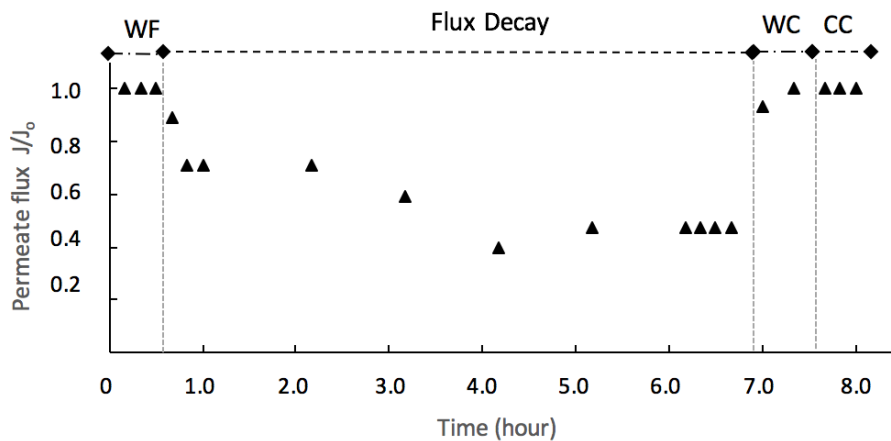


**Figure 3.6** – Flux decay over time for the effluent in which WC = water cleaning and CC = chemical cleaning with HCl 2% w/v

In addition, the EDX mapping also pointed out to a similar removal of the fouling layer, as shown in Figure 3.7.

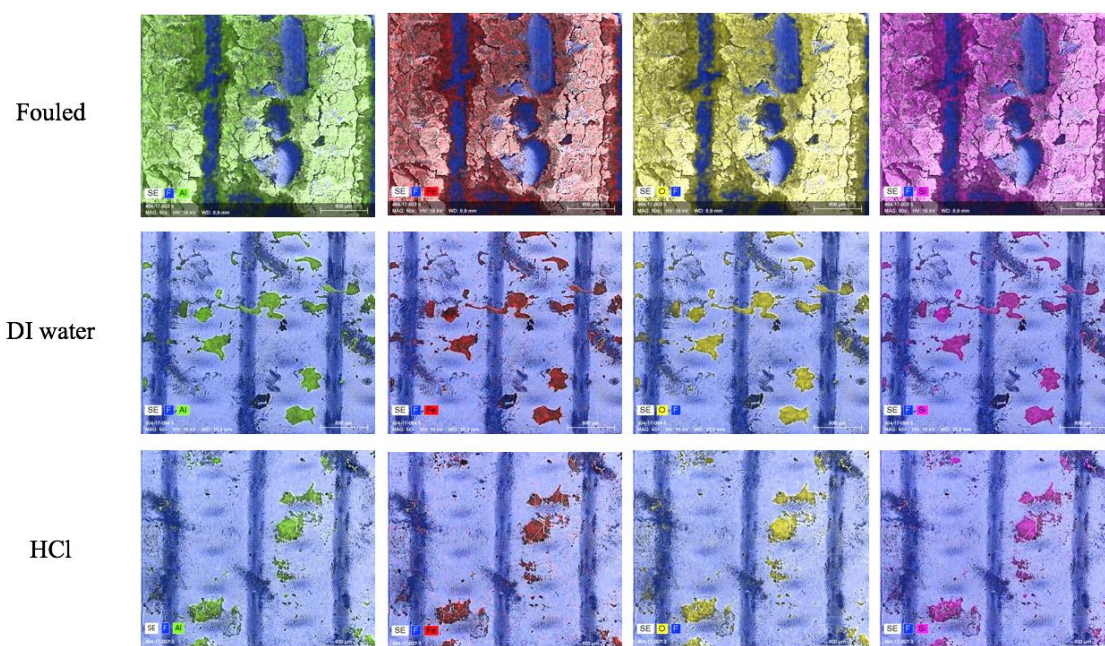


**Figure 3.7** – EDX mapping for the fouled membrane after cleaning with DI water and HCl (Al: Green, Fe: Red, O: Yellow, Si: Pink and F: Blue)

Thus, by seeing these results, one can conclude that the use of DI as a cleaning agent may be suitable in this case. Besides the obvious economical advantage of it, the

reduction in the chemicals usage is also a gain in several matters, since they have to be carefully stored and managed, require a treatment after their use and may cause environmental impacts in the case of accidents.

### 3.3.3 Membrane ageing

Figure 3.8 shows the SEM images for the days 0, 120 and 210, the measured membrane characteristics after a long-term exposure to the solution and Figure 3.9 presents the EDX mapping for the membrane at day 210. A flux decline was observed from day 0 to day 30, but it remained approximately constant until day 210. Conversely, the permeate conductivity increased over time, which indicates the progressive pore wetting caused by scaling suffered during the long-term exposure. Nevertheless, when comparing the feed and permeate salinity, one can see that the ions retention is still very high, despite the expressive conductivity factors found for days 180 and 210.

Regarding the SEM images, in contrast to the 6 hour filtration, scaling was developed through nucleation of  $\text{Al}_2\text{O}_3$  during the long-term exposure. This difference can be attributed to the way both fouling were developed. During the regular filtration, the feed cross-flow velocity creates a shear stress to the fouling layer, which hardens the nucleation of crystals, thus favoring the formation of amorphous structures. During the long-term exposure, on the other hand, the membrane was subjected to a static hot bath. As a consequence, there was no shear forces acting on the membrane surface, thus allowing the crystals to grow. Furthermore, Figure 3.9 shows a wide deposition of  $\text{Al}_2\text{O}_3$ , that can be justified by the enhancement attained in the nucleation of aluminum oxide when in the presence of iron oxide, since  $\text{Fe}_2\text{O}_3$  acts as a template or nucleation site for the  $\text{Al}_2\text{O}_3$  (RICHARDSON, 2009).

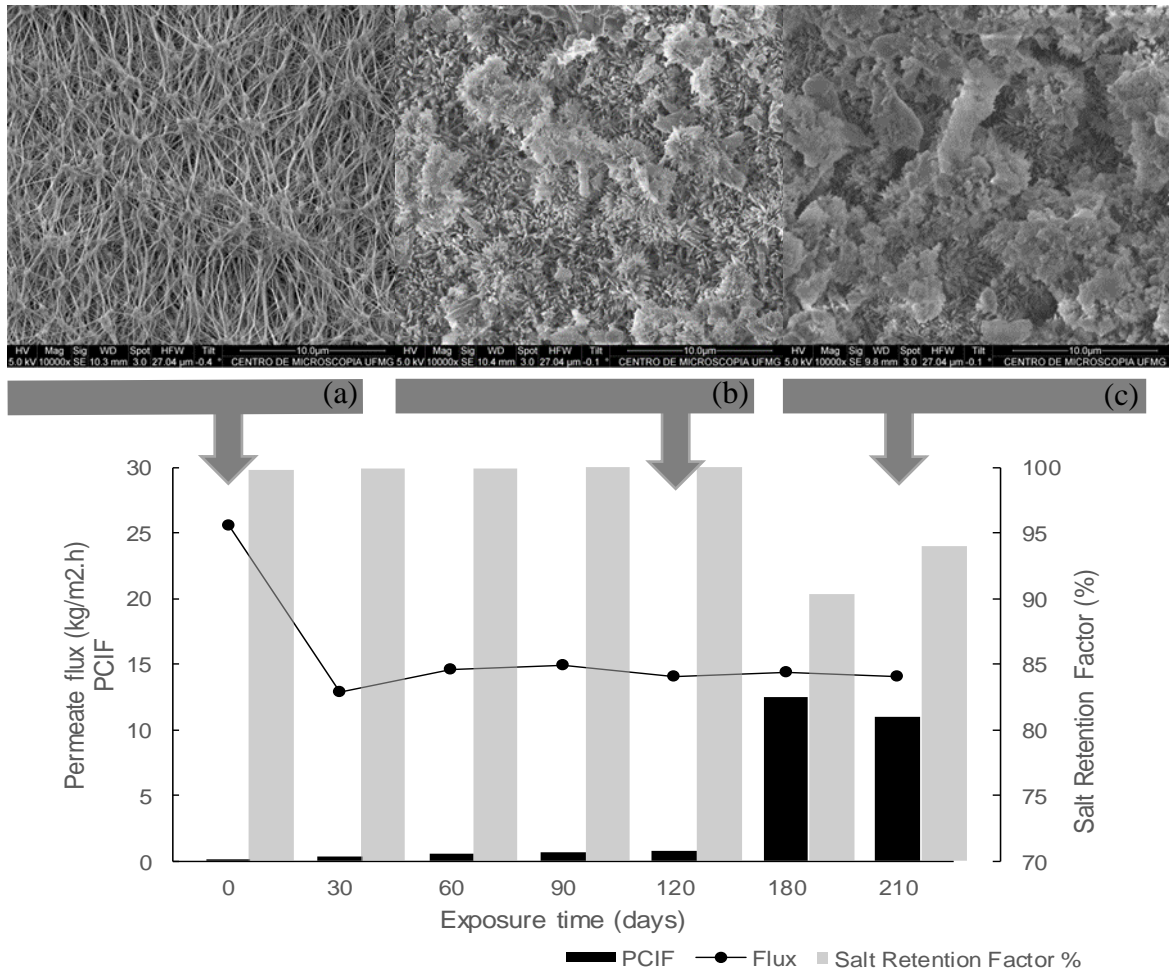


**Figure 3.8** – SEM images for the membranes at days 0, 120 and 210 (5000x), membrane main characteristics, and EDX mapping for the membrane at day 210

*PCIF = Permeate conductivity increasing factor*

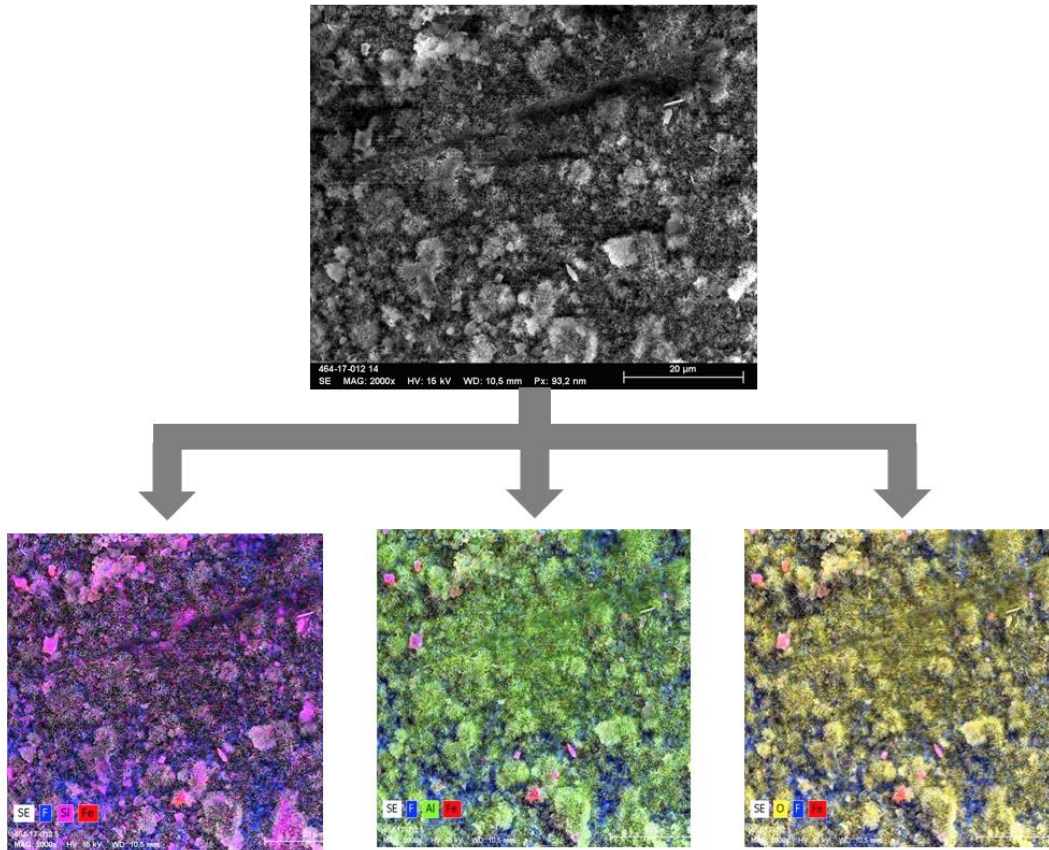


**Figure 3.9** – EDX mapping for the membrane at day 210 (Al: Green, Fe: Red, O: Yellow, Si: Pink and F: Blue)

Regarding the long-term exposure of the membranes to the solution and periodic cleaning, the SEM (Figure 3.10) image showed that there was only a partial removal of the fouling layer. EDX showed that the membrane integrity was maintained which was also corroborated by the water contact angle, measured at  $106.9 \pm 5.9^\circ$ .



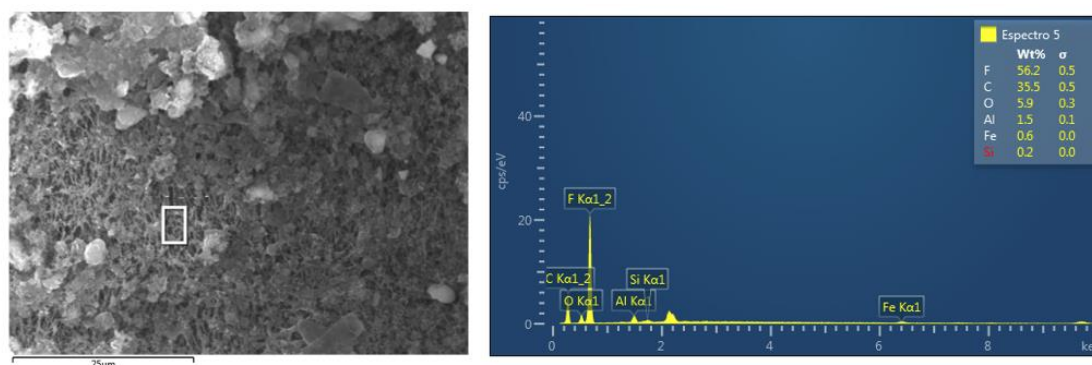


**Figure 3.10** –SEM images and EDX mapping for the membrane subjected to solution + DI water at 60°C

### 3.4 CONCLUSION

Membrane distillation is a robust treatment for water containing a great amount of suspended solids such as after the break of iron mining tailings dam. During the process, the flux decline can be mainly associated to the formation of a fouling layer in the cake form, responsible for adding resistance to filtration. In addition, fouling was found to be composed mainly for inorganic compounds, namely silica, alumina and hematite, characterized by the EDX analysis.

To control fouling, chemical agents were evaluated in a single cleaning step. It was observed that DI water at 60°C, HCl, and NaOH presented good removal efficiencies. However, since NaOH seemed to react with the selective layer and HCl did not present any real gain to the cleaning procedure, DI water at 60°C was considered as a suitable agent to membrane cleaning.

A study towards membrane ageing was also carried out. During the 210 of exposition, there was a decrease in both membrane permeability and retention. A SEM/EDX mapping showed a wide deposition of  $Al_2O_3$  as crystals, followed by the presence of  $SiO_2$  and  $Fe_2O_3$ . Despite the differences in the structures due to the absence of shear stress during the membrane ageing, DI water at 60° presented a partial removal of the fouling layer without compromising the membrane integrity, as observed in the on-site cleaning and the water contact measurement, respectively.

## **CHAPTER 4**

---

# **THERMAL BOUNDARY LAYER AND MASS FLUX PREDICTION MODELS FOR THE DESIGN OF A SEMI-PILOT MEMBRANE DISTILLATION STACK CELL**

## **4.1 INTRODUCTION**

Membrane Distillation (MD) is a non-isothermal process based on vapor-liquid equilibrium in which the driving force is the vapor pressure gradient between two phases separated by a microporous and hydrophobic membrane (DÍEZ and GONZÁLEZ, 2000; KHAYET, 2011). MD presents many interesting features such as (1) low operating temperature and hydrostatic pressure - when compared with conventional processes for distillation and pressure-driven membranes, respectively; (2) high rejection factor, with theoretical exclusion of 100% for non-volatile solutes; (3) less severe membrane fouling; and (4) possible association with renewable energy sources (LAWSON and LLOYD, 1997; BANAT and JWAIED, 2010; GUILLÉN-BURRIEZA et al., 2012). As a consequence to these characteristics, membrane distillation has been recently widely studied, and it is promised to be a cost-effective technology to treat water and wastewater (BANAT and SIMANDL, 1998; BAPPY, BAHAR and ARIFF, 2016; LE and NUNES, 2016).

The membrane distillation system can be presented under four different configurations, that differ one another from the method used for permeate cooling (CAMACHO et al., 2013). Among them, direct contact membrane distillation – DCMD is considered the simplest one, in which the cooling solution (normally water) is directly in contact to the membrane surface. As a consequence, the permeate is incorporated to this solution. DCMD is mainly applied to desalination and solute concentration (MANNA and PAL, 2016).

Despite its advantages among other processes, the majority of studies reported for MD are still in bench-scale (DÍEZ and GONZÁLEZ, 2000; ALKHUHIRI, DARWISH, and HILAL, 2012), and the lack of accessible commercial pilot-scale modules consists of a great challenge, specially in countries where this technology is not yet fully explored. Since MD is a process that couples heat and mass transfer, changes in membrane and channels size may affect directly the system performance, and therefore understanding and modelling these phenomena is fundamental. In this context, modelling can be divided into two phases: (1) thermal boundary layer estimation and (2) mass flux prediction.

For direct contact flat sheet membrane distillation – the configuration used in this paper, pilot modules are normally built by overlapping membranes in a flat sheet configuration (ANDERSSON, KJELLANDER and RODESJO, 1985). This design turns the estimation of the thermal boundary layer important, since the channel to be built must be thicker enough to ensure that the thermal boundary layers from two subsequent membranes do not overlap, compromising the bulk temperature that flows inside the channel. Besides, by being able to predict permeate flux given the specified entrance temperatures and flow properties, one can estimate overall production rate of the system, which allows a better control of the process.

Up to date, several attempts to model membrane distillation have already been developed and are summarized by El-Bourawi et al. (2006). However, most of them present a considerable deviation to experimental data (KHAYET, MENGUAL and ZAKRZEWSKA-TRZNADEL, 2006; DING, MA and FANE, 2003; FORTUNATO, BARBIERI and DRIOLI, 2000; IBRAHIM and ALSALHY, 2013), not representing a holistic approach. Moreover, when it comes to thermal boundary layer estimation, most of work were done one-dimensionally, which is actually an approximation of the real phenomena, and can contribute to a less accurate understanding of the process.

Hence, the propose of this paper was to develop a model that allow prediction of the average mass flux once entrance temperatures and flow properties. Additionally, the thermal boundary layer height developed along permeate and feed channels was also estimated using a bi dimensional energy balance and temperature profile for a direct contact membrane distillation system operating in counter-current. Finally, those models were used to predict and assess the design of a DCMD stack unit.

## **4.2 THEORY**

Figure 4.1 situates the system in space according to the three-dimensional coordinates used throughout the paper. It is defined as the whole membrane module, which includes the two flowing liquids and the membrane in between.



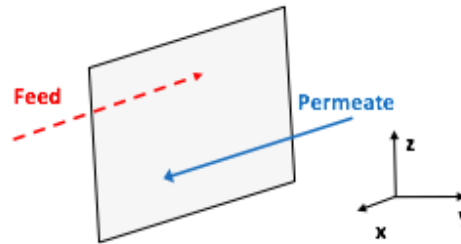


**Figure 4.1** – Representation of the system in the rectangular coordinate system used

Membrane plane is set in the  $y = 0$  plane. Meanwhile,  $x$  and  $y$  axis growth directions are reset depending on the channel being modelled. In the present work, for both channels, the convention was to have liquid entrance at  $x = 0$ , with  $x$  growing in the same direction it effectively moves. Regarding  $y$  axis, it was set to grow from the membrane to the opposite perpendicular wall surrounding each channel.

#### 4.2.1 Thermal Boundary Layer Estimation

In membrane distillation processes, Equation 4.1 can be used as the energy balance of permeate and feed channels once steady state is reached. As implied by the derivatives involved, the control volume for which the equation was derived is a point in space.

$$C_p \rho \, dy \, dz \, u \frac{\partial T}{\partial x} dx + C_p \rho \, dx \, dz \, v \frac{\partial T}{\partial y} dy + C_p \rho \, dx \, dy \, w \frac{\partial T}{\partial z} dz =$$

$$\left( \frac{\partial}{\partial x} \left( k \frac{\partial T}{\partial x} \right) dx \right) dy dz + \left( \frac{\partial}{\partial y} \left( k \frac{\partial T}{\partial y} \right) dy \right) dx dz + \left( \frac{\partial}{\partial z} \left( k \frac{\partial T}{\partial z} \right) dz \right) dx dy$$

Equation 4.1

In Equation 4.1,  $C_p$ ,  $\rho$  and  $k$  represent liquid phase's specific heat capacity at constant pressure condition, density and thermal conductivity, respectively; and  $u$ ,  $v$  and  $w$  designate its velocity in  $x$ ,  $y$  and  $z$  direction, respectively. The terms found on the left side characterize advection, and the ones from the right side represent the variation in the amount of heat that passed in each of the three dimensions. Since it consists of a steady state, there is no heat generation or consumption, both sides must be equal in order to respect the first law of Thermodynamics.

For the membrane distillation process, Equation 4.2 can be used as an equivalent to equation 4.1, since the variation of temperature experienced in in  $z$  direction is expected to be the negligible when compared to the other directions.

$$C_p \rho u \frac{\partial T}{\partial x} + C_p \rho v \frac{\partial T}{\partial y} = \left( \frac{\partial}{\partial x} \left( k \frac{\partial T}{\partial x} \right) \right) + \left( \frac{\partial}{\partial y} \left( k \frac{\partial T}{\partial y} \right) \right) \quad \text{Equation 4.2}$$

Instead of solving Equation 4.2 to find the  $T(x, y)$  solution function, a temperature profile for the liquid phases can be assumed taking into consideration boundary conditions that must be respected by such a function to ensure that in fact it represents the system's reality. Further on, energy balance is used to find out how thermal boundary layer, which will be directly involved in the temperature profile proposed, must depend on  $x$  for the energy conservation principle to be satisfied. Such an approach for estimating thermal boundary layer profile is known as integral solution (BEJAN, 2004; CHAPMAN, 1994).

However, to serve the purpose of giving out the boundary layer profile, the energy balance given in Equation 4.2 must be adapted to a different control volume. Equation 4.3 presents a version of it written for a vertical line, (perpendicular to the  $y = 0$  plane), as control volume. In this equation,  $T_\infty$  represents liquid bulk temperature;  $T_w$  represents temperature at the membrane-liquid interface; and  $\delta_T(x)$  represents thermal boundary layer height-

$$\frac{d}{dx} \left( \int_0^{\delta_T(x)} C_p \rho u (T_\infty - T) dx dz dy \right) = q_m'' dx dz + q_v'' dx dz + q_x'' dx dz - C_p \rho v (T_\infty - T_w) dx dz \quad \text{Equation 4.3}$$

In Equation 4.3, by integrating the term found on its left side in respect to  $y$ , the energy difference of an entire vertical line is obtained, that is, this result provides a function in which each point has its own  $T(x, y)$  and, therefore, yields, for a vertical line, an overall variation in energy compared to an intact line at temperature  $T = T_\infty$ . Given the boundary layer theorization (CHAPMAN, 1994), it is only necessary to integrate it until  $y = \delta_T$ , since beyond that,  $T = T_\infty$  and, as a consequence, there is no temperature difference to account for.

Following the integral, the infinitesimal variation rate along  $x$  direction – that is, the derivative of that function with respect to  $x$  – is taken. The only reason for the difference between the energy of a line and the intact line to be changing along  $x$  is heat transfer across the line's boundaries. Thus, left side must equal the contribution of the heat transfer phenomena taking place at the boundaries. The next steps are to identify the phenomena and then, to write appropriated expressions for the calculation of each one of them to build up the right side of Equation 4.3.

Given the control volume for which Equation 4.3 is written, an immediate identifiable source would be conductive heat transferred to the membrane,  $q_m'' dx dz$ , due to the temperature gradient experienced. Along with that one, heat is also lost or received in each line due to phase transition happening at the membrane interface,  $q_v'' dx dz$ . Another energy variation source is the variation in conductive heat,  $q_x'' dx dz$ . However, it is assumed to be smaller than the other terms being thus neglected in many integral solution approaches (BEJAN, 2004; CHAPMAN, 1994; HOLMAN, 1983). Finally, the energy variation sources stated previously are not supplied only by energy variation of the fluid flowing in  $x$  direction – there is also a contribution of the fluid flowing in  $y$  direction,  $C_p \rho v (T_\infty - T_w)$ . This term is also often neglected in the energy balances though (HOLMAN, 1983), being thus also absent in this paper's approach. Hence, Equation 4.3 can be simplified into Equation 4.4.

$$C_p \rho \int_0^{\delta_T} u (T_\infty - T) dy = q_m'' + q_v'' \quad \text{Equation 4.4}$$

Since both  $q_m''$  and  $q_v''$  energy variation sources are located at the membrane interface and are in heat form, they will be referred to as wall heat flux, and respectively designated as  $q_w''$ . The previous definition is presented algebraically in Equation 4.5.

$$q_w'' \stackrel{\text{def}}{=} q_m'' + q_v'' \quad \text{Equation 4.5}$$

In the present modelling work, velocity profile in  $x$  direction was assumed to be the same as for a fully developed flow between two parallel plates. Equation 4.6 is used for  $u(y)$  (WELTY et al., 2008).

$$u = \frac{3}{2} u_m \left( 1 - \left( \frac{y-H}{H} \right)^2 \right) \quad \text{Equation 4.6}$$

In the previous equation,  $u_m$  stands for mean fluid velocity and  $H$  represents half of the channel's thickness value.

Lastly, to be able to use Equation 4.4 as a tool to predict the appropriate profile for  $\delta_T(x)$  given the function  $T(x,y)$  proposed, it is necessary that the only remaining variables are  $\delta_T$  and  $x$ . Therefore, expressions for both components of wall heat flux ( $q_m''$ ,  $q_v''$ ) must be derived.

#### 4.2.1.1 Constant wall heat flux

Considering the counter current nature of the flow, it is possible that constant wall heat flux in  $y$  direction represents an accurate condition to be assumed for the process, since the temperature difference between two opposite interfacial points are often approximately constant. The conductive heat transfer for membrane distillation can be calculated using the expression found in Equation 4.7 (QTAISHATA et al, 2008; MARTÍNEZ-DÍEZ and VÁZQUEZ-GONZÁLEZ, 1999; GRYTA and TOMASZEWSKA, 1998).

$$q_m'' = k_m \frac{(T_{w,f} - T_{w,p})}{\varepsilon} \quad \text{Equation 4.7}$$

In Equation 4.7, subscripts  $f$  and  $p$  are added to  $T_w$  to designate feed and permeate interfacial temperatures, respectively;  $k_m$  symbolizes membrane thermal conductivity; and  $\varepsilon$  represents membrane thickness. Since membrane phase is constituted of gaseous and solid phases, a usual approach is to assume the overall phase thermal conductivity to be a weighted mean of the individual solid and gaseous phases (PHATTARANAWIK, JIRARATANANON and FANE, 2003). Such an approach is described in Equation 4.8.

$$k_m = (1 - \phi)k_s + \phi k_f \quad \text{Equation 4.8}$$

In Equation 4.8,  $\emptyset$  represents membrane porosity; and  $k_s$  and  $k_f$  stand for the thermal conductivities of each the individual solid and vapour phases, respectively.

Based on the definition of phase transition heat,  $q_v''$ , Equation 4.9 can be written. In this equation,  $J$  represents the mass flux across the membrane; and  $\Delta H_{vap}$  is the energy associated to liquid-vapour phase transition.

$$q_v'' = J\Delta H_{vap} \quad \text{Equation 4.9}$$

Finally, the temperature profile model proposed must be such that it is capable of respecting the following boundary conditions

- I)  $T = T_\infty$  for  $y = \delta_T$ ;
- II)  $\left(\frac{\partial T}{\partial y}\right)_{y=\delta_T} = 0$ ;
- III)  $\left(\frac{\partial T}{\partial y}\right)_{y=0} = \frac{q_w''}{k}$  (and constant);
- IV)  $\left(\frac{\partial^2 T}{\partial y^2}\right)_{y=0} = \left(C_P \rho v \frac{\partial T}{\partial y} - \left(\frac{\partial}{\partial x} \left(k \frac{\partial T}{\partial x}\right)\right)\right)_{y=0}$ .

Condition I) comes from boundary layer theorization. Condition II) arises from the physical fact that no heat is gathered beyond boundary layer in  $y$  direction. Therefore, given Fourier's conductive heat flux expression, temperature derivative in respect to  $y$  must be zero. Boundary conditions III) specifically requires the profile  $T(x, y)$  of the liquid phase to be able to deliver a constant and specific value for  $\left(\frac{\partial T}{\partial y}\right)_{y=0}$  along the entire membrane extension to then honor the constant wall heat flux assumption previously made. Finally, boundary condition IV) comes from the fact that must be a third term on the right side of Equation 4.2 to account for phase transition heat contribution. Therefore, for its second derivatives at the interface, Equation 4.2 is expected to remain valid as it describes the heat transfer behavior along all other positions inside the channels. Thus, the only change in such equation is that because of the no slip condition, there is no fluid motion in  $x$  direction at the interfaces (PHATTARANAWIK et al, 2003), allowing Equation 4.2 to be equivalent to Equation 4.10 when written for the membrane interface.

$$\left(C_P \rho v \frac{\partial T}{\partial y}\right)_{y=0} = \left(\left(\frac{\partial}{\partial x}\left(k \frac{\partial T}{\partial x}\right)\right) + \left(\frac{\partial}{\partial y}\left(k \frac{\partial T}{\partial y}\right)\right)\right)_{y=0} \quad \text{Equation 4.10}$$

Because of the small width available for a high change in  $T(y)$  and  $\frac{\partial T}{\partial y}$ ,  $\frac{\partial^2 T}{\partial y^2}$  is expected to be considerable bigger than  $\frac{\partial^2 T}{\partial x^2}$ , being thus negligible. Therefore, Equation 4.10 can be simplified to Equation 4.11, implying in a possible second simplification on the fourth boundary condition.

$$\left(C_P \rho v \frac{\partial T}{\partial y}\right)_{y=0} = \left(k \left(\frac{\partial^2 T}{\partial y^2}\right)\right)_{y=0} \quad \text{Equation 4.11}$$

A generic function  $T(x, y)$  directly capable of fully satisfying the three first boundary conditions simultaneously is presented in Equation 4.12, in which  $N, a, b$  and  $c$  are constants (KAKAÇ and YENER, 1994). Despite the infinite number of combinations that can be made, the constants values must always cherish the boundary conditions the temperature profile is known to be subjected to.

$$T(x, y) = \pm N \delta_T \left(1 + a \frac{y}{\delta_T} + b \left(\frac{y}{\delta_T}\right)^2 + c \left(\frac{y}{\delta_T}\right)^3\right) + T_\infty \quad \text{Equation 4.12}$$

First term may be positive or negative depending on whether the liquid phase is receiving or losing energy. Applied to the membrane distillation process reality, positive sign is used for the permeate channel profile while the negative sign is used for the feed channels.

Because mass flux is supposed to be constant throughout the membrane extension, same is applied to fluid velocity in  $y$  direction, given the relation between these two parameters. This implies that the term  $\left(C_P \rho v \frac{\partial T}{\partial y}\right)_{y=0}$ , involved in the fourth boundary condition, is also supposed to remain constant throughout the interfacial regions. However, as it can be seen from the temperature profile proposed, the same does not remain valid for  $\left(\frac{\partial^2 T}{\partial y^2}\right)$  at the interface given its dependence to  $\delta_T(x)$ . Being the temperature profile proposed insufficient to fully respect all four boundary conditions,

constants  $a, b, c$  and  $N$  must be set in the way to at least minimize boundary condition IV error, thus maximizing the model validity.

#### 4.2.2 Mass flux prediction

Mass transfer mechanisms across the membrane in membrane distillation processes yields the linear model presented in Equation 4.13 (KHAYET, 2011; CAMACHO et al, 2013).

$$J = C\Delta p \quad \text{Equation 4.13}$$

In the previous equation,  $C$  is named membrane coefficient;  $J$  is the mass flux across the membrane; and  $\Delta p$  is the vapor pressure difference between both interfaces. It is important to highlight that membrane coefficient value can be assumed to depend only on membrane properties, thus remaining the same for different flow and module parameters (KHAYET, 2011).

It is noteworthy that flux estimation for MD processes usually requires no infinitesimal approach. That is because when designing a process, the interest lies in the overall recovery rate of the process. Therefore, having knowledge of the average flux,  $\bar{J}$ , is enough to serve such purpose, despite local flux possibly varying from point to point according to how temperature in feed and permeate interfaces change, and it can be calculated through Equation 4.13.

For the different liquid-gas phase equilibria states of water, its vapor pressure relates to temperature as shown in Equation 4.14 (KHAYET, 2011), in which measurement units are specified in brackets.

$$P[Pa] = EXP\left(23,238 - \frac{3841}{T[K]-45}\right) \quad \text{Equation 4.14}$$

Equations 4.15 and 4.16 presented below consist on a macroscopic energy balance for the membrane interfaces in feed and permeate channels, respectively.

$$\left\{ \begin{array}{l} K_m \frac{(T_{w,f} - T_{w,p})}{\varepsilon} + J\Delta H_{vap,f} = h(T_{\infty,f} - T_{w,f}) \end{array} \right. \quad \text{Equation 4.15}$$

$$K_m \frac{(T_{w,f} - T_{w,p})}{\varepsilon} + J\Delta H_{vap,p} = h(T_{w,p} - T_{\infty,p}) \quad \text{Equation 4.16}$$

Regarding Equations 4.15 and 4.16 derivation, expressions found on the left consist on the conductive heat flux passed along membrane phase and amount of energy associated to vaporization or condensation (in which  $K_m$  is the membrane heat transfer coefficient). On their right side, lies an expression used to calculate convective heat transfer exchanged between the entire liquid flowing phase and the membrane due to temperature difference. Because steady state is the one considered, all the heat that arrives at the interface must necessarily be consumed or transferred, thus the equality sign appears.

Heat of vaporization,  $\Delta H_{vap}$ , depends on the temperature in which phase transition takes place. Using thermodynamic data from steam water table (KORETSKY, 2013), Equation 4.17 is obtained. Units of measurement are specified in brackets.

$$\Delta H_{vap} \left[ \frac{kJ}{kg} \right] = -2,386T[K] + 3153 \quad \text{Equation 4.17}$$

The expression used for convective heat flux in Equations 4.15 and 4.16 previously presented is originally derived for constant interfacial temperature. However, there is no external factor causing the membrane interfaces to be at constant temperatures. Because of that, these constant interfacial temperatures are going to be referred to as virtual ones. Even though it might seem contradictorily at first, the fact that  $T_{w,f}$  and  $T_{w,p}$  are virtual variables does not cause any harm to the goal previously set – to be able to predict average mass flux using the linear model given in Equation 4.13. That is because the mass transfer equation must simply be derived in a way that allows it to simultaneously solve Equations 4.15 and 4.16 for that same average flux value. That can be managed by assigning the value for  $c$  that delivers the average mass flux of the process when the  $\Delta P$  value of the previous mentioned origin is used in Equation 4.13. In fact, interfacial temperatures can be more properly calculated using the modelling approach presented in section 4.1.1, which is derived in a more suitable way.



After membrane coefficient is properly obtained, Equation 4.13 can be used along with Equations 4.15 and 4.16, yielding Equations 4.18 and 4.19.

$$\left\{ \begin{array}{l} K_m \frac{(T_{w,f} - T_{w,p})}{b} + (c\Delta P)\Delta H_{vap,f} = h(T_{\infty,f} - T_{w,f}) \\ K_m \frac{(T_{w,f} - T_{w,p})}{b} + (c\Delta P)\Delta H_{vap,p} = h(T_{w,p} - T_{\infty,p}) \end{array} \right. \quad \begin{array}{l} \text{Equation 4.18} \\ \text{Equation 4.19} \end{array}$$

The system of equations is made of two equations involving two variables each, since  $\Delta P$  can be expressed in terms of the virtual wall temperatures. Because the equations are not equivalent to each other, there must be necessarily only one possible solution for the system, which will be the average mass flux for the process for any set of process conditions.

#### 4.2.2.1 Convective heat transfer correlations

The convective heat transfer coefficient involved in Equations 4.15 and 4.16 is determined through empiric correlations (HOLMAN, 1983). These involve both flow parameters and fluid properties and also concern which flow regime is experienced – laminar or turbulent. Several studies were made regarding which correlation offers a coefficient that is in better agreement with experimental results obtained for membrane distillation processes (PHATTARANAWIK et al., 2003; IZQUIERDO-GIL, GARCÍA-PAYO and FERNANDÉZ-PINEDA, 2009; SCHOFIELD, FANE and FELL, 1987). In the present work, five different correlations are evaluated for laminar flow. These are used to calculate Nusselt number that is further used to calculate  $h$ , as shown in Equation 4.20 (HOLMAN, 1983).

$$h = \frac{k}{D} Nu \quad \text{Equation 4.20}$$

In the previous equation,  $Nu$  is used to refer to the Nusselt number and  $D$  is the hydraulic diameter of the flowing channel. For flowing channels whose cross section is not circular, Equation 4.21 is used to calculate  $D$ , in which  $A$  is the cross section area and  $P$ , its perimeter (HOLMAN, 1983).

$$D = 4 \frac{A}{P} \quad \text{Equation 4.21}$$

The experimental Nusselt correlations investigated in the present work are Equations 4.22 to 4.27, being the fluid properties involved in them calculated for the film temperature (HOLMAN, 1983; PHATTARANAWIK et al., 2003).

$$Nu = 1,86 \left( \frac{RePr}{L/D} \right)^{\frac{1}{3}} \quad \text{Equation 4.22}$$

$$Nu = 4,36 + \frac{0,036 RePr \left( \frac{D}{L} \right)}{1 + 0,0011 \left( RePr \left( \frac{D}{L} \right) \right)^{0,8}} \quad \text{Equation 4.23}$$

$$\left\{ \begin{array}{l} Nu_{cooling} = 11,5 (RePr)^{0,23} \left( \frac{D}{L} \right)^{0,5} \\ Nu_{heating} = 15 (RePr)^{0,23} \left( \frac{D}{L} \right)^{0,5} \end{array} \right. \quad \text{Equation 4.24}$$

$$Nu = 3,66 + \frac{0,104 RePr \left( \frac{D}{L} \right)}{1 + 0,0106 \left( RePr \left( \frac{D}{L} \right) \right)^{0,8}} \quad \text{Equation 4.25}$$

$$Nu = 0,097 Re^{0,73} Pr^{0,38} \quad \text{Equation 4.26}$$

Each correlation gives out a different value for the convective heat transfer coefficient, and consequently yield a different mass transfer equation, given the modelling approach previously presented. Aside from mass transfer modelling, the correlations can also be used to predict overall convective heat transference in the channel. Equation 4.28 brings the convective heat transfer expression separately from the macroscopic energy balances presented previously. In this equation,  $\xi$  is used to denote the overall convective heat.

$$\xi = h(T_w - T_\infty) \quad \text{Equation 4.27}$$

However, as previously mentioned, constant interfacial temperature assumption may not be loyal to the system's reality. On the other hand, the amount of energy required for such a change can be generically calculated as shown in Equation 4.29.

$$\xi = u_m \rho C_p (T_{outlet} - T_{inlet}) \quad \text{Equation 4.29}$$

### 4.3 MATERIALS AND METHODS

In order to determine membrane coefficient to build a linear equation such as Equation 4.13 to model mass transfer, it was necessary to gather a set of solutions, collected experimentally. Because average mass flux is also involved in Equation 4.4, used to estimate thermal boundary layer height, the collection of data to calculate average mass flux was also required for such a purpose.

#### 4.3.1 Membrane characteristics

A flat sheet polytetrafluoroethylene (PTFE) in a non-woven polypropylene support membrane supplied by Sterlitech was used in all experiments. Membrane main characteristics are presented in Table 4.1 along with its constituent's thermal conductivity, required in the calculation of the overall phase's thermal conductivity.

**Table 4.1** – Membrane main characteristics and air thermal conductivity for the set of temperatures used during the experiments

Parameter	Value	Unit	Reference
Membrane porosity	0.7	$\mu\text{m}$	Xu et al. (2016)
Membrane overall thickness	170	$\mu\text{m}$	Manawi et al. (2014b)
PTFE thermal conductivity	0.25	W/m.K	Price and Jarrat (2002)
Air thermal conductivity	0.020 – 0.022	W/m.K	Phattaranawik et al. (2003)
Membrane thermal conductivity	0.0918	W/m.K	Equation 4.28

#### 4.3.2 Experimental setup

Tests were carried out in a direct contact membrane distillation (DCMD) bench scale unit (Figure 4.2) equipped with two diaphragm pumps (one for feed and another for distillate flows), two supply tanks, a semi-analytical balance (for distillate weighting), a hot plate with magnetic stirrer (for feed heating), four thermometers installed at the inlet

and outlet positions of feed and permeate channels, a cooling system for permeate and a DCMD Teflon module. The flow channel of the module used was 0.09207m short, 0.04572m high and 0.002m wide, having total membrane active area of 0.004209m<sup>2</sup> (STERLITECH CORPORATION, 2017) . Module dimensions can then be used to calculate hydraulic diameter in Equation 4.21, yielding 0.003832m.

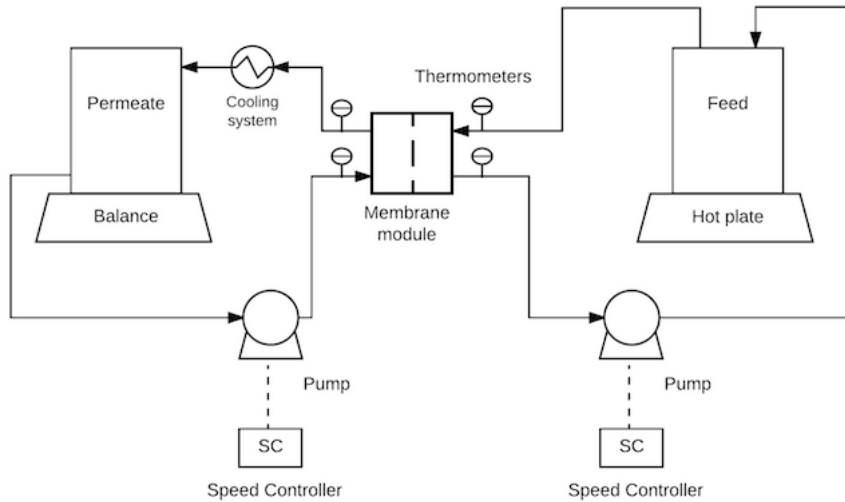


**Figure 4.2** – Schematic of the DCMD bench-scale unit

### 4.3.3 Experimental procedure

Tests were performed under three different conditions, that differ as to feed inlet temperature. Each assay consisted of using 2L of water as feed and 1L of distillate water as permeate. During all tests, the permeate temperature was maintained at 25°C by a cooling system. Since DCMD design was used, the permeate was integrated to the initial distillate. The feed and distillate inlet and outlet temperature were monitored, as well as the permeate mass increase over time. Because temperatures showed little variation in time, it was safe to consider that the values selected to represent a given time interval was in fact maintained throughout the majority of it. Table 4.2 summarizes the set of process condition used.

**Table 4.2** – Process conditions established to provide data to assist on the modelling

Condition	Feed reservoir temperature (°C)	Permeate reservoir temperature (°C)	Volumetric flow, $\dot{V}$ (L/h)	Mean fluid velocity, $u_m$ (m/s)
A	50			
B	55	25	33	0.1002
C	60			

#### 4.3.4 Mass flux prediction

To build the mass transfer equation, inlet temperatures and average flux data collected for each process condition were used to determine the shared solution ( $T_{w,f}, T_{w,p}$ ) between Equations 4.15 and 4.16 using each convective heat transfer correlation. The virtual wall temperature solutions obtained for each process condition were then used to calculate an equally virtual  $\Delta P$ , that was further put together with the respective experimental  $\bar{j}$  data to yield a linear regression. The linear fit was performed to give an algebraic link between points made out of the real  $\bar{j}$  data and virtual wall temperatures for a different set of process conditions.

Because every heat transfer correlation yields a different  $\Delta P$ , six mass transfer equations were obtained. Coefficient of determination,  $R^2$ , was used to evaluate each convective heat transfer correlation propensity to provide a mass transfer equation that delivers accurate values for the average flux when used together with the temperature solutions of Equations 4.15 and 4.16.

#### 4.3.5 Convective heat transfer analysis

The correlations potential to better describe overall convective heat transfer inside permeate and feed channels was also investigated for all three process conditions experiments performed. For each time data collected, wall temperature delivered by each correlation was used, along with the respective heat transfer coefficient, to calculate convective heat transfer as given in Equation 4.28, for both feed and permeate sides. Analogously, the experimental

data of inlet and outlet temperatures were used to calculate experimental convective heat transferred inside the module according to Equation 4.29 for feed and permeate sides.

To compare the results, the square of the difference between the energy values given by Equations 4.28 and 4.29 was taken for each time data collected and, further on, its average value was calculated. Finally, the square root of this average value obtained was calculated for each correlation for a given process condition, yielding a way to measure the deviation ( $\delta$ ) with smaller set of numbers.

#### **4.3.6 Thermal boundary layer estimation**

In the present work, thermal boundary layer was estimated for both permeate and feed sides for the different feed inlet temperature conditions in which experiments were performed via integral method, using Equation 4.12 as  $T(x, y)$ . To do so, it was necessary to set proper values for all the variables and parameters involved in Equation 4.4, leaving thus an equation relating  $\delta_T$  and  $x$  only. The fluid properties involved were assumed to be constant with temperature and, therefore, throughout the entire channel. Properties at the mean liquid temperature were taken as reference. Such mean temperature was estimated based on the virtual wall temperatures values obtained using the mass flux modelling approach, discussed previously in section 4.2.2.

Process parameters involved, such as average mass flux, bulk temperatures, liquid flow velocity were all either obtained directly from measurement or derived from calculation using the experimental data collected as presented in section 4.3. Membrane thermal conductivity calculated value can be found in Table 4.1.

In order to determine the function that better fitted the process characteristics among the family of temperature profiles represented generically in Equation 4.12, boundary conditions I) to III) were put together, yielding a system of three equations involving the four variables –  $a, b, c$  and  $N$ . Given the nature of such a system, one degree of freedom exists. Boundary condition IV) does not yield a direct relation between the constants to be used as a fourth equation, since it is mediated by  $\delta_T(x)$  value, as presented in Equation 4.30, given the format of the temperature profile proposed.

$$k \left( \pm N \frac{2b}{\delta_T} \right) = C_p \rho v \frac{\partial T}{\partial y} \quad \text{Equation 4.30}$$

It's inability to assist on a priori determination of the proper combination of constants requires Equation 4.4 to be solved first, being boundary condition IV)'s validity throughout membrane extension checked afterwards. Firstly, combinations of constants were then obtained by choosing values for  $b$  and calculating  $a, c$  and  $N$  that were in agreement with boundary conditions I) to III). Via trial and error, the most suitable temperature profile for the liquid phases can thus be obtained when checking upon boundary condition IV) results.

However, every combination of constants is expected to deliver a different  $\delta_T(x)$  profile. At first, in principle, that can make it possible for more than one temperature profile to be in good agreement with boundary condition IV), thus making it impossible to determine which temperature profile better represents the system's reality. To ascertain the uniqueness of the modelling result, its mathematical behavior was studied via experimenting different input values for  $b$  to evaluate the impact in the boundary condition IV) results.

Lastly, a value must be assumed a priori for the interfacial temperature difference,  $\Delta T$ , as it is also involved in Equation 4.4. Consequently, for model coherence, the  $\delta_T$  profile resultant for permeate and feed sides must, together with its respective  $N$  constant value, yield that same temperature difference in Equation 4.31 with good approximation.

$$\Delta T(x) = (-N_f \delta_{T,f}(x) + T_{\infty,f}) - (N_p \delta_{T,p}(x) + T_{\infty,p}) \quad \text{Equation 4.31}$$

With that said, interfacial temperature difference is both an input and an output in the present modelling. Besides influencing the outcome  $\delta_T(x)$  in Equation 4.4, it is also involved in boundary condition IV), thus also influencing its validity for a given  $T(x, y)$  profile solution associated to a set of constants  $a, b, c, N$ . Again, these are both evidences that the relative freedom of  $\Delta T$  value, at first, contributes for generating more than one  $T(x, y)$  profile that fits all the characteristics expected from such a function. Therefore, its influence on the results must also be investigated along with the constants. Such investigation was also performed via experimenting different input values and observing the impact on results.

Finally, in order to analyze the individual impact of both  $\Delta T$  and  $b$  input values on results, each parameter influence was investigated individually to further on analyze the possibility of convergence to more than one solution when changing both simultaneously.

## 4.4 RESULTS AND DISCUSSION

### 4.4.1 Experiments

Table 4.3 presents the process parameters obtained empirically for each process condition.

**Table 4.3** – Experimental data for each process condition

Condition	$T_{inlet,f}$ (°C)	$T_{outlet,f}$ (°C)	$T_{inlet,p}$ (°C)	$\bar{J}$ $\left(\frac{kg}{m^2 \cdot h}\right)$	$\sigma^*$ $\left(\frac{kg}{m^2 \cdot h}\right)$
A	44.2	42.3	25.1	26.2	8.1
B	48.4	46.6	25.4	26.3	10.0
C	52.1	49.7	25.2	26.6	13.1

\*Average mass flux standard deviation

### 4.4.2 Mass flux prediction

Table 4.4 presents the linear regression equation and  $R^2$  associated to the each of the five convective heat transfer correlations investigated. Based on coefficient of determination values, the set of correlations 4.24 – 4.25 resulted a better fit. Therefore, the linear function  $\bar{J}(\Delta P)$  delivered by them is expected to yield a more accurate value for the average flux when used together with Equations 4.15 and 4.16.



**Table 4.4** – Corresponding linear regression equation and  $R^2$  for each of the heat coefficient correlations

<b>Correlation</b>	<b>Corresponding linear regression (<math>y = ax + b</math>)</b>	<b><math>R^2</math></b>
4.22	$0.0012x - 0.208$	0.936
4.23	$0.0014x - 0.3182$	0.920
4.24 – 4.25	$0.0006x + 0.1562$	0.973
4.26	$0.0009x - 0.0572$	0.942
4.27	$0.0007 + 0.323$	0.958

According to the mass transfer equation provided by correlations 4.24 – 4.25, the coefficient for the PTFE supported membrane is  $6.02 \times 10^{-7} \frac{kg}{m^2 \cdot s \cdot Pa}$ , value similar to the one found in other works involving such membrane material (PHATTARANAWIK et al, 2003).

#### **4.4.3 Convective heat transfer analysis**

The accuracy provided by the convective heat transfer correlations in predicting overall convective heat transfer given in Equation 4.28 was evaluated using the deviation  $\delta$  described in section 4.3.5. The values are presented in Table 4.5 for each channel and condition experimented on. For  $\delta$ , smaller number indicates better heat transfer prediction for the process. The set of correlations 4.24 - 4.25 presented better overall results for such a purpose as well.

**Table 4.5** – Comparison between experimental data and constant wall temperature model energy variation predictions

Condition	Correlation	Permeate channel $\delta$	Feed channel $\delta$
A		12.7	52.7
B	<b>4.22</b>	7.89	49.6
C		41.1	62.9
A		43.5	64.3
B	<b>4.23</b>	7.34	50.5
C		29.1	56.3
A		8.5	48.3
B	<b>4.24 - 4.25</b>	16.5	45.8
C		28.4	56
A		10	50.6
B	<b>4.26</b>	10.9	47.7
C		35.7	59.7
A		10	50.6
B	<b>4.27</b>	12.9	46.9
C		58.8	76.9

As it can be seen from the results presented in Table 4.5, relative high deviations were found, especially for the feed channel. In particular, the lower accuracy of feed results can be interpreted as a sign of higher heat loss beyond the boundaries of the system. Such a statement is supported by the higher temperature difference between feed channel and its surroundings, thus causing a more intense heat loss.

#### 4.4.4 Thermal boundary layer estimation

Thermal boundary layer modelling results must necessarily start with the study of influence of both  $\Delta T$  and  $b$  on the results, once such path is used not only to check for the uniqueness of the  $T(x, y)$  solution, but also offers guidance to the trial and error method used to find the solution itself.

For different values of  $b$ , it was observed that when diminishing it, both  $N$  and  $\delta_T(x)$  values became smaller. As a direct consequence of the temperature profile format, temperature variation across the interface on feed and permeate channels became smaller, causing a higher outcome  $\Delta T$ . The variation in thermal boundary layer height for every  $x$  position was much

lower in intensity compared to the one in  $N$  and  $b$  itself, thus considerable decrease was observed in the value of  $k \frac{\partial^2 T}{\partial y^2}$ , involved in boundary condition IV). However, no variation was caused to  $C_p \rho v \frac{\partial T}{\partial y}$  value as it has no relation to the set of constants used to build an specific temperature profile.

On the other hand, diminishing the  $\Delta T$  input value for a same  $b$  resulted in a smaller  $\delta_T(x)$ . However, for low intensity changes in  $\Delta T$  no significant change was observed in thermal boundary layer height. That was true specially for low input values of temperature difference, a scenario in which phase transition heat flux contributes more intensely to the total wall heat flux and, consequently, to the value  $\delta_T$  must assume to satisfy Equation 4.4. A smaller value for  $\delta_T(x)$  leads to higher values for  $k \frac{\partial^2 T}{\partial y^2}$  in boundary condition IV) expression. However, smaller values are expected for  $C_p \rho v \frac{\partial T}{\partial y}$ , as the derivative must converge to a smaller value in the interface to account for the decrease in interfacial heat flux.

Combining the effects of  $b$  and input  $\Delta T$  in the results, gradual directed changes on their respective input values are made until a solution  $T(x, y)$  which yields a match in input and outcome  $\Delta T$  while simultaneously being in good agreement with boundary condition IV) is found. Afterwards, the intensity of the changes in the results associated to each of the two parameters allow further verification of the possibility of convergence to another solution. It was observed that, for a change of any magnitude in  $\Delta T$  input value, it is impossible to change  $b$  to continue matching both the outcome  $\Delta T$  and boundary condition IV) simultaneously. That happens due to the lack of synergy between the variation intensity of  $C_p \rho v \frac{\partial T}{\partial y}$  and  $k \frac{\partial^2 T}{\partial y^2}$  and of input and outcome  $\Delta T$ . The impossibility of convergence to more than one temperature profile for the process successfully grants then the uniqueness of the solution obtained from the modelling approach used.

As previously mentioned, it is virtually impossible to keep boundary condition IV) satisfied throughout the entire membrane extension. Although it is possible to keep deviation low for the middle-end portion of the flow in a given channel, the same does not remain valid for the initial portion due to the intense  $\delta_T$  variation, intrinsic of the temperature model proposed in

such a portion. Figure 4.3 presents the boundary layer profiles resulting from a modelling that prioritizes bigger accuracy – in the order of 80% – in boundary condition IV) for the middle-end portion of the flow in both permeate and feed channels for all the three feed inlet conditions experimented. Table 4.6 is presented along to inform the respective coefficients and input interfacial temperature difference values associated to the  $T(x, y)$  solution of each channel in each feed inlet condition.

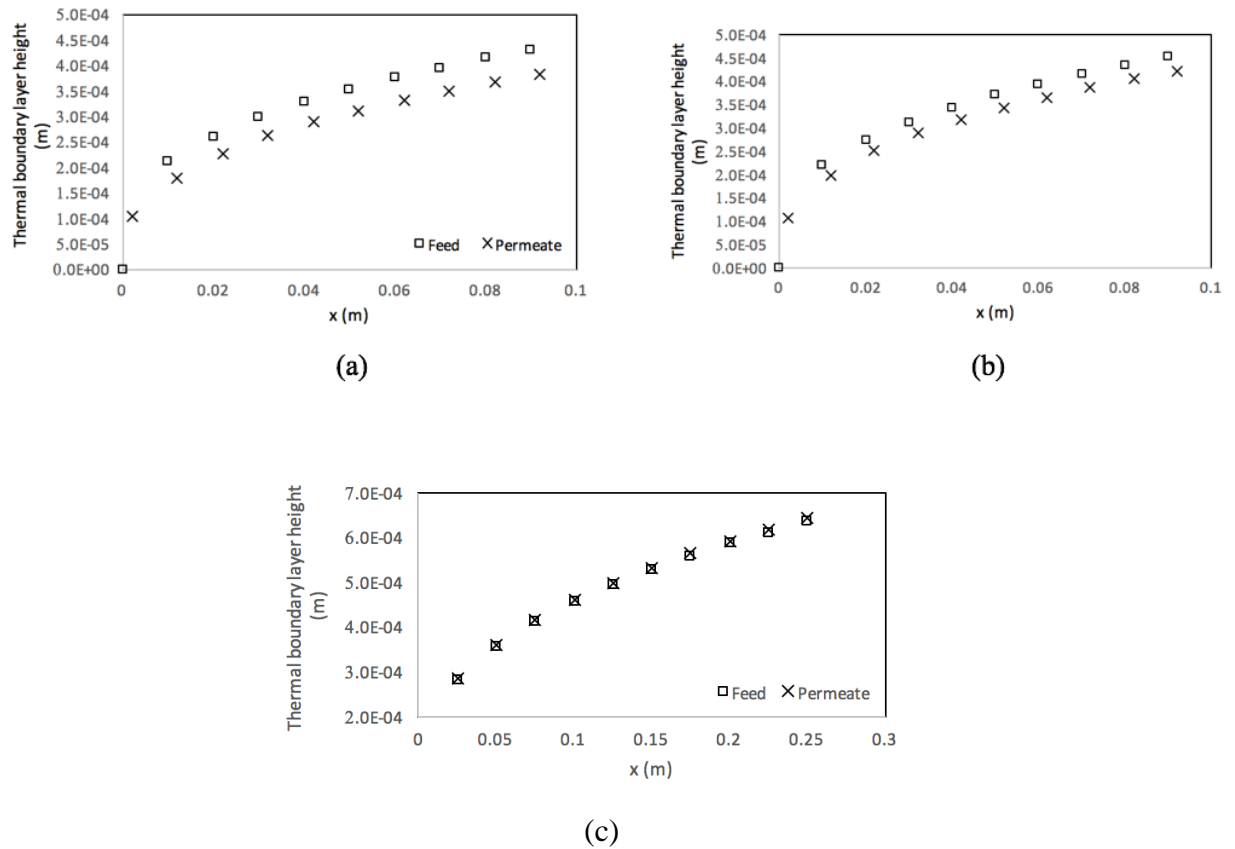


**Figure 4.3** – Thermal boundary layer height predicted by the temperature profile resultant from the modelling in feed and permeate channels for condition (a) A; (b) B and (c) C

**Table 4.6** – Respective temperature profile solutions obtained for feed and permeate channels for each feed inlet temperature condition modelled

<b>Condition</b>	<b>Feed temperature profile</b>	<b>Permeate temperature profile</b>	<b>input</b>
A	a = 1.49805	a = 1.49820	10
	b = 0.00390	b = 0.00360	
	c = -0.5019	c = -0.50180	
	N = 13018	N = 17861	
B	a = 1.49670	a = 1.4976	12.7
	b = 0.00500	b = 0.0048	
	c = -0.5025	c = -0.5024	
	N = 14120	N = 17080	
C	a = 1.49675	a = 1.49675	14
	b = 0.00650	b = 0.00650	
	c = -0.5032	c = -0.5032	
	N = 16984	N = 17651	

Smooth increase in boundary layer height was observed for both feed and permeate channel as feed inlet temperature increased. This is justified by the increased values of interfacial temperature difference, which implies in more heat gathered at the interface and, ultimately, in a higher  $\delta_T(x)$ , according to the temperature profile format proposed, to properly satisfy Equation 4.4. It was also observed in the graphical representation of the functions  $\delta_T(x)$  for each condition that permeate boundary layer height was more sensitive to the increase in interfacial temperature difference compared to feeds.

Regarding the constant interfacial temperature difference assumption, it was found to be impossible to keep the exact same value constant across the entire membrane length, being the deviation higher on its initial and final portions. Such behavior is independent of the feed inlet temperature condition, being rather due to the intrinsic logic associated to the interfacial temperature variation of the profile proposed. Figure 4.4 is presented to illustrate interfacial temperature difference variation course across membrane length.

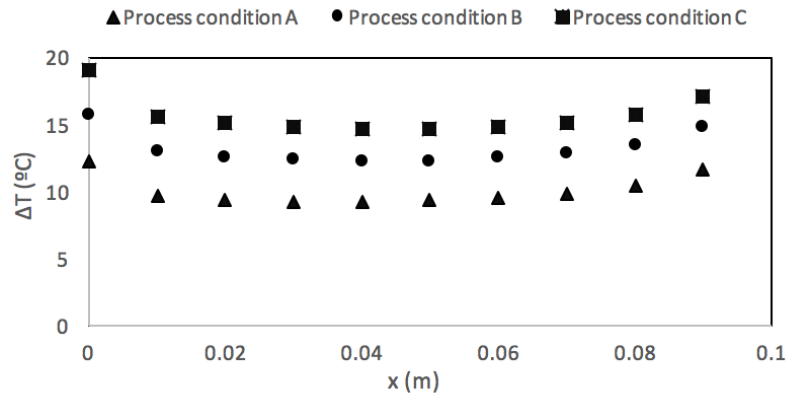


**Figure 4.4** – Illustration of  $\Delta T$  behavior delivered specifically by the temperature profiles solutions of each of the three feed inlet temperature condition

*Note: position is expressed taking feed channel as reference.*

A similar behavior was observed for the respective water vapor pressure difference between opposite interfacial sites, as shown graphically in Figure 4.5. Despite its exponential relation to temperature, water vapor pressure difference between membrane interface showed relatively little change across membrane length, being the divergence high specifically for the inlet portion of feed flow. Such high divergences were not observed for the outlet portion though.

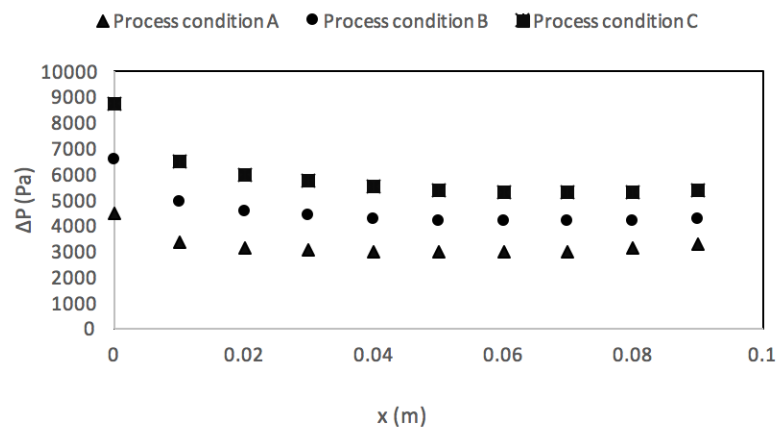


**Figure 4.5** – Illustration of  $\Delta P$  behavior delivered specifically by the temperature profiles solutions of each of the three feed inlet temperature condition

*Note: position is expressed taking feed channel as reference.*

Because of the good coherence with the constant wall heat flux assumption, boundary condition IV) and with the value of  $\Delta T$  used as input Equation 4.4, it is very likely that both channel's temperature profiles proposed represent, with good approximation, the system's reality in the middle portion of the flow. However, the big divergences in the wall heat flux value and high errors for boundary condition IV) obtained for the extremities of the channels reveals that the modelling does not represent well the exact temperature profile prevailing on each channel. Supported by the results, one can speculate what a more appropriate temperature profile should be like in the initial and final portion of the flows.

Given boundary layer theory, any other temperature profile  $T(x, y)$  also shares boundary condition I) and II) and must respect the energy balance given in Equation 4.4, assuming all the simplifications made to get to such equation remain valid. Each temperature profile can be designed to depend on  $x$  and  $y$  in different ways, thus having its own intrinsic heat loss profile for both directions. However, in any of them, for the beginning of the flow, even though temperature variation in  $y$  direction may be intense to account for a possibly large wall heat flux, interfacial temperature is still the closest to bulk temperature as it can be.

Rationalizing for the feed channel, given the exponential dependence of vapor pressure with temperature, its inlet portion of the flow must indeed have a higher  $P$  as feed interfacial temperature is still closer to bulk temperature. A possibly higher vapor pressure and interfacial temperature differences both implicate in higher wall heat flux. Because of such deviation expected in  $q''_w$  compared to the approximately constant value assumed,  $\delta_T$  value in the inlet portion may be smaller to support a bigger amount of interfacial heat transfer. However, it must be big enough to ultimately match the  $\delta_T$  values found for the middle portion of the flow in the current model. As expected from a continuous function, the more appropriate thermal boundary layer profile must have its behavior smoothly match the behavior found for the middle portion in the current model. That is because model coherence indicates that  $\delta_T(x)$  follows a similar behavior as the one found for such region. Hence, in

order to attenuate the increase in wall heat flux and support the smooth connection, the appropriate  $T(x, y)$  profile in the adjacent permeate channel must predict higher interfacial temperatures and shorter thermal boundary layer than the ones found for the final portion of its flow. Both factors synergistically support higher wall heat flux values as more intense interfacial temperature variation across  $y$  would prevail. As a consequence of the higher values of interfacial temperatures in the final portion of permeate channel, an attenuation on the increase of both  $\Delta T$  and  $\Delta P$  and, consequently, in  $q_w''$ , is expected in such a region. The smaller increase in wall heat flux allows boundary layer height on feed's side to catch up with the profile found for the middle portion, as the required intensity of its shortening diminishes. In short terms, the results of the current model lead to believe that the actual height of the thermal boundary layer in the end portion of the permeate flow is smaller than the one predicted, thus being overestimated in such region.

Same reasoning applies to the inlet portion of the permeate channel. However, the smaller feed interfacial temperatures in the adjacent region does not cause  $q_v''$  to be as big as it is on its own inlet portion. Thus, a smaller attenuation on feed's thermal boundary layer drop of interfacial temperature are expected. Ultimately, thermal boundary layer height on the outlet portion of feed's side is not as overestimated as permeates.

Lastly, it must be recognized though that the only reason the temperature profile proposed fits well boundary condition IV) for a reasonable portion of the system was due to the small membrane length used. Given the temperature profile's intrinsic variation rates intensity in  $x$  and  $y$  directions to account for the energy loss in every plane  $xy$ ,  $\delta_T$  keeps increasing with  $x$ . The thermal boundary layer height continuous growth leads, as a consequence, to the continuous increase in boundary condition IV)'s error across membrane length.

#### **4.4.5 Stack module design**

The modelling rationalized for the DCMD was also used to predict the behavior and assess the design of a small pilot stack module. Table 4.7 presents the outcomes of the modeling in terms of permeate production.



**Table 4.7** – Operational conditions, membrane dimensions, expected flux, and permeate production

<b>Parameter</b>	<b>Value</b>	<b>Unit</b>
$T_{\text{feed,in}}$	60	°C
$T_{\text{perm,in}}$	25	°C
L	0.25	m
b	0.002	m
h	0.4	m
Velocity	0.10	m/s
Number of membranes	3	-
Membrane active area	0.3	m <sup>2</sup>
Expected flux	14.42	kg/m <sup>2</sup> .h
Expected permeate production	103.80	kg/day

It was chosen to stack three membranes with smaller size in order to obtain a bigger membrane area without compromising the validity of the model. Figure 4.6 presents the boundary layer profile for a 80% of accuracy in boundary condition IV) for the middle-end portion of the flow in both permeate and feed channels. The boundary profile found for both feed and permeate are very similar, presenting a smooth increase in boundary layer height, as observed in all conditions for the smaller module. The similarity lies on the fact that the  $\Delta T_{\text{interfacial}}$  is the same for both streams, as shown in Table 4.8.

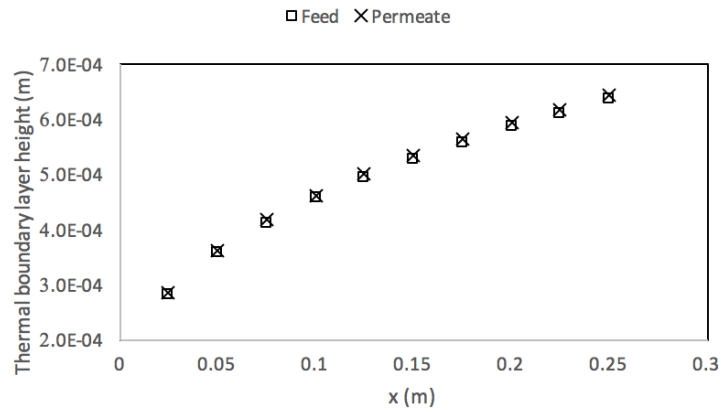


**Figure 4.6** – Thermal boundary layer height predicted by the temperature profile resultant from the modelling in feed and permeate channels for the stack module designed  
*Note: position is expressed taking feed channel as reference.*

**Table 4.8** – Respective temperature profile solutions obtained for feed and permeate channels for the stack module designed

Parameter	Feed	Permeate
a	1.495	1.495
b	0.01	0.01
c	-0.505	-0.505
N	18980	19578
$\Delta T_{interfacial}$	16	16

In addition, the temperature profile for each of the membranes is shown in Figure 4.7. As seen for the process conditions in the smaller module, a higher deviation on the initial and final portions of the membrane was also observed in this case.

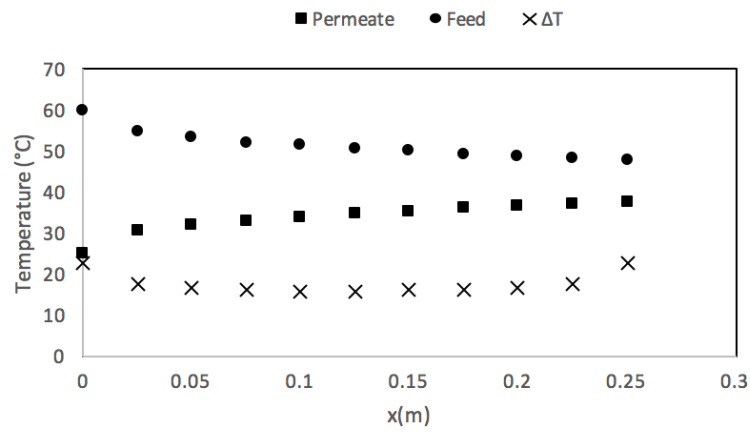
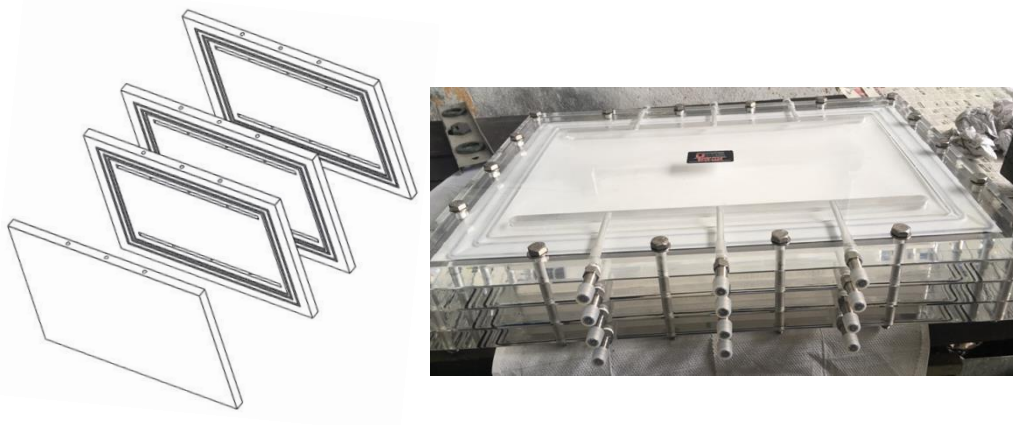


**Figure 4.7** – Illustration of  $\Delta T$  behavior delivered specifically by the temperature profiles solutions for the small pilot

*Note: position is expressed taking feed channel as reference.*

In sight of the similarity between the results found on the small and the module to be built, including the accuracy in developing the boundary layer profile, a stack DCMD module was built using the dimensions defined in Table 4.7. The module was machined in acrylic sheets, as it can be seen in Figure 4.8. As for its functioning, it is expected to be tested and experimental data will be confronted to the modelling developed.



#### 4.5 CONCLUSION

Linear models for average mass flux calculation based on virtual interfacial temperatures given by a macroscopic energy balance was obtained for all the convective heat transfer correlations investigated. Their capability of properly predicting the overall convective heat transferred inside the module through Equation 4.28 was also investigated. The set of correlations 4.24 and 4.25 were the ones that delivered the most accurate model for average mass flux prediction, being also the ones to better represent the overall convective heat transfer taking place in the system.

Thermal boundary layer could be successfully modelled for the middle portion of the channels using the temperature profile proposed in Equation 4.12 and the respective constant wall heat flux assumption. However, because of the form on which its second derivative in respect to  $y$  depends upon  $\delta_T$  and the intensity of the latest's variation, the membrane sheet used must not be too long for boundary condition IV), and consequently the profile proposed, to remain valid with good approximation. Based on the lack of coherence of results for the extremities of the membrane, the real temperature profile and thermal boundary layer are not well represented in the present modelling. However, an oriented interpretation of the results pointed out for an overestimated boundary layer height for both permeate and feed channels on its respective outlet portion of the flow. Therefore, despite not offering an accurate representation of the system's temperature in such regions, the model still offers reliability when designing a membrane sheet overlap in membrane distillation processes.

In sight of the results of the results obtained for the model, it was used to assess the development of a stack direct contact membrane distillation module. It was seen that the model was still valid for membrane with dimensions of 0.25 x 0.4 m, with over 80% accuracy for the boundary layers estimation. The height of the boundary layer, due to its size, did not cause any harm to the stack model developed, since the membrane channels were much thicker than them. Regarding the permeate flux, an amount of 103.4kg of permeate is expected per day, produced using a total membrane area of 0.3m<sup>2</sup>.

# **CHAPTER 5**

---

## **FINAL CONSIDERATIONS**

In this work, the use of membrane distillation to treat water with different degrees of contamination by tailings from an iron mining dam was investigated. In Chapter 2, the influence of feed turbidity and operational parameters such as feed pretreatment, feed temperature, and cross-flow velocity was evaluated regarding its impacts on the system. When treating solutions with different amounts of suspended solids, it was noticed that a feed turbidity until 300 NTU did not affect the membrane performance very severely, since no wetting time or wetting rate were observed. However, at higher turbidities, a pretreatment should be carried out in order to avoid a premature membrane damage. In this context, the ultrafiltration presented the best technical results both for preventing flux decay and wetting time. Regarding feed temperature, it was observed a deviation between the expected and the experimental flux, which can be attributed to the temperature polarization phenomenon. This effect increases along with the temperature gradient. Yet, the minimum amount of heat demanded for generating 1kg of permeate was found for the temperature of 70°C, being the recommended temperature in this case. For the cross-flow velocity assessment, it was noticed that an increase in the Re number increased the permeate flux. However, this decrease is less prominent after the threshold value of 0.18 m/s, from which the energy added to increase cross-flow velocity does not contribute to a better efficiency of the process anymore.

In Chapter three, fouling was characterized and an agent was chosen for cleaning. SEM/EDX and FTIR analysis showed that fouling was mainly composed by inorganic fouling, being silica, alumina and hematite the main foulant agents. As a consequence, HCl and water at 60°C presented the best results for the partial removal of the fouling layer, but HCl did not seem to bring any gain to the process efficiency. In addition, a test to evaluate membrane ageing was carried out. It was observed a decrease in both permeate flux and saline retention. A SEM analysis showed the nucleation and growth of Al<sub>2</sub>O<sub>3</sub> over the membrane, which can be the cause for permeate flux decrease and membrane wetting. Despite the structural differences between the fouling layer formed during the regular filtration and the ageing procedure, the effect of the cleaning agent was the same in both cases, which indicates that DI water at 60°C can be used as a cleaning agent without compromising the integrity of the membrane.

Finally, in Chapter four, two models for thermal boundary layer estimation and mass flux prediction were developed for a direct contact membrane distillation system. For the first

model, a bi-dimensional temperature profile was developed to predict thermal boundary layer height using the integral method, in which the model results agreed with the assumptions made with 80% accuracy or higher. The results indicated that the thermal boundary layer profile obtained can be safely used for designing a membrane module with flat sheet overlapping. However, in order to maintain the model's accuracy, the membrane should not be too long, since the model demonstrated deviations in the membranes limits. For mass flux prediction, five convective heat transfer coefficient correlations used to deliver the average mass flux model were compared and evaluated regarding its capability of predicting the overall heat transferred in the process. Once defined the most suitable correlation, an equation for average mass flux calculation was determined using macroscopic energy balance. Hereinafter, the models were successfully used to assess the development of a stack direct contact membrane distillation module with dimensions of 0.25 x 0.4 m. The height of the boundary layer, due to its size, did not cause any harm to the stack model developed, and an amount of 103.4kg of permeate was expected per day, produced using a total membrane area of 0.3m<sup>2</sup> (the system was composed by 3 membranes).

## **CHAPTER 6**

---

### **SUGGESTIONS FOR FUTURE WORK**



The following studies are suggested for future work:

- Economical assessment of the feed pretreatment techniques;
- Assess the effect of permeate temperature on MD performance;
- Evaluate the conjugation of membrane distillation with renewable sources of energy, such as solar energy;
- Perform an economical evaluation of the DCMD system as a solution for water treatment during emergency situation;
- Optimize the chemical cleaning agent chosen towards its concentration and cleaning time;
- Increase the exposure time of the membrane to the effluent and perform a long-term filtration with cleaning procedures, to confront the eventual differences found in pilot-scale and the results obtained in laboratory scale;
- Compare the results experimentally obtained for the small-pilot constructed with those predicted by the models;

# **CHAPTER 7**

---

## **REFERENCES**

ACERO, J. L.; BENITEZ, F. J.; LEAL, A. I.; REAL, F. J.; TEVA, F. Membrane filtration technologies applied to municipal secondary effluents for potential reuse. *Journal of Hazardous Materials*, v. 177 (1), p. 390-398, 2010.

AGUIAR, A.; ANDRADE, L.; GROSSI, L.; PIRES, W.; AMARAL, M. Acid mine drainage treatment by nanofiltration: A study of membrane fouling, chemical cleaning, and membrane ageing. *Separation and Purification Technology*, v. 192, p. 185-195, 2018.

ALKHUDHIRI, A.; DARWISH, N.; HILAL, N. Membrane distillation: A comprehensive review. *Desalination*, v.287 p. 2-18, 2012.

ALKHUDHIRI, A.; HILAL, N. Air gap membrane distillation: A detailed study of high saline solution. *Desalination*, v. 403, p. 179-183, 2017.

AL-OBAIDANI, S.; CURCIO, E.; MACEDONIO, F.; PROFIO, G.; DRIOLI, E. Potential of membrane distillation in seawater desalination: Thermal efficiency, sensitivity study and cost estimation. *Journal of Membrane Science*, v. 323, p. 85-98, 2008.

AN A.; GUO, J.; JEONG, S.; LEE, E.; TABATABAI, S.; LEIKNES, T. High flux and antifouling properties of negatively charged membrane for dyeing wastewater treatment by membrane distillation. *Water Research*, v. 103, p. 362-371, 2016.

ANDERSSON, S.; KJELLANDER, N.; RODESJO, B.. Design and field tests of a new membrane distillation desalination process. *Desalination*, v. 56, p. 345-354, 1985.

ANDRADE, L. *Caracterização de rejeitos de mineração de ferro, in natura e segregados, para aplicação como material de construção civil*. Viçosa: UFV, 96p. 2014 (PhD thesis).

ANDRADE, L.; RICCI, B.; GROSSI, L.; AGUIAR, A.; PIRES, W.; AMARAL, M. Nanofiltration applied in gold mining effluent treatment: Evaluation of chemical cleaning and membrane stability. *Chemical Engineering Journal*, v. 323, p. 545-556, 2017.

APHA. *Standard methods for the examination of water and wastewater*. American Public Health Association, Washington, DC, 2012.

BLANPAIN, P.; LALANDE, M. Investigation of fouling mechanisms governing permeate flux in the crossflow microfiltration of beer. *Filtration Separation*, v. 34 p. 1065-1069, 1997.

BAKER, R.W. *Membrane technology and applications*, 2. Ed. John Wiley & Sons Ltd, England, 2004.

BANAT, F.; JWAIED, N. Autonomous Membrane Distillation Pilot Plant Unit Driven by Solar Energy: Experiences and Lessons Learned. *International Journal of Sustainable Water & Environmental Systems*, v. 1, p.21-24, 2010.

BANAT, F.; SIMANDL, J. Desalination by membrane distillation: a parametric study. *Separation Science and Technology*, v. 33, p. 201–226, 1998.

BAPPY, M.; BAHAR, R.; ARIFF, T. Low energy and low cost freshwater production by membrane distillation. IN: 2016 International Conference on Industrial Engineering and Operations Management. Kuala Lumpur (2016).

BBC. *2010 membrane and separation technology research review*. BBC Research, 2011.

BBC. *Major Reverse Osmosis System Components for Water Treatment: The Global Market*. BBC Research, 2014.

BEJAN, A. *Convection heat transfer*. New Jersey: John Wiley & Sons, 2004.

BNDES. *Perspectivas da Energia Solar e o Apoio do BNDES ao Setor*. São Paulo, 2014.

BRASIL. *Portaria nº 2914 de 12 de Dezembro de 2011. Dispõe sobre os procedimentos de controle e de vigilância da qualidade da água para consumo humano e seu padrão de potabilidade*. Publicado no D.O.U.

BRASIL. *Resolução CONAMA nº357, de 17 de Março de 2005. Classificação de águas, doces, salobras e salinas do Território Nacional*. Publicado no D.O.U.

CAMACHO, L.; DUMÉE, L.; ZHANG, J.; LI, J.; DUKE, M.; GOMEZ, J. GRAY, S. Advances in Membrane Distillation for Water Desalination and Purification Applications. *Water*, v. 5, p. 94-196, 2013.

CATH, T.; ADAMS, V.; CHILDRESS, A. Experimental study of desalination using direct contact membrane distillation: a new approach to flux enhancement. *Journal of Membrane Science*, v. 228, p. 5-16, 2004.

CHAPMAN, A. *Heat Transfer*. 4 ed. London: Collier Macmillan Publishers, 1994.

COMITÊ DE BACIA DO RIO DOCE. *Diagnóstico Consolidado da Bacia do Rio Doce*. Brasil, 2005.

CRISCUOLI, A.; CARNEVALE, M.C.; DRIOLI, E. Evaluation of energy requirements in membrane distillation. *Chemical Engineering and Processing: Process Intensification*, v. 47, p. 1098-1055, 2008.

CURCIO, E.; JI, X.; PROFIO, G.; SULAIMAN, A. FONTANANOVA, E.; DRIOLI, E. Membrane distillation operated at high seawater concentration factors: role of the membrane on CaCO<sub>3</sub> scaling in presence of humic acid. *Journal of Membrane Science*, v. 346, p. 263-269, 2010.

CURCIO, E.; DRIOLI, E. Membrane distillation and related operations – A review. *Separation and Purification Reviews*, v. 34, p.35–86, 2005.

DARTON, T.; ANNUNZIATA, U.; PISANO, F.; GALLEGGO, S. Membrane autopsy helps to provide solutions to operational problems. *Desalination*, v. 167 (0), p. 239-245,2004.

DIÉZ, L.; GONZÁLEZ, M.. A method to evaluate coefficients affecting flux in membrane distillation. *Journal of Membrane Science*, v. 173, p. 225-234, 2000.

DING, Z.; MA, R.; FANE, A. A new model for mass transfer in direct contact membrane distillation. *Desalination*, v. 15, p. 217–227, 2003.

DRIOLI, E.; ALI, A.; MACEDONIO, F. Membrane distillation: Recent developments and perspectives. *Desalination*, v. 356, p. 56-84, 2015.

EPA <https://www.epa.gov/water-research/relative-risk-pharmaceuticals-wastewater>

EL-BOURAWI, M.; DING, Z.; MA, R.; KHAYET, M. A framework for better understanding membrane distillation separation process. *Journal of Membrane Science*, v. 285, p. 4-29, 2006.

FAVERO, C. *Uso e degradação de solos na microrregião de Governador Valadares*. 2011. 80 p. Tese (Doutor em Ciências), Departamento de Pós-Graduação em Solos e Nutrição de Plantas - Universidade Federal de Viçosa, Viçosa, 2001.

FORTUNATO, L.; BARBIERI, G.; DRIOLI, E. Direct contact membrane distillation: modelling and concentration experiments. *Journal of Membrane Science*, v. 166, p. 1–11, 2000.

FRANCIS, L.; GHAFFOR, N.; ALSAADI, A.S.; NUNES, S.P.; AMY, G.L. Performance evaluation of the DCMD desalination process under bench scale and large scale module operating conditions. *Journal of Membrane Science*, v. 455, p. 103-112, 2014.

FUNDAÇÃO ESTADUAL DO MEIO AMBIENTE (FEAM). *Inventário de barragens do estado de minas gerais*. Belo Horizonte, 2016.

FUNDAÇÃO JOÃO PINHEIRO. *Perfil demográfico do estado de Minas Gerais 2000*. Belo Horizonte, 2000.

GE, J.; PENG, Y.; LI, Z.; CHEN, P.; WANG, S. Membrane fouling and wetting in a DCMD process for RO brine concentration. *Desalination*, v. 344, p. 97-107, 2014.

GOMES, M. A. *Caracterização tecnológica no aproveitamento do rejeito de minério de ferro*. Ouro Preto: UFOP. 77p. 2009. (Master Thesis)

GUEDES, C. D.; PEREIRA, J.; LENA, J.; PAIVA, J.; LIMA, R. Coagulação/floculação de suspensões ricas em óxidos de ferro por sulfato de alumínio. *Química Nova*, v. 27 (5), p. 715-719, 2004.

GUILLÉN-BURRIEZA, E.; MAVUKKANDY, M.; BILAD, M.; ARAFAT, H. Understanding wetting phenomena in membrane distillation and how operational parameters can affect it. *Journal of Membrane Science*, v. 515, p. 163-174, 2016.

GUILLEN-BURRIEZA, E.; RUIZ-AGUIRRE, A.; ZARAGOZA, G.; ARAFAT, H. Membrane fouling and cleaning in long term plant-scale membrane distillation operations. *Journal of Membrane Science*, v. 468, p. 360-372, 2014.

GUILLÉN-BURRIEZA, E.; THOMAS, R.; MANSOOR, B.; JOHNSON, D.; HILAL, N. Effect of dry-out on the fouling of PVDF and PTFE membranes under conditions simulating intermittent seawater membrane distillation (SWMD). *Journal of Membrane Science*, v. 515, p. 126-139, 2013.

GUILLÉN-BURRIEZA, E.; ZARAGOZA, G.; MIRALLES-CUEVAS, S.; BLANCO, J. Experimental evaluation of two pilot-scale membrane distillation modules used for solar desalination. *Journal of Membrane Science*, v. 409-410, p. 264-275, 2012.

GRYTA, M. Effect of iron oxides scaling on the MD process performance. *Desalination*, v. 216 (1-3), p. 88-102, 2007.

GRYTA, M. Fouling in direct contact membrane distillation. *Journal of Membrane Science*, v. 325, p. 383-394, 2008.

GRYTA, M. Influence of polypropylene membrane surface porosity on the performance of membrane distillation process. *Journal of Membrane Science*, v. 144, p. 211-222, 1998.

GRYTA, M. Polyphosphates used for membrane scaling inhibition during water desalination by membrane distillation. *Desalination*, v. 285, p. 170-176, 2012.

GRYTA, M.; TOMASZEWSKA, M. Membrane distillation of NaCl solution containing natural organic matter. *Journal of Membrane Science*, v. 181, p. 279-287, 2001.

GRYTA, M.; TOMASZEWSKA, M. Heat transport in the membrane distillation process. *Journal of Membrane Science*, v. 144, p. 211-222, 1998.

GRYTA, M.; GRZECHULSKA-DAMSEL, J.; MARKOWSKA, A.; KARAKULSKI, K. The influence of polypropylene degradation on the membrane wettability during membrane distillation. *Journal of Membrane Science*, v. 326, p. 493-512, 2009.

GWON, E.-M.; YU, M.-J.; OH, H.-K.; YLEE, Y.-H. Fouling characteristics of NF and RO operated for removal of dissolved matter from groundwater. *Water Research*, v. 37, n. 12, p. 2989-2997, 2003.

HABERT, A.C.; BORGES, C.; NOBREGA, R. *Processos de separação por membranas*, 1. ed., Rio de Janeiro: e-papers, 2006.

HOLMAN, J. P. *Transferência de Calor*. São Paulo: McGraw-Hill, 1983.

HSU, S.; CHENG, K.; CHIOU, J. Seawater desalination by direct contact membrane distillation. *Desalination*, v. 143 (3), p. 279-287, 2002.

- IBRAHIM, S.; ALSALHY, Q. Modelling and simulation for direct contact membrane distillation in hollow fiber modules. *AIChE Journal*, v. 59, p. 589–603, 2013.
- INSTITUTO MINEIRO DE GESTÃO DE ÁGUAS (IGAM). *Qualidade das águas superficiais em Minas Gerais em 2013*. Belo Horizonte, 2014.
- INSTITUTO MINEIRO DE GESTÃO DE ÁGUAS (IGAM). *Acompanhamento da Qualidade das Águas do Rio Doce Após o Rompimento da Barragem da Samarco no distrito de Bento Rodrigues – Mariana/MG*. Belo Horizonte, 2016.
- INSTITUTO BRASILEIRO DE MINERAÇÃO (IBRAM). *Panorama da mineração em Minas Gerais*. Brasília, 2016.
- IZQUIERDO-GIL, M.A.; GARCÍA-PAYO, M.C.; FERNANDÉZ-PINEDA, C. Air gap membrane distillation of sucrose aqueous solutions. *Journal of Membrane Science*, v.155, p. 291-307, 2009.
- JACOB, J.; PRADANOS, P.; CALVO, J.I.; HERNANDEZ, A.; JONSSON, G. Fouling kinetics and associated dynamics of structural modifications. *Colloids and Surfaces: Physicochemical and Engineering Aspects*, v. 138 p. 173-183, 1998.
- KAKAÇ, S.; YENER, Y. *Convective Heat Transfer*. 2 ed. Boca Raton: CRC Press, 1994.
- KHAN, E.; MARTIN, A. Water purification of arsenic contaminated drinking water via air gap membrane distillation (AGMD). *Periodica Polytechnica Mechanical Engineering*, v. 58, p. 47-53, 2014.
- KHAYET, M. Membranes and theoretical modeling of membrane distillation: A review. *Advances in Colloidal Interface Science*, v.164, p. 56-88, 2011.
- KHAYET, M.; MATSUURA, T. *Membrane Distillation: Principles and Applications*. 1 Ed. Netherlands: Elsevier, 2011.
- KHAYET, M.; MENGUAL, J.I.; ZAKRZEWSKA-TRZNADEL, G. Direct contact membrane distillation for nuclear desalination, part II: experiments with radioactive solutions. *International Journal of Nuclear Desalination*, v. 2, p. 56, 2006.
- KLÜPFEL, A.; FRIMMEL, F. Nanofiltration of river water-fouling, cleaning and micropollutant rejection. *Desalination*, v. 250, p. 10005-1007, 2010.
- KNYAZKOVA, T.V.; MAYNAROVICH, A.A. Recognition of membrane fouling: testing of theoretical approaches with data on NF of salt solutions containing a low molecular weight surfactant as a foulant. *Desalination*, v. 126 (1–3), p. 163-169, 1999.
- KORETSKY, M.D. *Engineering and Chemical Thermodynamics*. Oregon: John Wiley & Sons, 2013.

- LAWAL, D; KHALIFA, A. Flux Prediction in Direct Contact Membrane Distillation. *International Journal of Materials, Mechanics and Manufacturing*, v. 2, p. 302-308, 2014.
- LAWSON, K.; LLOYD, D. Review: Membrane Distillation. *Journal of Membrane Science*, v.124, p. 1-23, 1997.
- LE, N.; NUNES, S. Materials and membrane technologies for water and energy sustainability. *Sustainable Materials and Technology*, v. 7, p. 1-28, 2006.
- LIU, CHEN, L.; ZHU, L. Fouling mechanism of hydrophobic polytetrafluoroethylene (PTFE) membrane by differently charged organics during direct contact membrane distillation (DCMD) process: An especial interest in the feed properties. *Journal of Membrane Science*, v. 548, p. 123-135, 2018.
- MANNA, A.; PAL, P. Solar-driven flash vaporization membrane distillation for arsenic removal from groundwater: Experimental investigation and analysis of performance parameters. *Chemical Engineering and Processing: Process Intensification*, v. 99, p. 51-57, 2016.
- MANAWI, Y.M. ; KRAISHEH, M.; FARD, A.K.; BENYAHIA, F.; ADHAM, S. A predictive model for the assessment of the temperature polarization effect in direct contact membrane distillation of high salinity feed. *Desalination*, v. 341, p. 38-49, 2014a.
- MANAWI, Y.M.; KHRAISHEH, M.; FARD, A.K.; BENYAHIA, F.; ADHAM, S. Effect of operational parameters on distillate flux in direct contact membrane distillation (DCMD): Comparison between experimental and model predicted performance. *Desalination*, v. 336, p. 110-120, 2014b.
- MARTÍNEZ-DÍEZ, L.; VÁZQUEZ-GONZÁLEZ, M.I. Temperature and concentration polarization in membrane distillation of aqueous salt solutions. *Journal of Membrane Science*, v. 156, p. 265-273, 1999.
- MERICQ, J.P.; LABORIE, S.; CABASSUD, C. Vacuum membrane distillation for an integrated seawater desalination process. *Desalination and Water Treatment*, v. 9, p. 287-296, 2009.
- NARIYOSHI, Y.N.; PANTOJA, C.E. Destilação com membranas aplicada para concentração de soluções aquosas de cloreto de sódio: modelagem matemática. In: XX CONGRESSO BRASILEIRO DE ENGENHARIA QUÍMICA, 2014, São Paulo.
- PANTOJA, C.E.; NARIYOSHI, Y.N.; SECKLER, M.M. Membrane Distillation Crystallization Applied to Brine Desalination: A Hierarchical Design Procedure. *Industrial & Engineering Chemistry Research*, v. 54 (10), p. 2776-2793, 2015.
- PHATTARANAWIK, J; FANE, A.; PASQUIER, A.; BING, W. A novel membrane bioreactor based on membrane distillation. *Desalination*, v. 223 1-3, p. 386-395, 2008.



- PHATTARANAWIK, J.; JIRARATANANON, R.; FANE, A.G. Heat transport and membrane distillation coefficients in direct contact membrane distillation. *Journal of Membrane Science*, v. 212, p. 177-193, 2003.
- PEREIRA, E.; MARTINS, F.; ABREU, S.; RÜTHER, R. *Atlas brasileiro de energia solar*, 1. Ed, Brasil, 2006.
- PENG, Y.; GE, J.; LI, Z.; WANG, S. Effects of anti-scaling and cleaning chemicals on membrane scale in direct contact membrane distillation process for RO brine concentrate. *Separation and Purification Technology*, v. 154, p. 22-26, 2015.
- PRICE, D.; JARRAT, M. Thermal conductivity of PTFE and PTFE composites. *Thermochimica Acta*, v. 392-393, p. 231-236, 2002.
- PROFIO, G.; JI, X.; CURCIO, E.; DRIOLI, E. Submerged hollow fiber ultrafiltration as seawater pretreatment in the logic of integrated membrane desalination systems. *Desalination*, v. 269 1-3, p. 128-135, 2011.
- QIN, W.; XIE, Z.; NG, D.; YE, Y.; JI, X.; GREY, S.; ZHANG, J. Comparison of colloidal silica involved fouling behavior in three membrane distillation configurations using PTFE membrane. *Water Research*, v. 130, p. 343-352, 2018.
- QU, D.; WANG, J.; HOU, D.; LUAN, Z.; FAN, B.; ZHAO, C. Experimental study of arsenic removal by direct contact membrane distillation. *Journal of Hazardous Materials*, v. 173, p. 874-879, 2009.
- QTAISHATA, M.; MATSUURAA, T.; KRUCZEKA, B.; KHAYETB, M. Heat and mass transfer analysis in direct contact membrane distillation. *Desalination*, v. 219, p. 272-292, 2008.
- REGULA, C.; CARRETIER, E.; WYART, Y.; GÉSAN-GUIZIOU, G.; VINCENT, A.; BOUDOT, D.; MOULIN, P. Chemical cleaning/disinfection and ageing of organic UF membranes: a review. *Water Research*, v. 56, p. 325-365, 2014.
- RICHARDS, L.; RICHARDS, B.S.; SCHÄFER, A.I. Renewable energy powered membrane systems: Inorganic contaminant removal from Australian groundwaters. *Membrane Water Treatment*, v. 2, n. 4, p. 239-250, 2011.
- RICHARDSON, T. *Shreir's Corrosion*. Oxford: Elsevier, 2009.
- SAFFARINI, R.; SUMMERS, E.; ARAFAT, H.; LIENHARD, J. Technical evaluation of stand-alone solar powered membrane distillation systems. *Desalination*, v. 286, p. 332-341, 2012.
- SANMARTINO, J.; KHAYET, M.; GARCÍA-PAYO, M. Reuse of discarded membrane distillation membranes in microfiltration technology. *Journal of Membrane Science*, v. 539, p. 273-283, 2017.

SCHWANTES, R.; CIPOLLINA, A.; GROSS F.; KOSCHIKOWSKI J.; PFEIFLE, D.; ROLLETSCHEK, M.; SUBIELA, V. Membrane distillation: Solar and waste heat driven demonstration plants for desalination. *Desalination*, v. 323, p. 93-106, 2013.

SCHÄFER, A.; FANE, A.; WAITE, T. *Nanofiltration: Principles and Applications*. Oxford: Elsevier, 2005.

SCHOFIELD, R.W.; FANE, A.; FELL, C.J.D. Heat and mass transfer in membrane distillation. *Journal of Membrane Science*, v. 33, p. 299-313, 1987.

SETHI, S.; WIESNER, M. R. Cost modeling and estimation of cross-flow membrane filtration processes. *Environmental engineering science*, v. 17 (2), p. 61-79, 2000.

SOHRABI, M.; MADAENI, S.; KHOSRAVI, M.; GHAEDI, A. Chemical cleaning of reverse osmosis and nanofiltration membranes fouled by licorice fouled solutions. *Desalination*, v. 267, p. 93-100, 2011.

SRISURICHAN, S.; JIRARATANANON, R.; FANE, A.G. Humic acid fouling in the membrane distillation process. *Desalination*, v. 174 (1), p. 63-72, 2005.

SRISURICHAN, S.; JIRARATANANON, R.; FANE, A.G. Mass transfer mechanisms and transport resistances in direct contact membrane distillation process. *Journal of Membrane Science*, v. 227, p. 186-194, 2006.

STERLITECH CORPORATION. *CF042D-FO Cell Assembly and Operation Manual*, in: Manual CF042D-FO Cell, 2017.

TIJING, L.; WOO, Y.; CHOI, J.; LEE, S.; KIM, S.; SHON, H. Fouling and its control in membrane distillation—A review. *Journal of Membrane Science*, v. 475, p. 215-244, 2015.

WANG, P.; CHUNG, T.S. Recent advances in membrane distillation processes: Membrane development, configuration design and application exploring. *Journal of Membrane Science*, v. 474, p. 39-56, 2015.

WANG, J.; QU, D.; TIE, M.; REN, H.; PENG X.; LUAN Z. Effect of coagulation pretreatment on membrane distillation process for desalination of recirculating cooling water. *Separation and Purification Technology*, v. 64, p. 108-115, 2008.

WANG, Z.; LIN, S. Membrane fouling and wetting in membrane distillation and their mitigation by novel membranes with special wettability. *Water Research*, v. 112, p. 38-47, 2017.

WARSINGER, D.; SWAMINATHAN, J.; GUILLEN-BURRIEZA, E.; ARAFAT, H.; LIENHARD, J. Scaling and fouling in membrane distillation for desalination applications: A review. *Desalination*, v. 356, p. 294-313, 2015.

WISE URANIUM PROJECT. Chronology of major tailing dam failure. Disponível em: < <http://www.wise-uranium.org/mdaf.html> >. Acessado em 04/11/16.

WELTY, J.; WICKS, C.; WILSON, R.; RORRER, G.. *Fundamentals of Momentum, Heat, and Mass Transfer*. Oregon: John Wiley & Sons, 2008.

XU, J.; SINGH, Y.B.; AMY, G.L.; GHAFFOR, N. Effect of operating parameters and membrane characteristics on air gap membrane distillation performance for the treatment of highly saline water. *Journal of Membrane Science*, v. 512, p. 73-82, 2016.

YABE, M.; OLIVEIRA, E. Metais pesados em águas superficiais como estratégia de caracterização de bacias hidrográficas. *Química nova*, v. 21 (25) p. 551-556, 1998.

YUAN, W.; KOCIC, A.; ZYDNEY, A.L. Analysis of humic acid fouling during microfiltration using a pore blockage-cake filtration model. *Journal of Membrane Science*, v. 198, p. 51-62 2002.

YUNA, Y.; MAB, R.; ZHANG, W.; FANEC, A.G.; LIA, J. Direct contact membrane distillation mechanism for high concentration NaCl solutions. *Desalination*, v. 199, p. 251-262, 2006.

ZHANG, J.; GREY, S.; LI, J. Modelling heat and mass transfers in DCMD using compressible membranes. *Journal of Membrane Science*, v. 387-388, p. 7-16, 2012.